

DELFT UNIVERSITY OF TECHNOLOGY

---

# Evaluating Constant Failure Rates in Storm Surge Barriers

---

A Statistical Framework Applied to Censored Component  
Lifetimes of the Oosterscheldekering

By

Jelle Epema

Tracks: Financial Engineering & Hydraulic Engineering  
Faculties: Applied Mathematics & Civil Engineering  
At the Delft University of Technology  
To be defended publicly on Tuesday, November 7, 2023

*Chair:*

Prof. dr. ir. Matthijs Kok TU Delft

*Supervisors:*

Dr. Piao Chen TU Delft

Ir. Leslie Mooyaart TU Delft — Rijkswaterstaat

*Committee*

Prof. dr. Geurt Jongbloed TU Delft

Dr. ir. Alexander Bakker TU Delft — Rijkswaterstaat

Dr. Ronald van Nooijen TU Delft



## Nomenclature

Symbol	Description
$\lambda$	Scale parameter
$\kappa$	Shape parameter
$t_i$	Observed lifetime
$t_{i0}, t_{i1}$	Interval limits for interval-censored lifetimes
$\delta_{Ri}, \delta_{Ii}$	Indicator variables for right- and interval-censoring
$\boldsymbol{\theta}$	Parameter vector in multi-parameter models
$\mathbf{H}$	Hessian matrix
$\nabla\mathcal{L}$	Gradient vector of the log-likelihood function
$C$	Censoring time
$S(t; \lambda)$	Survival function
$f(t; \lambda)$	Probability density function
$F(t; \lambda)$	Cumulative distribution function
$T_i$	Actual lifetime
$H_0$	Null hypothesis
$H_1$	Alternative hypothesis
$F$	Distribution under consideration
$F_0$	Specified distribution for comparison
$n$	Group size of components
$\delta_i$	Indicator variable for censoring

## Preface

This MSc Thesis signifies the conclusion of my academic tenure at Delft University of Technology. The research was conducted in partnership with Rijkswaterstaat, and focuses on the crucial issue of storm surge barrier reliability, with specific emphasis on the Oosterscheldekering.

I wish to extend profound gratitude to my supervisory team, whose guidance was instrumental in the successful completion of this work. Prof. Dr. ir. Matthijs Kok, Prof. Dr. Geurt Jongbloed, Dr. Piao Chen, Dr. ir. Alexander Bakker, Dr. Ronald van Nooijen, and Ir. Leslie Mooyaart have each played a pivotal role in shaping my understanding and facilitating the realization of this project.

Special recognition is due to Leslie Mooyaart and Piao Chen, who provided unwavering support and indispensable insights throughout the research process. Their timely feedback and readiness for dialogue have been invaluable. Additionally, I express my gratitude for the late-stage assistance provided by Alexander.

The research aims to rigorously evaluate the assumption of constant failure rates in storm surge barriers, an especially salient issue given the Netherlands' heightened susceptibility to flood events. Although the findings are not definitive, they introduce pivotal questions that challenge existing risk assessment methodologies. It is my aspiration that this work serves as a foundational component for subsequent research, especially by employing more comprehensive datasets to yield conclusive results.

Acknowledgment is also owed to FLEET CLEANER, who have not only facilitated my professional development but also provided an environment conducive to my thesis work during off-hours.

Lastly, I wish to convey my sincere appreciation to my family and friends, whose steadfast support has made this intellectually demanding undertaking a fulfilling journey.

# Contents

<b>1</b>	<b>Introduction</b>	<b>7</b>
<b>2</b>	<b>Current Methods, Limitations, and Literature Review on Failure Rate Assessment</b>	<b>9</b>
2.1	Current Methodologies for Analyzing Closure Reliability in Dutch Storm Surge Barriers . . . . .	9
2.2	Assumptions in PRA Methods Supporting ProBO . . . . .	10
2.3	Limitations of Current Risk Evaluation Methods for Storm Surge Barriers	11
2.4	Challenges in the Literature to Constant Failure Rates . . . . .	12
<b>3</b>	<b>Data Sources, Processing and Storage for Failure Rate Assessment.</b>	<b>15</b>
3.1	Background . . . . .	15
3.1.1	Use of Empirical Data . . . . .	15
3.1.2	Justification for a Data-Centric Approach . . . . .	15
3.2	Raw Data Description . . . . .	15
3.2.1	Raw Data Sources . . . . .	15
3.2.2	Maintenance Groups . . . . .	16
3.2.3	Type-Codes . . . . .	17
3.2.4	Relations Between Type Codes and Maintenance Groups . . . . .	18
3.2.5	Objects . . . . .	19
3.2.6	Malfunctions . . . . .	19
3.2.7	Missing Data . . . . .	20
3.2.8	Data Consistency . . . . .	21
3.3	Data Preprocessing and Database Construction . . . . .	22
3.3.1	Preprocessing Data . . . . .	22
3.3.2	Constructing the Database . . . . .	23
3.3.3	Structuring Tables . . . . .	23
3.3.4	Visualising the Database . . . . .	23
3.4	Constructed Component Database . . . . .	24
3.5	Availability of Data for Assessing Constant Failure Rates . . . . .	26
<b>4</b>	<b>Statistical Framework for Failure Rate Assessment</b>	<b>29</b>
4.1	Background and Rationale for Enhanced Reliability Analysis . . . . .	29
4.1.1	Current Approaches in Reliability Analysis . . . . .	29
4.1.2	Identification of Research Gap . . . . .	30
4.1.3	Proposed Framework for Addressing Research Gap . . . . .	30
4.1.4	Rationale for Model Selection . . . . .	30
4.1.5	Framework Implementation and Validation Details . . . . .	30
4.2	Statistical Assessment Framework . . . . .	30
4.2.1	Data Characteristics . . . . .	30
4.2.2	Statistical Foundation . . . . .	31
4.2.3	Likelihood Functions for Censored Data . . . . .	33
4.2.4	Numerical Parameter Fitters: Newton-Raphson Method . . . . .	38

4.2.5	Assessing Models . . . . .	39
4.3	User Interface and Database . . . . .	42
4.4	Summary . . . . .	43
<b>5</b>	<b>Assessment of Component Failure Rates via Statistical Framework</b>	<b>45</b>
5.1	Background . . . . .	45
5.2	Method . . . . .	46
5.2.1	Data Preparation . . . . .	47
5.2.2	Model Fitting . . . . .	47
5.2.3	Model Assessment . . . . .	48
5.2.4	Assumptions and Limitations . . . . .	49
5.3	Results . . . . .	50
5.3.1	Failure Scenarios and Object Lifetimes . . . . .	50
5.3.2	Model Fits . . . . .	52
5.3.3	Graphical Assessment of Model Fits . . . . .	55
5.4	Summary . . . . .	63
5.4.1	Implications . . . . .	64
5.4.2	Recommendations for Future Research . . . . .	64
<b>6</b>	<b>Discussion and Conclusion</b>	<b>66</b>
6.1	Discussion . . . . .	66
6.2	Conclusion . . . . .	67
6.3	Contributions . . . . .	67
6.4	Recommendations . . . . .	68
6.4.1	Future Research Strategies . . . . .	68
<b>A</b>	<b>Maintenance Groups SVKO</b>	<b>73</b>
<b>B</b>	<b>Type-codes SVKO</b>	<b>78</b>
<b>C</b>	<b>Unified Modeling Language</b>	<b>81</b>
<b>D</b>	<b>Type-codes: Detailed Breakdown</b>	<b>82</b>
<b>E</b>	<b>Hessian Matrix</b>	<b>84</b>
<b>F</b>	<b>Validation Simplified Bootstrap Method</b>	<b>85</b>
<b>G</b>	<b>Detailed Description of Python Packages</b>	<b>88</b>
G.1	Pandas . . . . .	88
G.2	FastAPI . . . . .	88
G.3	SQLAlchemy . . . . .	88
G.4	Python-DotEnv . . . . .	88
G.5	Uvicorn . . . . .	88
G.6	NumPy . . . . .	88
G.7	Psycpg2 . . . . .	88

G.8 Reliability . . . . .	89
G.9 Alembic . . . . .	89
G.10 Surpyval . . . . .	89
<b>H Plots of Failure Scenarios</b>	<b>90</b>
H.1 Failure Scenario - LBDIM . . . . .	90
H.2 Failure Scenario - LBDINM . . . . .	91
H.3 Failure Scenario - LBGC . . . . .	92
H.4 Failure Scenario - LBKLO . . . . .	93
H.5 Failure Scenario - LBPRC . . . . .	94
H.6 Failure Scenario - LBPRNI . . . . .	95
H.7 Failure Scenario - LBQENM . . . . .	96
H.8 Failure Scenario - LBREL . . . . .	97
H.9 Failure Scenario - LBSWAM . . . . .	98
H.10 Failure Scenario - LBSWB . . . . .	99
H.11 Failure Scenario - LEDGSN . . . . .	100
H.12 Failure Scenario - LEDSSN . . . . .	101
H.13 Failure Scenario - LERA38 . . . . .	102
H.14 Failure Scenario - LEVSSN . . . . .	103
H.15 Failure Scenario - LESS . . . . .	104
H.16 Failure Scenario - LHGR . . . . .	105
H.17 Failure Scenario - LHSV T . . . . .	106
<b>I Comparative Analysis of Failure Scenarios Based on Model Fits</b>	<b>107</b>
<b>J Data Types</b>	<b>109</b>
<b>K Closure Data Analysis</b>	<b>110</b>
K.1 Literature Review . . . . .	110
K.1.1 Challenges in Failure Data Analysis . . . . .	110
K.1.2 Review of Data-Driven Methods . . . . .	110
K.1.3 Methodological Implications for This Thesis . . . . .	111
K.2 Methodology . . . . .	111
K.2.1 Methodology Framework . . . . .	111
K.2.2 Rule of Three and Closure Reliability . . . . .	112
K.2.3 Bayesian Analysis in the Context of Storm Surge Barrier Closures	112
K.2.4 Combining Different Closure Types for Enhanced Data Analysis	114
K.2.5 Comparative Analysis and Evaluation of Conservatism . . . . .	115
K.2.6 Assumptions, Limitations, and Evaluation of Methods . . . . .	115
K.3 Results . . . . .	116
K.3.1 Observed Closure Data . . . . .	116
K.3.2 Rule of Three Analysis . . . . .	117
K.3.3 Bayesian Analysis . . . . .	119
K.4 Discussion . . . . .	121
K.4.1 Reflecting on Data . . . . .	121

K.4.2	Reflecting on the Limitations . . . . .	121
K.4.3	Reflecting on the Results . . . . .	122
<b>L</b>	<b>Bayesian Inference for Parameter Estimation</b>	<b>123</b>
<b>M</b>	<b>Rule of three</b>	<b>124</b>
<b>N</b>	<b>Proof of Beta-Binomial Conjugacy</b>	<b>125</b>
<b>O</b>	<b>Storm Surge Barrier Closure Database</b>	<b>126</b>
<b>P</b>	<b>Overview of the Oosterscheldekering</b>	<b>128</b>
<b>Q</b>	<b>Overview of the Hollandsche IJsselkering</b>	<b>130</b>
<b>R</b>	<b>Overview of the Maeslantkering</b>	<b>131</b>
<b>S</b>	<b>Overview of the Hartelkering</b>	<b>132</b>
<b>T</b>	<b>Individual Double Degree Thesis Division</b>	<b>133</b>

# 1 Introduction

The Netherlands is uniquely vulnerable to flooding due to its low-lying geography, with nearly half of its landmass situated below sea level [20]. This geographical challenge has led to the development of specialized flood defense systems. Among these, storm surge barriers hold a pivotal role. These barriers, which were introduced following the catastrophic 1953 flood in the province of Zeeland as part of the Deltaplan [21], are designed to be both flexible and robust. They remain open to allow for the regular flow of water and maritime navigation but can be closed promptly when a storm surge poses a flooding risk.

The reliability of these closures is critical for the effectiveness of storm surge barriers. For instance, a study on the Hollandsche IJsselkering (HIJK) demonstrated that the expected water levels behind the barrier are significantly influenced by the reliability of its closure [26]. A reliable closure reduces the expected water level and thereby the risk of flooding. Conversely, if the barrier is less reliable, the flood risk increases.

The Probabilistic Operation, and Maintenance (ProBO) framework is essential for maintaining closure reliability in storm surge barriers [2]. Initially developed for the Maeslant barrier, the ProBO method employs rigorous risk analysis techniques, borrowing from high-safety sectors like nuclear power [12]. This approach relies on detailed risk models that utilize fault or event trees, and incorporate various failure data such as human errors, software issues, component defects, and external events like lightning strikes [31]. A key principle in the implementation of ProBO at storm surge barriers is the assumption of component failure rates remain constant over time, provided that regular preventive maintenance is conducted [2, 32].

The risk analysis methodology supporting ProBo exhibits limitations in its approach to estimating failure rates of storm surge barriers [31]. Specifically, while it employs Bayesian updates to fine-tune failure rate estimates, it holds the assumption that component failure rates are constant in time. This static assumption tends to overlook potential variations in component failure rates. If these rates increase, the closure reliability of the barrier decreases. Neglect of the dynamic nature of these rates could lead to underestimation of expected water levels behind the barrier. Conversely, a reduction in failure rates may result in overly conservative reliability estimates. Therefore, examining the potential variation in component failure rates over time is a crucial area of research for enhancing flood risk management practices.

The central research question of this thesis is: Is the assumption of constant failure rates in time for storm surge barriers valid?

To address this question, the thesis will explore:

1. Does existing literature challenge the assumption of time-constant failure rates in storm surge barriers?
2. Is there empirical data that can be used to assess variations in storm surge barrier

failure rates over time?

3. How can statistical methods be applied to this data to evaluate the assumption of constant failure rates?
4. Does a time-variable failure rate model provide a statistically better fit to the existing data than a constant rate model?

### **Chapter 2: Literature Review on ProBO Method and Dynamic Reliability**

This chapter starts with an introduction to the ProBO methodology as it is currently applied to assess the reliability of storm surge barriers. It then identifies and discusses any shortcomings in this methodology, particularly focusing on whether it assumes constant failure rates. The chapter ends by reviewing evidence in the literature that suggests the possibility of time-varying failure rates. This structured approach aims to answer the first research sub-question.

### **Chapter 3: Data Description and Pre-processing**

This chapter is dedicated to addressing the second research sub-question. It begins by describing the dataset used in the thesis: its source, types of data, and characteristics. The chapter then details the steps taken to prepare and pre-process this data, including any cleaning, transformation, or coding required. Lastly, it discusses how the prepared data is structured to be suitable for the subsequent statistical analysis.

### **Chapter 4: Development of Statistical Framework for Failure Rate Assumptions**

This chapter addresses the third research sub-question by establishing the statistical methods and framework for evaluating failure rate assumptions. The chapter details the criteria for selecting appropriate statistical models and introduces the goodness-of-fit metrics that will be used for model evaluation.

### **Chapter 5: Empirical Evaluation of Failure Rate Assumptions**

Building upon the framework developed in Chapter 4, this chapter addresses the fourth research sub-question. It begins with the application of two distinct models to the available data: one model assumes constant failure rates, while the other allows for variability. The chapter concludes by employing the previously introduced goodness-of-fit metrics to compare the fit of these two models. The results are then discussed to determine whether a time-variable failure rate model provides a statistically superior fit to the data.

### **Chapter 6: Discussion, Conclusion, Contribution and Recommendations**

In the final chapter, findings from earlier chapters are synthesised to address the key research question: Does a time-variable failure rate model provide a statistically better fit to the existing data than a constant rate model? This chapter offers a discussion, the conclusion, contributions, the recommendations, and proposed future research.

## 2 Current Methods, Limitations, and Literature Review on Failure Rate Assessment

In this chapter, the current methods to assess the closure reliability of storm surge barriers are discussed. First, an overview of the current approach is provided. Second, the limitations of this approach are discussed.

### 2.1 Current Methodologies for Analyzing Closure Reliability in Dutch Storm Surge Barriers

The risk models employed in ProBO are grounded in Performance-based Risk Analysis (PRA) methodologies. The PRA methodology can be applied to ensure that Dutch storm surge barriers meet the essential criteria for Reliability, Availability, Maintainability, and Safety (RAMS) [19]. The PRA is a detailed analytical method involving techniques such as fault trees to pinpoint risks affecting barrier reliability [2]. For critical infrastructure like storm surge barriers, the PRA offers a quantitative assessment of reliability, resulting in a conservative performance evaluation [2, 19].

The initial step in evaluating the closure reliability of a storm surge barrier is setting a failure rate requirement, serving as a benchmark for reliability assessments [19]. For example, the Maeslant Barrier is mandated by Dutch Water Law to at least have a failure probability of 1 in 100 for each individual closure operation [1]. Subsequently, a functional and system analysis is conducted to map the system and identify the essential subsystems required for its intended operation [31]. This analysis includes factors like external events, human actions, and hardware and software components that may affect performance [19].

In the evaluation of storm surge barrier reliability, qualitative risk analysis serves to pinpoint failure modes and assess their consequences [19]. A failure mode is a specific way in which the system can fail; for example, a hardware malfunction that prevents the barrier from fully closing and allows water to pass through. Tools like Failure Mode and Effect Analysis (FMEA) provide a detailed breakdown, extending to individual mechanical and software components [31]. The SVKO case underscores this granularity by identifying failure modes associated with solenoids.

For a more nuanced risk assessment, fault tree analysis (FTA) is employed [19]. FTA delineates the combinations of failure modes, such as hardware malfunctions, that can culminate in a closure failure. Additionally, FTA offers quantification of the primary failure event [31], thus serving as a multi-faceted risk assessment tool.

Building on the qualitative risk analysis, quantitative risk models like fault trees are used to determine likelihood of a storm surge barrier failing to close [31]. Figure 1 presents an example of a fault tree quantitative risk model for the failure to close of a storm surge barrier. These types of quantitative models incorporate failure probabilities of components or events, and use Boolean algebra to calculate the probability of

the primary failure event. The sources for the failure probabilities used in the quantitative analysis can include performance statistics from manufacturers or component reliability databases. When existing data are not sufficient, expert estimates are used to complete the analysis [31].

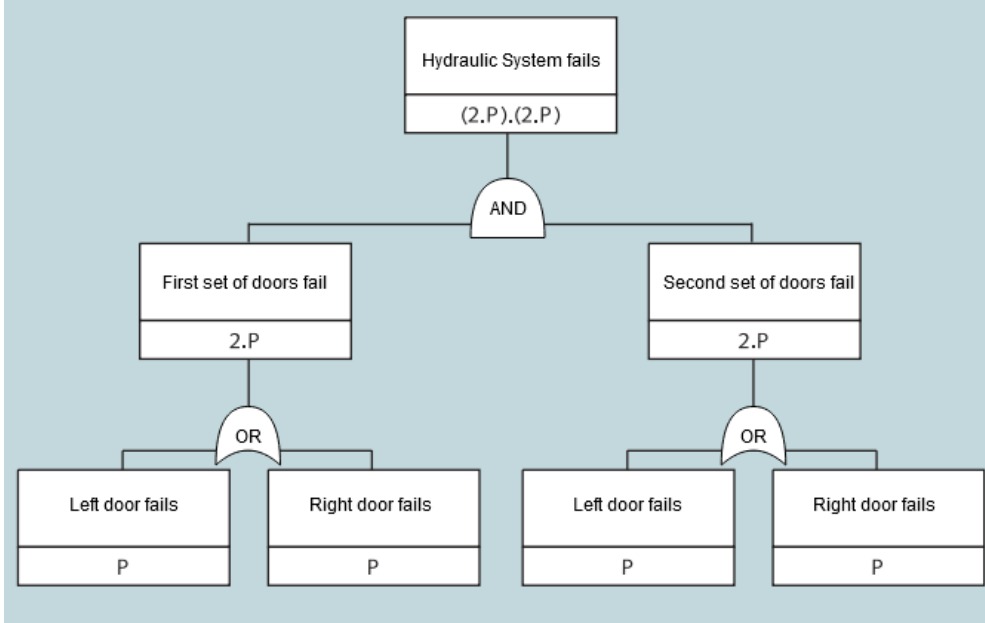


**Figure 1:** Fault tree depicting the failure to close of a hydraulic system consisting of two sets of doors. The failure modes that could result in the failure of the system are both the first and second set of doors failing. A set of doors fails when one of the doors fails. The failure probability is presented by  $P$ . Since the failure of one door has probability  $P$ , the failure probability of a set of doors is  $2P$ . The system only fails if both sets of doors fail, with each set of doors having a probability of  $2P$ , the overall failure probability of the system is  $4P^2$  [31]

## 2.2 Assumptions in PRA Methods Supporting ProBO

The implementation PRA methods that support ProBO relies on specific key assumptions. These assumptions serve to simplify the some of the reliability behavior of storm surge barrier components, reducing the complexity of the risk analysis as this behavior, such as aging, does not have to be accounted for.

The first key assumption deals with the condition of a component after maintenance. It is assumed that a component is “as good as new” after repair or replacement [19]. Operators of storm surge barriers commonly adopt this assumption in their analyses.

The second key assumption states that the failure rates of components remain con-

stant over time, provided that a preventive maintenance (PM) strategy is followed [19]. Generally, mechanical components exhibit failure rates that follow a bathtub curve, as illustrated in Figure 2. In this curve, failure rates are initially elevated due to nascent faults, commonly referred to as the "child-disease" phase. These rates subsequently stabilize after the initial faults are addressed and later escalate owing to long-term degradation. A PM strategy aims to preemptively replace components before they enter the wear-out phase. The adoption of a PM strategy is standard practice among operators, thereby justifying the assumption of constant failure rates when modeling the reliability of a storm surge barrier.

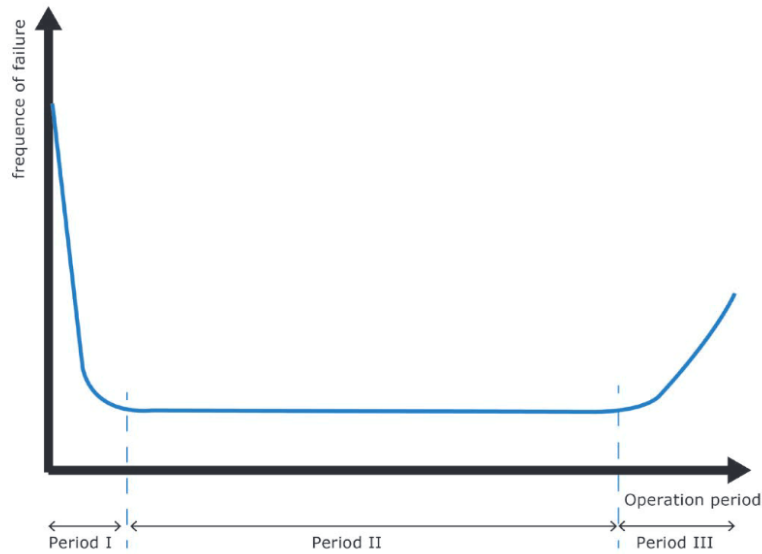


**Figure 2:** Bathtub curve depicting the three key phases of component failure rates over time [19].

During the operational phase of a storm surge barrier, adjustments to initial failure rate estimates are possible. Using operational data, and Bayesian updating methods, the initial risk estimates can be revised [19]. After a revision, the failure rates are once again assumed to be constant, in line with the second key assumption.

### 2.3 Limitations of Current Risk Evaluation Methods for Storm Surge Barriers

The risk analysis methodologies used to support ProBO, contain limitations that can affect the reliability assessments of these barriers. One such limitation is the inherent conservatism in the model [2, 19]. This conservatism can be exacerbated when all system redundancies are mapped in great detail [2]. Additionally, the conservatism

may be further intensified by conservatively estimated model parameters [2]. One specific model parameter contributing to this conservatism is the assumption that component failure rates remain constant over time. This assumption is at odds with the potentially dynamic nature of storm surge barriers, which can be affected by various factors including maintenance, repairs, upgrades, and aging.

In actuality, complex repairable systems like storm surge barriers often exhibit failure rates that are not constant but dynamic [18, 22, 28, 29]. These dynamic failure rates can be influenced by various factors such as maintenance, repairs, upgrades, and aging. Although the risk analysis methodologies supporting ProBO typically assume that maintenance and repairs restore components to their “as-new” state, this assumption may not always hold true. Incremental modifications, repairs, and updates can either extend or reduce the original lifespans of individual components, thereby influencing the overall system reliability.

## 2.4 Challenges in the Literature to Constant Failure Rates

In storm surge barriers, the approach to component-level reliability often mirrors that used for non-repairable systems. This employs “renewal theory”, where a failed component is replaced, bringing the system back to an “as new” state. This process is called a Homogeneous Poisson Process (HPP), which assumes a constant probability of failure over any given time interval [7]. For example, if failures for a hydraulic cylinder in a storm surge barrier are assumed to follow HPP, the probability of its failure remains the same between each failure, irrespective of its operational age or recent maintenance history.

In repairable systems like storm surge barriers, components such as hydraulic cylinders are often repaired rather than replaced. To account for the varying failure probabilities of these components over time, statistical methods based on a Non-Homogeneous Poisson Process (NHPP) are more appropriate [7]. The NHPP allows for a changing failure probability, which can be influenced by several factors. For instance, the probability of failure for a hydraulic cylinder may decrease as maintenance crews become more skilled at repairs or implement effective preventive measures. Conversely, the failure probability may increase if repairs do not fully restore the component to its original “as new” condition. Therefore, methods that incorporate NHPP are more adept at capturing the dynamic nature of failure rates in repairable systems. This is especially pertinent for components such as hydraulic cylinders, which are more likely to undergo repair rather than replacement. As maintenance and repair methodologies evolve, NHPP-based methods offer a more accurate representation of the changing failure rates.

Building on the relevance of models that account for variable failure rates, a study focused on aircraft engines further substantiates their applicability [33]. Like storm surge barriers, aircraft engines are complex systems that are repairable and subject to rigorous safety standards. This makes them a pertinent comparison in terms of system complexity, maintenance protocols, and reliability criteria. The study employed

a Weibull model to analyze aircraft engine data and found that it could precisely forecast the time before an overhaul was required. Moreover, the study confirmed that the failure rate of these engines is not constant but varies over time [33]. This evidence strengthens the argument for adopting models that account for variable failure rates in the reliability assessments of storm surge barriers.

Much like the approach taken for storm surge barriers, the nuclear industry also frequently employs models that assume constant failure rates for components in their system reliability assessments [23, 31]. Both types of infrastructure—nuclear power plants and storm surge barriers—are critical and have stringent safety requirements, making them comparable in the context of reliability modeling. A study in the nuclear industry challenged this assumption, revealing that failure rates can indeed vary over time, often due to system updates and improvements [23]. Models that account for variable failure rates, such as Weibull, are found useful in capturing these variations. Beyond their descriptive capabilities, these models also offer actionable insights for maintenance strategies. They can evaluate the economic benefits of changing a maintenance approach and identify shifts in failure trends—insights valuable for both general monitoring and long-term life cycle management.

The utility of models that account for variable failure rates extends beyond merely describing failure rates; they can also serve as a guide for optimizing maintenance policies for storm surge barriers [23, 33]. By capturing the variable nature of component failure rates, these models can inform more adaptive and cost-effective maintenance strategies. The adaptability of these models allows for the prediction of failures, which is crucial for planning maintenance activities. For instance, if the model indicates a decreasing failure rate due to improved repair procedures, maintenance intervals could be extended, leading to cost savings. Conversely, if the failure rate is increasing, more frequent inspections could be scheduled to mitigate risks [23, 33]. This adaptability in maintenance planning not only enhances the reliability but also potentially extends the lifespan of critical components within the barrier. A side note is that both studies suffered from a lack of data, mainly due to the scarcity of actual failures [23, 33].

The traditional “bathtub curve” often used to describe failure rates may not be fully applicable to repairable systems like storm surge barriers [18]. If the system undergoes continuous repairs or improvements, the failure rate could deviate from this curve, especially in the continuous and wear-out phases. This deviation underscores the limitations of using constant failure rates and highlights the need for more dynamic models [6].

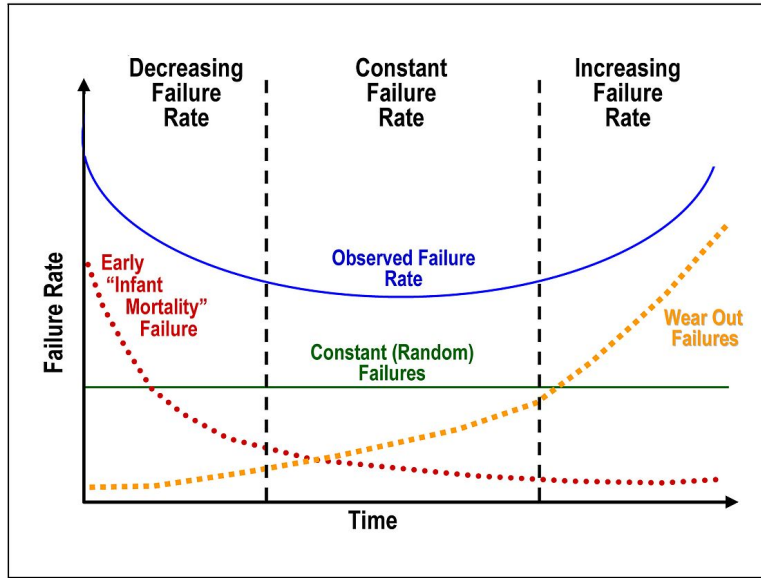


**Figure 3:** Example of the bathtub curve illustrating the dynamic nature of failure rates [6].

In summary, the research sub-question: “Does existing literature challenge the assumption of time-constant failure rates in storm surge barriers?” is affirmatively answered. Studies from related fields such as the nuclear industry and aircraft engine maintenance support this claim. Models that provide a more nuanced understanding of variable component failure rates challenge the assumption of time-constant failure rates. This evidence contributes to the broader inquiry posed by the main research question: “Is the assumption of constant failure rates in time for storm surge barriers valid?” Given the findings presented, there is a compelling case for re-evaluating this assumption in the reliability assessments of storm surge barriers.

## 3 Data Sources, Processing and Storage for Failure Rate Assessment.

This chapter details the data used to study component failure rates in storm surge barriers. The primary data for this analysis is SVKO component malfunction data, supplied by the operator of the SVKO. To handle this data efficiently, it is stored in a database developed using the PostgreSQL language.

### 3.1 Background

To evaluate storm surge barrier component failure rates, relying on empirical data from real-world observations can be informative. This approach provides an avenue to scrutinize the widely accepted assumption of constant failure rates. Analyzing actual component behaviors over time can provide insight into changing reliability. Consequently, this nuanced understanding may provide insights into the system's evolving reliability.

#### 3.1.1 Use of Empirical Data

Empirical data has been used in various sectors to question and refine assumptions about variations in component failure rates over time. In the nuclear sector, time-to-failure data serves as a basis for such evaluations [23]. The aviation industry, especially in aircraft engine maintenance, turns to time-to-removal data to gain similar insights [33]. In case of storm surge barriers, empirical data detailing the total lifetime and observed malfunctions have been used. Researchers have coupled this data with Bayesian methods to update existing failure rates [4, 8].

#### 3.1.2 Justification for a Data-Centric Approach

Relying on empirical data, akin to the methodologies adopted in the nuclear and aviation sectors, ensures a grounded and realistic approach to analysis. A data-driven methodology facilitates objective evaluations based on actual observations, which in turn increases the credibility and realism of the conclusions drawn.

### 3.2 Raw Data Description

This subsection presents a comprehensive description of the raw data for SVKO components, along with the methods employed for data processing and analysis.

#### 3.2.1 Raw Data Sources

Two primary sources contribute to the raw data for SVKO components: the RWS Bayesian Update BMS (RBU) Excel sheet and the Data Update 2016 Faalkansanalyse Stormvloedkering Oosterschelde (DU16) report. These documents contain malfunction data collected between May 10, 2010, and June 30, 2016, originating from the BMS+

maintenance and management software [8]. In these sources, 1501 malfunctions, 554 maintenance groups and 611 Type Codes are reported.

While the SVKO has been operational for 37 years, the data covers approximately 6 years. This leaves an estimated 31 years of operational history without observed malfunction data. Given the limited timeframe of the data, the 1501 malfunctions recorded are likely only a fraction of the total malfunctions that have occurred since the SVKO became operational in 1986. Figure 4 shows that the sources used in this study only cover roughly 16% of the total operational time.

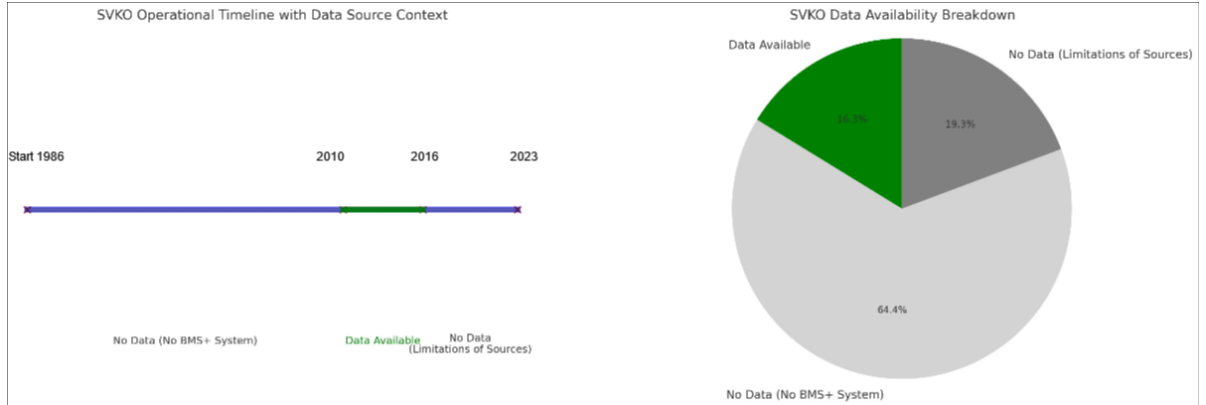


**Figure 4:** Illustration of the period for which observations on malfunctions are available for this research compared to the total operational time.

### 3.2.2 Maintenance Groups

RBU lists 554 maintenance groups, each distinguished by unique codes and descriptions. Although DU16 does not provide an explicit definition, it is inferred that a maintenance group includes components with similar functionalities or types and, therefore, similar maintenance needs. For instance, cylinders are grouped under the code H-ZC, and motor-controlled switches are classified as E-VM. Among these 554 maintenance groups, only 92 are included in the failure analysis. These 92 groups are specifically relevant to the storm surge barrier's closure reliability. The remainder are excluded as they are not included in the failure model of the SVKO [8]. A comprehensive list of these 92 maintenance groups can be found in Appendix A.

For each of these 92 groups, data are collected on total failures, failures relevant to closure, and the number of operational components. As an example of a failure that does not impact the closure, the B-GC group experienced a deviation in the value measured and that returned by the sensor, which was determined to have no effect on the closure performance [8]. The "total components" figure is inferred to represent the number of operational components within each group. This inference is based on

a calculated total observed time, which, when divided by the number of components, consistently results in 53,616 hours, the number of hours between start and end time of the observation period.

**Table 1:** Sample of Maintenance Groups records [8].

Code	Description	Total Failures	Relevant Failures	Total Components
B-DI	Digital input module	7	6	1786
B-GC	Graycode-giver	12	9	372

Table 1 shows the "Graycode-giver" (B-GC) has 12 total failures, 9 relevant to closure, among 372 components in the maintenance group that are in operation at any given time. Similarly, the "Digital input module" (B-DI) group shows 7 total failures, 6 of which are relevant to closure, with a total of 1786 operational components.

### 3.2.3 Type-Codes

RBU includes 611 Type-codes that represent various failure modes. Although DU16 does not explicitly define what a Type-code is, it can be inferred that a Type-code describes a specific failure mode often linked to a particular type of component and the nature of its failure. For example, the Type-code "LEDGSN" is described as "Diesel generator does not start". Failure modes can vary in their clarity; for instance, the Type-code "LBDOM" is ambiguously described as "Output Module Detectable".

Out of the 611 Type-codes, 88 are directly associated with the maintenance groups included in the failure model. Table 2, showing a sample of records, demonstrates that the Type-code "BDIM" refers to a noticeable failure in the Digital Input Module, falling under the B-DI maintenance group, which has 1786 components operational at any given moment. Similarly, the Type-code "LBGC" indicates a malfunction in the Graycode-giver, associated with the B-GC maintenance group, comprising 372 operational components. An overview of all the Type-codes can be found in Appendix B

**Table 2:** Sample of selected records for Type Codes [8].

Code	Description	Maintenance Groups	Code Maintenance Group	Components in Group
LBDIM	Noticeable Digital Input Module Failure	Digital Input Module Control OSK	B-DI	1786
LBDINM	Unnoticeable Digital Input Module Failure	Digital Input Module Control OSK	B-DI	1786
LBGC	R14 Graycode-giver 1 North Not Functioning	Graycode-giver	B-GC	372

Table 2 demonstrates that the Type-code “LBDIM” refers to a noticeable failure in the Digital Input Module, falling under the B-DI maintenance group, which consists of 1786 operational components. Similarly, the Type-code “LBGC” indicates a malfunction in the Graycode-giver, associated with the B-GC maintenance group, comprising 372 operational components.

### 3.2.4 Relations Between Type Codes and Maintenance Groups

In the dataset, a multifaceted relationship exists between type codes and maintenance groups. A single Type-code can correspond to one or multiple maintenance groups, and inversely, a single maintenance group can be linked to one or various type codes [8].

Firstly, a single type code may relate to multiple maintenance groups in two ways:

1. Failure modes of components that result in the malfunction of a larger system or machine, like a diesel generator, are unified under a single type code. For such instances, the study perceives the machine as a singular unit with one Type-code ‘Diesel-generator does not start’ [8].
2. A type code can represent components that perform similar functions across different maintenance groups. For instance, switches of varying voltage levels but with identical functions might be grouped under one Type-code ‘Does not switch’. In this scenario, the study aggregates the total number of components across these maintenance groups [8], so the number of components associated with the Type-code is the total sum of all components in the maintenance groups.

Secondly, a single maintenance group can be associated with multiple type codes, indicating various failure modes for components within that group. Each observed malfunction of interest is then assigned its appropriate type code, as reflected in the raw data [8]. For concrete examples, refer to Table 3. The type code “LHSV T” is associated with different maintenance groups, demonstrating that a single failure mode can be relevant for multiple types of machinery. Similarly, the maintenance group H-SV5 has two Type-codes, LHSV T and LHOV.

**Table 3:** Example of Type Codes and Corresponding Maintenance Groups [8].

Type-code	Description	Maintenance Group (Code and Description)
LHSVT	Solenoid 4/3 control valve 15 does not open	H-SV5 (Solenoid Valve POS15)
LHOV	Hydraulically-controlled valve 15 does not open	H-SV5 (Solenoid Valve POS15)
LHSVT	Solenoid 4/2 slide valve 38 does not open	H-SV8 (Solenoid Valve POS38)
LHSVT	Solenoid 4/2 slide valve 17 does not close	H-SV7 (Solenoid Valve POS17)
LHSVT	Solenoid 4/2 slide valve 38 does not close	H-SV8 (Solenoid Valve POS38)

### 3.2.5 Objects

In the excel a list of objects is included. An "object" specifically means a component in use at a designated location. Each object is assigned a unique object code and description. Special characters in object codes, such as asterisks or slashes, are removed for the sake of data processing simplicity.

Table 4 shows examples of such objects. Note that all objects in the table are part of the same maintenance group 'B-DI'. This implies that these objects have similar operational roles and are managed under the same set of maintenance protocols.

**Table 4:** Example of Objects and Their Attributes [8].

Object Name	Description	Maintenance Group
=H01+26:LC1-EDI.1.U0119	Digital Input	B-DI
=H01+26:LC1-EDI.2.U0129	Digital Input	B-DI
=H01+26:LC1-EDI.3.U0139	Digital Input	B-DI

### 3.2.6 Malfunctions

The study documents 1501 malfunctions recorded between 20 May 2010 and 30 June 2016. It categorizes these into malfunctions that are critical and non-critical to the closure reliability of the SVKO storm surge barrier [8]. Specifically, 308 malfunctions are related to 92 maintenance groups that affect closure reliability. 87 of these 308 malfunctions are identified as having a direct impact on the closure reliability of the SVKO [8]. Each record in the malfunction data is initially allocated to a maintenance

group; this allocation can be updated [8]. The 87 malfunctions identified as directly impacting the closure reliability are also associated with 17 unique Type-Codes.

Table 5 provides a concise view of selected malfunction records. It includes the initial and updated maintenance groups, object code, malfunction number, date and time of occurrence, detectability, and Type-code. For example, the first record in the table indicates a malfunction initially assigned to the B-PM-T maintenance group and later updated to B-DI, marked as detectable. Conversely, the third record lacks a Type-code, signifying it is not critical to the barrier’s reliability [8].

**Table 5:** Example of Partial Malfunction Records [8].

Initial Maintenance Group	Malfunction Number	Object Code	Date and Time	Detectable	Updated Maintenance Group	Type-code
B-PM-T	353514	=S14+26:LC2	3/09/2011 1:30	Yes	B-DI	LBDIm
E-DG:DB	618010	=A01+73*CBB:30- ETANK	30/09/2015 14:15	No	E-DG:DB	
B-PM-T	822387	=R21+11:GN- EU290	05/11/2010 14:23	No	B-PM-T	LBGC

The raw data for each malfunction record originally contains 37 fields. For the purpose of this study, which focuses on lifetime analysis, only select fields are included in Table 5. These selected fields comprise the initial and updated maintenance groups, object code, malfunction number, date and time of occurrence, detectability, and Type-code. The maintenance groups and Type-code are crucial for grouping malfunctions and evaluating their impact on component lifetimes. The malfunction number serves as a unique identifier for individual malfunction records. Object code is utilized to ascertain whether a specific component at the same position has experienced multiple failures. Finally, the detectability of a malfunction is essential for choosing the appropriate analysis method.

### 3.2.7 Missing Data

Several limitations are present in the available data set, particularly concerning the timing of component failures and their operational status. Failures that are undetectable during regular operation are only recorded upon SVKO testing, and the exact occurrence dates remain unspecified. A supplemental document indicates the test closure dates for the SVKO, thus providing an interval between the last successful test and the detection of the malfunction. However, neither the primary report nor the accompanying Excel sheet contain comprehensive lists of test dates.

Additional shortcomings include the absence of data on component replacement times and the resumption of normal functionality. This lack of information complicates the task of determining the specific start dates for each component within the SVKO. The data set also omits the initial operational dates of components and any failures that may have occurred prior to the observation period. This results in uncertainty regarding the start date of each component’s initial lifetime if it was already operational at the beginning of the observation period.

The number of components and failures within maintenance groups, along with the six-year duration of the observation period, allow for certain inferences about component lifetimes. For instance, the B-DI maintenance group, which includes digital input modules, reports only 7 failures among 1786 components during this period. Considering that industrial-grade input modules have documented lifetimes ranging between 15 and 20 years [15], it becomes evident that the six-year observation period may not adequately represent the potential longevity of these components.

In the context of reliability analysis, this relatively short observational period poses a risk of underestimating the system’s actual reliability. Limited data could artificially elevate observed failure rates, thus not accurately reflecting the longer-than-expected lifetimes of certain components, such as digital input modules. This mismatch has implications for interpreting failure patterns over time and may conceal trends related to component degradation or improvement.

### 3.2.8 Data Consistency

A check of data samples reveals discrepancies in the malfunctions associated with the diesel generator. The dataset shows 10 components for Type-Codes LEDGSN and LEDSSN. Closer inspection reveals 20 failures attributed to LEDGSN, involving 18 unique objects.

The discrepancies may be due to:

- Data entry errors, possibly exemplified by truncated object codes:

Possible truncated code: *A01 + 74CBB* : 30

Full intended code: *A01 + 74CBB* : 30*EG001*

- Misclassification or incomplete documentation of the operational objects.

Given the unclear attribution of the reported malfunctions to the initially documented 10 objects, we have opted to base our analysis on the 18 unique object codes that have been explicitly recorded. This choice avoids speculative allocation of failures and is thus considered more pragmatic.

Implications of an increased object count include: A diluted failure rate per object, possibly suggesting a more robust system than if a lower count were used. they could affect the reliability analysis and maintenance strategies for the diesel generators.

### 3.3 Data Preprocessing and Database Construction

This section outlines the methodology employed for the transformation and preparation of raw data, as initially presented in Section 3.2. It discusses the procedures for data cleaning, the establishment of the database structure, the maintenance of data relationships, and the methods used to provide an overview of the created database.

#### 3.3.1 Preprocessing Data

Data preprocessing comprises a series of structured steps designed to enhance data identifiability, standardization, and quality for subsequent analysis.

**Identification Enhancement:** To distinguish between Type Codes more effectively, a prefixed ID is added. For instance, “LBDIM” is converted to “1-LBDIM”.

**Character Normalization:** Special characters are removed from the dataset. For example, the string “=R31+11:GN-EU270” is simplified to “R3111GNEU270”. All text strings are also converted to uppercase, which is advantageous for data manipulation in programming languages such as Python.

**Temporal Cross-Referencing:** A search algorithm is utilized to correlate the most recent SVKO test dates, obtained from a supplementary document, with dates of malfunction detection. This serves to estimate the approximate time of failure for each component.

**Boolean Standardization:** The detectability field, initially containing various spellings of ‘Yes’ and ‘No’, is standardized to Boolean values of ‘True’ or ‘False’.

**Lifetime Dataset Initialization:** The dataset accounting for component lifetimes is initialized on May 20, 2010. If a component experiences a malfunction, the period from May 20, 2010, to the malfunction date is recorded as one lifetime. A new lifetime commences from this malfunction date, extending either to the next malfunction or to the observation period’s end date, June 30, 2016. As an illustrative example, consider Type-code LBGC, which consists of 372 operational objects. Of these, 7 unique objects experience a total of 9 malfunctions. Initially, all 372 objects have lifetimes that begin on May 20, 2010. Among them, 365 continue without malfunction until the end of the observation period. For the 7 malfunctioning objects, an additional 16 lifetimes are generated due to the 9 malfunctions, making the total 381 lifetimes for LBGC.

**Censoring Types:** If a component remains functional at the observation period’s conclusion on June 30, 2016, its lifetime is termed “censored” [16]. This implies that the object has been operational until the end of the observation period, but its future lifespan remains uncertain. Additional types of censoring are recognized, such as “interval censoring,” where the exact time of malfunction is not known. In such cases, the interval between the last successful test and the detection of malfunction is recorded. Lifetimes are categorized based on their type of censoring, a crucial factor for subsequent statistical analyses, as elaborated in Chapter 4.

This approach to data preprocessing ensures that the dataset is in a suitable format for the comprehensive statistical analyses that follow.

### **3.3.2 Constructing the Database**

The component data are organized in a structured database managed using PostgreSQL, an open-source object-relational database management system. PostgreSQL is chosen for its capacity to manage large datasets and execute intricate queries. The database consists of multiple tables, each housing records of distinct data points related to components. Every record in these tables is assigned an internal database ID, serving multiple purposes:

1. Identifies and groups related records
2. Defines explicit relationships between records in different tables

The construction of the database involves the following steps:

1. Gather relevant component data from the SVKO report [8].
2. Create a database schema that specifies the structure of tables and the relationships between them.
3. Identify potential correlations between records across multiple tables.
4. Assign an internal database ID to each record for easier identification and linkage.
5. Populate the PostgreSQL database, utilizing SQL for effective data management.

### **3.3.3 Structuring Tables**

Tables in the database are designed with specific columns, data types, and attributes to meet the study's requirements. For example, a component database might include columns for component type and failure mode, with data type specified as "Text". Data integrity is maintained using constraints like primary keys (PK) and foreign keys (FK). The table structure is also optimized to facilitate the types of queries expected to be executed, ensuring efficient performance.

### **3.3.4 Visualising the Database**

Unified Modeling Language (UML) diagrams are used to offer a visual representation of the database structure. These diagrams display the organization and relationships between tables and attributes, aiding in a better understanding of the component data and facilitating subsequent analysis. A more detailed description of UML can be found in appendix C.

### 3.4 Constructed Component Database

The SVKO database developed for this study consists of four main tables: the MaintenanceGroups table, the FailureTypeCode table, the FailureTypeCodeChangeHistory table, and the MalfunctionRecord table. These tables collectively store and organize data related to the operations of the storm surge barrier components.

The *Maintenance Group Table* holds all the maintenance groups of the SVKO. Each record in this table contains an ID, a maintenance group identifier, and a description of the maintenance group. Figure 5 shows the UML diagram for the Maintenance Group table.

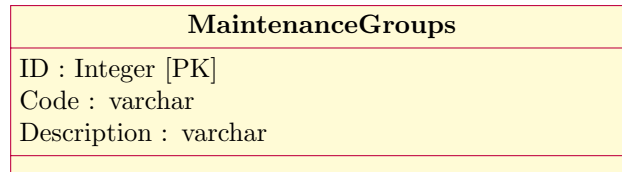


**Figure 5:** The UML diagram of the Maintenance Group table. The attributes are ID (Integer, primary key), Code (Text), and Description (Text).

The *FailureTypeCode Table* provides information on type-codes of storm surge barrier components. Each record contains an ID, a Type-code, and a description of the Type-code. Figure 6 illustrates the UML diagram for the FailureTypeCode table.

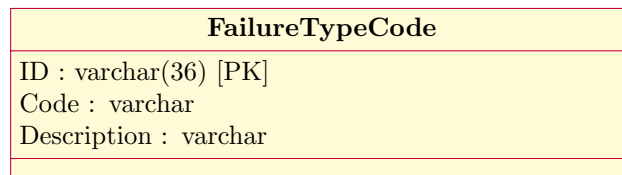


**Figure 6:** The UML diagram of the FailureTypeCode table. The attributes are ID (varchar(36), primary key), Code (varchar), and Description (varchar).

The *FailureTypeCodeChangeHistory Table* captures the historical changes in failure frequencies and the number of components associated with each Type-code. This allows for nuanced data analysis, especially when failure attributes evolve over time. Each record in this table includes an ID, a reference to the associated Type-code, the failure frequency, the number of components, and the start and end dates for the validity of this data. The UML diagram for the FailureTypeCodeChangeHistory table is shown in Figure 7.

<b>FailureTypeCodeChangeHistory</b>
ID : varchar(36) [PK]
FailureTypeCodeID : varchar(36) [FK]
FailureFrequency : float8
NumberOfComponents : int4
StartDate : date
EndDate : date

**Figure 7:** The UML diagram of the FailureTypeCodeChangeHistory table. The attributes are ID (varchar(36), primary key), FailureTypeCodeID (varchar(36), foreign key), FailureFrequency (float8), NumberOfComponents (int4), StartDate (date), and EndDate (date).

The *MalfunctionRecord Table* logs component malfunctions. It includes attributes such as the maintenance group ID, malfunction number, object code ID, a description of the malfunction, the date and time of the event, the visibility of the malfunction (observable or hidden), the associated failure type code ID, and the last test date. The UML diagram for the MalfunctionRecord table is presented in Figure 8.

<b>MalfunctionRecord</b>
ID : varchar(36) [PK]
MaintenanceGroupID : varchar(36) [FK]
MalfunctionNumber : int4
ObjectCodeID : varchar(36) [FK]
Description : varchar
EventDate : date
EventTime : time
Observable : bool
FailureTypeCodeID : varchar(36) [FK]
LastTestDate : date

**Figure 8:** UML diagram of the MalfunctionRecord table. Attributes include ID (varchar, primary key), MaintenanceGroupID (varchar, foreign key), MalfunctionNumber (int4), ObjectCodeID (varchar, foreign key), Description (varchar), EventDate (date), EventTime (time), Observable (bool), FailureTypeCodeID (varchar, foreign key), and LastTestDate (date).

Figure 9 showcases the relationships between tables in the SVKO component database. Arrows denote foreign key connections, while cardinality symbols, such as “1..” and “0..”, indicate the number of instances between tables. This diagram provides an overview of the interconnected tables, fostering efficient data analysis and management.

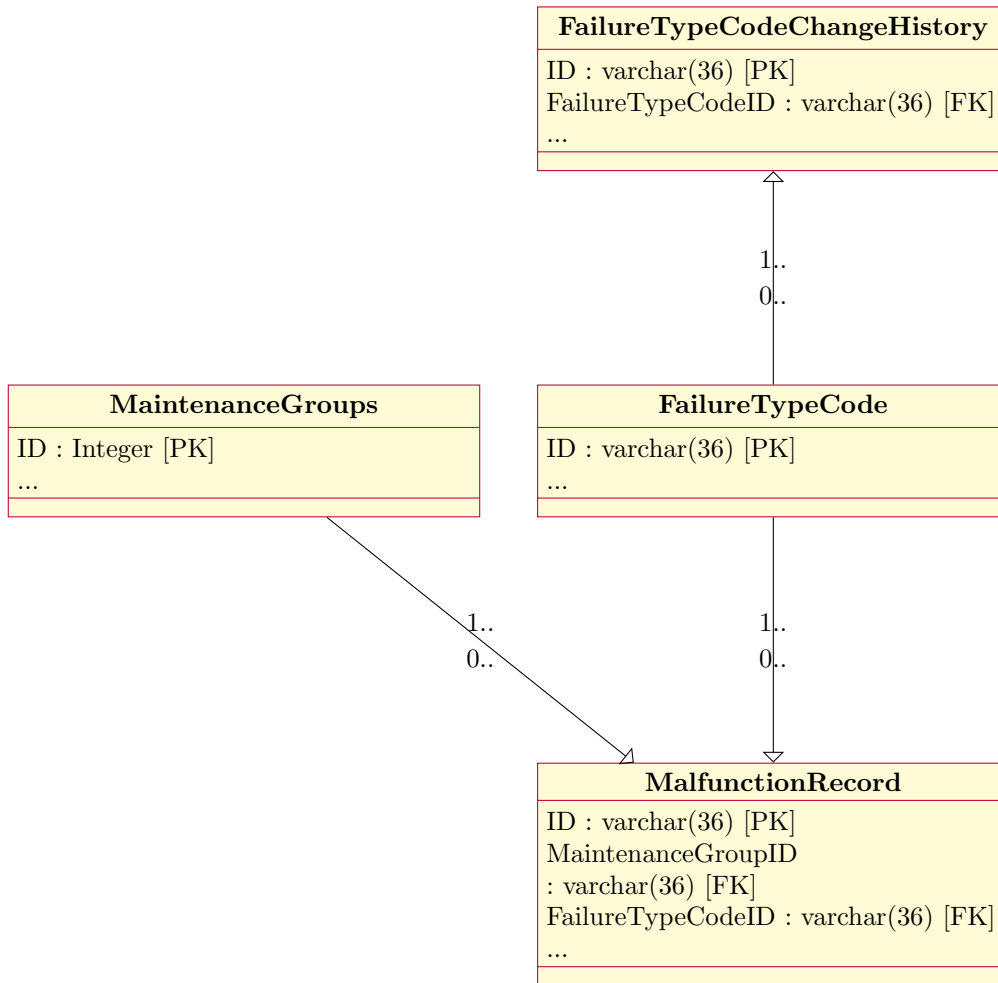


**Figure 9:** A holistic UML diagram depicting the relationships between tables in the SVKO component database. Arrows represent foreign key connections, and cardinality symbols (e.g., 1..\* and 0..) illustrate the number of instances between tables. This diagram aids in grasping the database structure and ensures efficient data analysis and management.

In summary, the SVKO database is an organized system designed for the efficient storage, retrieval, and analysis of data related to the reliability of storm surge barrier components.

### 3.5 Availability of Data for Assessing Constant Failure Rates

To address the sub-research question—“Is there empirical data available to assess variations in storm surge barrier failure rates over time?”—the data sources confirm that

such empirical data do exist. The BMS Excel sheet and the DUA16 report collectively offer malfunction data covering 6 years within the SVKO's 37-year operational span. A total of 1501 malfunctions have been documented, of which 87 malfunctions related to 17 unique Type-codes are directly pertinent to the SVKO's closure reliability. These 87 malfunctions form lifetime datasets that are suitable for fitting models. A summary of this data, organized by Type-code, can be found in Table 6. For instance, Type-code LBQENM is associated with 15 failures among 992 components, resulting in a dataset that encompasses 1007 lifetimes.

While the available data are adequate for initial analyses, it is advisable for future research to include additional data for a more comprehensive and robust assessment. This is particularly relevant given that the BMS+ system is assumed to remain operational, thereby continuing to accumulate new malfunction data.

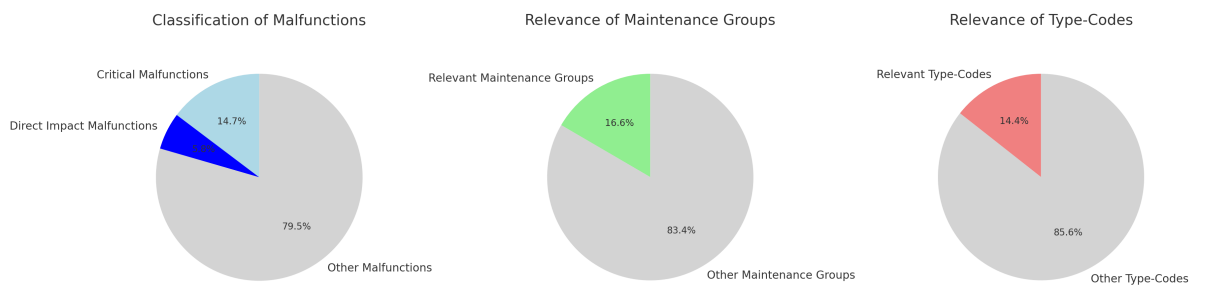


**Figure 10:** Visualization of the proportion of available data that is related to the closure failure of the SVKO storm, relative to their totals.

**Table 6:** Number of failures and number of components for each Type Code, classified by lifetime scenario. Detailed explanations of the abbreviations and column descriptions can be found in the appendix D.

Type Code	Description	Lifetime Scenario	Failures (No.)	Components (No.)	Lifetimes (No.)
1-LBDIM	Failure digital input module	Observable Failure	2	1786	1788
2-LBDINM	Failure digital input module	Unobservable Failure	4	1786	1790
3-LBGC	Bug gray code module	Unobservable Failure	9	372	381
4-LBKLO	Interruption safely closure cable	Unobservable Failure	1	3	4
5-LBPRC	Failure I-O digital module	Observable Failure	9	260	269
6-LBPRNI	Failure network interface I-O module	Observable Failure	1	260	261
7-LBQENM	Failure QE module	Unobservable Failure	15	992	1007
8-LBREL	Failure relay	Unobservable Failure	1	1240	1241
9-LBSWAM	Computer bug switch type A in mid section	Observable Failure	2	256	258
10-LBSWB	Computer bug switch type B	Observable Failure	1	256	257
11-LEDGSN	Failure start diesel generator	Unobservable Failure	20	18	38
12-LEDSSN	Failure motor controlled switch	Unobservable Failure	2	18	20
13-LERA38	Failure 380V transformer container earth leakage	Observable Failure	1	79	80
14-LEVSSN	Failure motor controlled switch of 10kV transformer	Unobservable Failure	6	42	48
15-LESS	Signal failure local computer to 10kV transformerfield	Unobservable Failure	1	17	18
16-LHGR	Function failure charging rectifier	Observable Failure	9	63	72
17-LHSV	Switching failure solenoid	Observable Failure	1	384	385

## 4 Statistical Framework for Failure Rate Assessment

This chapter addresses an unexplored question in the literature: How can statistical methods challenge the assumption of constant failure rates in storm surge barriers? While existing studies have primarily focused on updating failure rates using Bayesian methods [4,8], these works do not assess the validity of assuming constant failure rates. This chapter aims to fill this research gap by outlining statistical methods specifically designed to question this assumption. These methods will be applied to data analysis in subsequent chapters.

The study introduces a specific framework centered on empirically determining failure rates over time. This framework employs two key statistical models for analysis: the exponential and Weibull distributions. The exponential model assumes a constant failure rate and is commonly utilized in the context of storm surge barrier reliability [5]. On the other hand, the Weibull distribution accommodates variable failure rates and is favored in reliability theory [16]. The choice between these models is guided by their prevalence and versatility in existing research. Both models aim to estimate the hazard function, a key parameter in describing failure rate over time, as emphasized in statistical literature [16].

The chapter begins with a Background section to establish foundational context. Following this, it delves into the characteristics of the data that influence model selection, referencing constraints and conditions elaborated in chapter 3. The chapter then presents the mathematical foundations of the framework, which include the Nelson-Aalen estimator for deriving the empirical hazard function. It also outlines the lifetime models—Exponential and Weibull—that the study employs and provides the methodology for their application to the data. Tests devised to evaluate the appropriateness of the chosen models are discussed in the succeeding section. The chapter concludes with an overview of a code repository to facilitate future work, followed by a summary that focuses on how the methods presented address the research question.

### 4.1 Background and Rationale for Enhanced Reliability Analysis

Reliability assessment in storm surge barriers is instrumental for resource allocation and public safety. Accurate predictive models are a prerequisite for informed risk management and policy decisions. Underestimating the reliability can result in unnecessary allocation of resources. On the other hand, overestimating reliability could jeopardize the safety behind the storm surge barrier.

#### 4.1.1 Current Approaches in Reliability Analysis

As detailed in Chapter 2, current methodologies for reliability analysis predominantly employ the assumption of constant failure rates for components of storm surge barriers. This assumption is valid under the condition of regular preventive maintenance and proactive testing [2, 19].

### 4.1.2 Identification of Research Gap

The critical research gap resides in the empirical validation, or lack thereof, of the assumption of constant failure rates, specifically in the context of storm surge barriers.

### 4.1.3 Proposed Framework for Addressing Research Gap

To address this research gap, this chapter outlines a comprehensive analytical framework, to analyse the available data, which is discussed in Chapter 3. The framework incorporates two statistical lifetime models: the Exponential and Weibull distributions.

### 4.1.4 Rationale for Model Selection

The Exponential model, commonly used as a reference for constant failure rates, assumes a constant rate of failure [16]. The exponential model is also one of the models used to model component lifetimes in storm surge barriers [5]. Conversely, the Weibull distribution allows for both constant and variable failure rates [16]. Both models can be used to estimate the hazard function, a crucial metric for understanding failure rates over time [16].

### 4.1.5 Framework Implementation and Validation Details

The proposed framework will utilize statistical tools such as the Nelson-Aalen estimator to derive the empirical hazard function. To compare model performance, the Akaike Information Criterion (AIC) will be employed. Hypothesis testing methods like the Kolmogorov–Smirnov test are used to assess the fit of the models to the data. Additional validation will include visualization of the models and the data, to assist in model selection if AIC and hypothesis testing do not provide satisfactory results. A code repository will contain the implementation codes, enhancing the reproducibility and future adaptability of the study.

## 4.2 Statistical Assessment Framework

This section introduces the statistical framework that can be used to assess the constant failure rate assumption.

### 4.2.1 Data Characteristics

The characteristics of the available data, delineated in Chapter 3, influence the design and implementation of the statistical framework of this thesis.

**Failure Scenarios** For the purpose of this analysis, Type-codes are employed as the failure scenarios. This choice is motivated by two main reasons. First, the Type-codes encompass various failure modes and are instrumental for identifying and grouping malfunctions, as highlighted in Table 3 and Table 5. Second, the original study from

which this dataset is derived also uses Type-codes for updating failure rates and assessing system reliability [8]. Adopting Type-codes as failure scenarios thus not only provides a structured approach but also ensures consistency with the existing literature.

**Censoring Types and Treatment** Secondly, the data contains instances of right-censoring, interval-censoring, and left-censoring, each affecting statistical analysis [16].

**Interval and Right-Censoring** Interval censoring occurs when a failure is identified within a specific time frame rather than a distinct point in time. For instance, components under failure scenario 8-LBREL undergo periodic tests at intervals denoted as  $0 = a_0 < a_1 < \dots < a_m < \infty$ . Failure may occur within the interval  $(a_{j-1}, a_j]$  [16]. Right-censoring is observed when the data collection period terminates before all components fail, leaving incomplete failure information [16]. These forms of censoring necessitate specialized statistical methods to handle the incomplete data.

**Left-Censoring** Although the data inherently contains left-censoring, it is not considered in the analysis. This exclusion aligns with the treatment in the original study, which assumes that the lifetimes of components start at the onset of the observation period [8]. The decision not to consider left-censoring is deemed justifiable as it does not contradict the methodology employed in the original study.

**Assumptions on Operational Components** The framework presumes a constant count of operational components for each failure scenario throughout the observation period. This assumption is justified by two key factors. First, no data are available on repair or replacement times for failed components. Second, the original study implicitly maintains this constant count when calculating total observed lifetime hours [8]. This simplifies the analysis and aligns with the original study's methodology.

#### 4.2.2 Statistical Foundation

This section covers the statistical foundation and the approach to parameter estimation used in this study.

**Reliability Functions** The probability density function (pdf), denoted as  $f(t; \lambda)$ , describes the distribution of probabilities for a continuous random variable  $t$  across its possible values. In this expression,  $\lambda$  represents one or more parameters that shape this distribution.

Derived from the pdf, the cumulative distribution function (cdf) quantifies the probability that a continuous random variable  $t$  will take a value less than or equal to a specific point. It provides the cumulative probability from the lower bound of the distribution up to a given value of  $t$ .

$$F(t; \lambda) = P(T \leq t) \tag{1}$$

Building on the cdf, the reliability function, also known as the survival function, quantifies the probability that a component or system will function beyond a specified time  $T$ :

$$S(t; \lambda) = P(T > t) \quad (2)$$

The hazard function, denoted by  $h(t)$ , quantifies the instantaneous failure rate at a specific time  $t$ , conditional on the component having survived until that time. It is mathematically represented as:

$$h(t) = \frac{f(t)}{S(t)} \quad (3)$$

Subsequent to the hazard function is the cumulative hazard function  $H(t)$ , which serves as an integrative measure of risk over time. This function is calculated as the integral of the hazard function  $h(u)$  from 0 to  $t$ :

$$H(t) = \int_0^t h(u) du \quad (4)$$

The shape of  $H(t)$  offers pivotal insights into the system's reliability characteristics and is subject to detailed interpretation in reliability analyses. The function can manifest in several forms, each indicative of specific reliability behaviors:

1. **Increasing** ( $H'(t) > 0$ ): An upward trend in the cumulative hazard function signifies a failure rate greater than zero, indicative of an increasing risk over time.
  - **Linear Increase:** A linearly increasing  $H(t)$  often implies a constant failure rate and is generally modeled by the Exponential distribution [16].
  - **Non-Linear Increase:** A nonlinearly increasing  $H(t)$  suggests that the failure rate itself may be a function of time, often indicative of wear-out, aging mechanisms [16].
2. **Constant** ( $H'(t) = 0$ ): A constant or horizontal cumulative hazard function denotes  $h(t) = 0$ , which could suggest an extremely reliable system or may require further examination for data truncation or censoring issues.
3. **Decreasing** ( $H'(t) < 0$ ): A downward trend is generally not physically interpretable as it implies a negative failure rate.
4. **Complex or Mixed Shapes:** These can occur in systems with multiple contributing factors to reliability. A complex  $H(t)$  shape could emerge from a blend of "burn-in" failures, constant hazard rates, and wear-out mechanisms.

**Non-Parametric Estimation using Nelson-Aalen** In this study, the Nelson-Aalen estimator is employed for the non-parametric estimation of the cumulative hazard function. The Nelson-Aalen estimator computes the cumulative hazard function  $H(t)$  without making assumptions about a specific distribution for the data at hand [3,14]. Mathematically, it is expressed as follows:

$$H(t) = \sum_{t_i \leq t} \frac{d_i}{n_i} \quad (5)$$

In the equation,  $d_i$  signifies the number of events at time  $t_i$ , and  $n_i$  is the number at risk just before  $t_i$ . Utilizing this method has the benefit of using the observed data directly to provide an empirical estimation of the hazard function. The choice for using the Nelson-Aalen estimator is guided by its general simplicity in application and the study's specific focus on the hazard function. Additional information on Nelson-Aalen can be found in appendix F.

Note that Nelson-Aalen can only be used for complete and right censored lifetimes.

**Parametric Estimation Using Maximum Likelihood Estimation** In this study, the Maximum Likelihood Estimation (MLE) method is used to estimate the parameters for the Exponential and Weibull models. MLE assumes that the observed data conform to the specified distribution, such as Exponential or Weibull. The aim is to find the optimal parameters, such as  $\lambda$ , that maximize the likelihood of the observed data. In contrast to non-parametric methods, MLE requires an assumption about the distribution of data. This assumption enables the quantification of the likelihood of the observed data for different potential values of  $\lambda$ , or other parameters. The study opts for MLE due to its proven applicability to censored lifetime data, a common characteristic in reliability studies [16]. Mathematically, the likelihood function within the MLE framework is defined as:

$$L(\lambda) = \prod_{i=1}^n f(t_i; \lambda) \quad (6)$$

This equation measures how well the model, determined by parameters such as  $\lambda$ , fits the observed data. The primary goal is to maximise this function to identify the value of  $\lambda$  that makes the observed data most probable under the model. The form of the likelihood function can vary depending on the data characteristics—complete lifetimes, right-censored, or interval-censored.

#### 4.2.3 Likelihood Functions for Censored Data

In this section, likelihood functions for various censoring scenarios in component malfunction data are derived. These scenarios encompass both complete and right-censored lifetimes, as well as interval and right-censored lifetimes. The symbol  $\lambda$  serves as a placeholder, representing either a single parameter or a vector of parameters depending on the specific statistical distribution under study.

In failure scenarios of the SVKO where the component malfunction is observable, the data set includes both complete lifetimes and right-censored lifetimes. Specifically, for a group of size  $n$ , the lifetime  $T_i$  of a unit can exceed the censoring time  $C$ . Therefore, two scenarios are possible: either  $T_i > C$  or  $T_i \leq C$ . In the former, the lifetime is not fully observed, while in the latter, it is.

The observed lifetime  $t_i$  depends on whether it is censored or not. To distinguish between these scenarios, an indicator variable  $\delta_i$  is introduced. The variable  $t_i$  and the indicator  $\delta_i$  are defined as follows:

$$t_i = \min(T_i, C), \quad \& \quad \delta_i = I(T_i \leq C) \quad (7)$$

Both  $t_i$  and  $\delta_i$  are treated as random variables.

Given these definitions, the joint probability of observing the data points  $(t_i, \delta_i)$  is:

$$P(t_i, \delta_i) = \begin{cases} P(T_i > C), & \text{if } t_i = C, \delta_i = 0 \\ f(t_i), & \text{if } t_i = T_i, \delta_i = 1 \end{cases} \quad (8)$$

Consequently, the joint probability density function (pdf) of  $(t_i, \delta_i)$  can be expressed as [16]:

$$f(t_i; \lambda)^{\delta_i} P(T_i > C)^{1-\delta_i} \quad (9)$$

By incorporating this joint pdf into the likelihood function, the expression for right-censored data becomes:

$$L(\lambda) = \prod_{i=1}^n f(t_i; \lambda)^{\delta_i} S(t_i; \lambda)^{1-\delta_i} \quad (10)$$

Here,  $S(t_i; \lambda)$  represents the survival function, as given in equation 2.

In failure scenarios of the SVKO where the component malfunction is unobservable, the data set includes both interval-and right censoring.

In the case of interval-censoring, the lifetime  $T_i$  of a component is confined to a specific interval  $(t_{i_0}, t_{i_1}]$ . In this context,  $t_{i_0}$  and  $t_{i_1}$  denote the times at which tests were conducted. Specifically,  $t_{i_0}$  is the time of the preceding test, and  $t_{i_1}$  is the time of the following test. The probability of a unit failing within this interval is calculated as  $P(t_{i_0} < T_i \leq t_{i_1})$ , which can be expressed as:

$$P(t_{i_0} < T_i \leq t_{i_1}) = F(t_{i_1}) - F(t_{i_0}) \quad (11)$$

Thus, the likelihood function for interval-censored data can be formulated as:

$$L(\lambda) = \prod_{i=1}^n [F(t_{i_1}; \lambda) - F(t_{i_0}; \lambda)] \quad (12)$$

To accommodate both interval and right-censoring in the data, the likelihood function is modified. Specifically, if a component has not failed by the end of the observation period at time  $C$ , its lifetime is considered to fall within the interval  $(C, \infty)$ . Consequently, the probability of failure for such a component is calculated as follows:

$$F(\infty; \lambda) - F(C; \lambda) = 1 - F(C; \lambda) \quad (13)$$

$$= S(C; \lambda) \quad (14)$$

Hence, in case of interval and right censoring, the likelihood function can be expressed as:

$$L(\lambda) = \prod_{i=1}^n S(t_{i_0}; \lambda)^{\delta_{Ri}} [F(t_{i_1}; \lambda) - F(t_{i_0}; \lambda)]^{\delta_{Ii}} \quad (15)$$

with indicators  $\delta_{Ii}$  and  $\delta_{Ri}$  defined as:

$$\delta_{Ii} = \begin{cases} 1, & \text{if the lifetime is interval censored} \\ 0, & \text{otherwise} \end{cases} \quad (16)$$

$$\delta_{Ri} = 1 - \delta_{Ii} \quad (17)$$

The analysis employs the log-likelihood function and its derivative to maximize the likelihood function. The log-likelihood function simplifies the task of finding the derivative. It is obtained by taking the natural logarithm of the likelihood function. This transformation often leads to a function that is easier to differentiate.

Upon obtaining the derivative of the log-likelihood function, the first step is to look for a closed-form solution. The approach consists of the following steps:

1. Differentiate the log-likelihood function with respect to the parameters.
2. Equate the first-order derivative to zero and solve for the parameters.

A closed-form solution, if found, provides optimal parameter values that maximize the likelihood function for the given data.

**Exponential Distribution** The estimation of the parameter  $\lambda$  for the Exponential distribution fitted to complete and right censored lifetimes commences with inserting exponential pdf and survival function into equation 10, which results in:

$$L(\lambda) = \prod_{i=1}^n e^{-\lambda t_i} \delta_i^{(1)} \quad (18)$$

It follows that the loglikelihood is given by:

$$l(\lambda) = \log L(\lambda) = \sum_{i=1}^n (\log \lambda - \lambda t_i) \delta_i^{(1)} \quad (19)$$

The derivative of  $l(\lambda)$  with respect to  $\lambda$  is

$$\frac{dl}{d\lambda} = \frac{\sum_{i=1}^n \delta_i^{(1)}}{\lambda} - \sum_{i=1}^n t_i \delta_i^{(1)} \quad (20)$$

Solving  $\frac{dl}{d\lambda} = 0$  yields a closed-form solution for  $\hat{\lambda}$ :

$$\hat{\lambda} = \frac{\sum_{i=1}^n \delta_i^{(1)}}{\sum_{i=1}^n t_i \delta_i^{(1)}} \quad (21)$$

For interval and Right-Censored Lifetimes the exponential pdf and survival function are inserted into equation 12, which results in:

$$L(\lambda) = \prod_{i=1}^n (e^{-\lambda t_{i1}} - e^{-\lambda t_{i0}})^{\delta_i^{(2)}} \quad (22)$$

Here,  $\delta_i^{(2)}$  is an indicator variable set to one for interval-censored observations and zero otherwise. The log-likelihood function is then

$$l(\lambda) = \sum_{i=1}^n \delta_i^{(2)} \log (e^{-\lambda t_{i1}} - e^{-\lambda t_{i0}}) \quad (23)$$

The derivative  $l(\lambda)$  with respect to  $\lambda$  is given by:

$$\frac{dl}{d\lambda} = \sum_{i=1}^n \delta_i^{(2)} \frac{-t_{i1} e^{-\lambda t_{i1}} + t_{i0} e^{-\lambda t_{i0}}}{e^{-\lambda t_{i1}} - e^{-\lambda t_{i0}}} \quad (24)$$

The equation for  $\frac{dl}{d\lambda}$  is nonlinear in terms of  $\lambda$ , stemming from the combination of exponential functions and linear coefficients. The summation captures differences across various lifetime data points, adding layers of complexity to the equation. Given this intricate structure, obtaining a closed-form solution through algebraic means becomes challenging. Therefore, a numerical approach is adopted in this thesis to determine the equation's roots.

**Weibull Distribution** In case of the Weibull distribution, the scale parameter  $\lambda > 0$  and the shape parameter  $\kappa > 0$  are estimated. The Weibull pdf is represented by:

$$f(t; \lambda, \kappa) = \frac{\kappa}{\lambda} \left( \frac{t}{\lambda} \right)^{\kappa-1} e^{-\left(\frac{t}{\lambda}\right)^\kappa} \quad (25)$$

With cdf and survival functions:

$$F(t; \lambda, \kappa) = 1 - e^{-\left(\frac{t}{\lambda}\right)^\kappa} \quad (26)$$

$$S(t; \lambda, \kappa) = e^{-\left(\frac{t}{\lambda}\right)^\kappa} \quad (27)$$

where  $t$  is the lifetime.

For complete and Right-Censored Lifetimes, the Weibull pdf and survival function are inserted into equation 10, which results in:

$$\begin{aligned} L(\lambda, \kappa) &= \prod_{i=1}^n \left( \kappa \left( \frac{t_i}{\lambda} \right)^{\kappa-1} e^{-\left( \frac{t_i}{\lambda} \right)^\kappa} \right)^{\delta_i} \left( e^{-\left( \frac{t_i}{\lambda} \right)^\kappa} \right)^{1-\delta_i} \\ &= \kappa^{\sum_i \delta_i} \prod_{i=1}^n \left( \frac{t_i}{\lambda} \right)^{\kappa \delta_i - \delta_i} e^{-\left( \frac{t_i}{\lambda} \right)^\kappa} \end{aligned} \quad (28)$$

It follows that the log likelihood is given by:

$$l(\lambda, \kappa) = \sum_i \delta_i \ln(\kappa) + \sum_i (\kappa \delta_i - \delta_i) \ln \left( \frac{t_i}{\lambda} \right) - \sum_i \left( \frac{t_i}{\lambda} \right)^\kappa \quad (29)$$

The derivative of the log likelihood function is given by:

$$\begin{aligned} \frac{\partial l(\lambda, \kappa)}{\partial \kappa} &= \sum_i \delta_i \frac{1}{\kappa} + \sum_i \delta_i \ln \left( \frac{t_i}{\lambda} \right) - \sum_i \ln \left( \frac{t_i}{\lambda} \right) \left( \frac{t_i}{\lambda} \right)^\kappa \\ \frac{\partial l(\lambda, \kappa)}{\partial \lambda} &= - \sum_i (\kappa \delta_i - \delta_i) \frac{t_i}{\lambda^2} + \kappa \sum_i \left( \frac{t_i}{\lambda} \right)^{\kappa-1} \frac{t_i}{\lambda^2} \end{aligned} \quad (30)$$

setting these equations to zero, then solving for  $\kappa$  and  $\lambda$  results in the following non-linear equations:

$$\begin{aligned} \frac{1}{\kappa} \sum_i \delta_i + \sum_i \delta_i \ln \left( \frac{t_i}{\lambda} \right) - \sum_i \ln \left( \frac{t_i}{\lambda} \right) \left( \frac{t_i}{\lambda} \right)^\kappa &= 0 \\ (\kappa - 1) \sum_i \delta_i \frac{t_i}{\lambda^2} + \kappa \sum_i \left( \frac{t_i}{\lambda} \right)^{\kappa-1} \frac{t_i}{\lambda^2} &= 0 \end{aligned} \quad (31)$$

Due to the complexity of these specific non-linear functions, it is assumed that there are no closed form solutions to determine  $\kappa$  and  $\lambda$ . Hence to derive the parameters, a numerical solver should be used.

For interval and right-Censored lifetimes, the Weibull pdf and survival function are inserted into equation 15, producing:

$$L(\lambda, \kappa) = \prod_{i=1}^n \left[ e^{-\left( \frac{t_{i0}}{\lambda} \right)^\kappa} \right]^{\delta_{Ri}} \left[ \left( 1 - e^{-\left( \frac{t_{i1}}{\lambda} \right)^\kappa} \right) - \left( 1 - e^{-\left( \frac{t_{i0}}{\lambda} \right)^\kappa} \right) \right]^{\delta_{Ii}} \quad (32)$$

A simplified version is presented by:

$$L(\lambda, \kappa) = \prod_{i=1}^n \left[ e^{-\left( \frac{t_{i0}}{\lambda} \right)^\kappa} \right]^{\delta_{Ri}} \left[ e^{-\left( \frac{t_{i0}}{\lambda} \right)^\kappa} - e^{-\left( \frac{t_{i1}}{\lambda} \right)^\kappa} \right]^{\delta_{Ii}} \quad (33)$$

The log-likelihood function then becomes:

$$l(\lambda, \kappa) = \sum_{i=1}^n \delta_{Ri} \log \left( e^{(-\frac{t_{i0}}{\lambda})^\kappa} \right) + \delta_{Ii} \log \left( e^{(-\frac{t_{i0}}{\lambda})^\kappa} - e^{(-\frac{t_{i1}}{\lambda})^\kappa} \right) \quad (34)$$

The derivative of the log likelihood function with respect to  $\kappa$  and  $\lambda$  is:

$$\begin{aligned} \frac{\partial l(\lambda, \kappa)}{\partial \kappa} &= \sum_{i=1}^n \delta_{Ri} \left( -\frac{t_{i0}}{\lambda} \right)^\kappa \log \left( \frac{t_{i0}}{\lambda} \right) e^{(-\frac{t_{i0}}{\lambda})^\kappa} \\ &\quad + \delta_{Ii} \left( \left( -\frac{t_{i0}}{\lambda} \right)^\kappa \log \left( \frac{t_{i0}}{\lambda} \right) e^{(-\frac{t_{i0}}{\lambda})^\kappa} - \left( -\frac{t_{i1}}{\lambda} \right)^\kappa \log \left( \frac{t_{i1}}{\lambda} \right) e^{(-\frac{t_{i1}}{\lambda})^\kappa} \right) \\ \frac{\partial l(\lambda, \kappa)}{\partial \lambda} &= \sum_{i=1}^n \delta_{Ri} \kappa \left( -\frac{t_{i0}}{\lambda^2} \right)^\kappa e^{(-\frac{t_{i0}}{\lambda})^\kappa} \\ &\quad + \delta_{Ii} \kappa \left( \left( -\frac{t_{i0}}{\lambda^2} \right)^\kappa e^{(-\frac{t_{i0}}{\lambda})^\kappa} - \left( -\frac{t_{i1}}{\lambda^2} \right)^\kappa e^{(-\frac{t_{i1}}{\lambda})^\kappa} \right) \end{aligned} \quad (35)$$

Setting the above equations to zero and then solving for  $\kappa$  and  $\lambda$  results in the following non-linear equations:

$$\begin{aligned} &\sum_{i=1}^n \delta_{Ri} \left( -\frac{t_{i0}}{\lambda} \right)^\kappa \log \left( \frac{t_{i0}}{\lambda} \right) e^{(-\frac{t_{i0}}{\lambda})^\kappa} \\ &\quad + \delta_{Ii} \left( \left( -\frac{t_{i0}}{\lambda} \right)^\kappa \log \left( \frac{t_{i0}}{\lambda} \right) e^{(-\frac{t_{i0}}{\lambda})^\kappa} \right. \\ &\quad \left. - \left( -\frac{t_{i1}}{\lambda} \right)^\kappa \log \left( \frac{t_{i1}}{\lambda} \right) e^{(-\frac{t_{i1}}{\lambda})^\kappa} \right) = 0, \\ &\sum_{i=1}^n \delta_{Ri} \kappa \left( -\frac{t_{i0}}{\lambda^2} \right)^\kappa e^{(-\frac{t_{i0}}{\lambda})^\kappa} \\ &\quad + \delta_{Ii} \kappa \left( \left( -\frac{t_{i0}}{\lambda^2} \right)^\kappa e^{(-\frac{t_{i0}}{\lambda})^\kappa} \right. \\ &\quad \left. - \left( -\frac{t_{i1}}{\lambda^2} \right)^\kappa e^{(-\frac{t_{i1}}{\lambda})^\kappa} \right) = 0. \end{aligned} \quad (36)$$

Due to the complexity of these specific non-linear functions, it is assumed that there are no closed form solutions to determine  $\kappa$  and  $\lambda$ . Hence to derive the parameters, a numerical solver should be used.

#### 4.2.4 Numerical Parameter Fitters: Newton-Raphson Method

When a closed-form solution is not attainable, numerical optimization methods are employed for parameter estimation. The Newton-Raphson method serves as a robust solution for solving the MLE [16].

**Newton-Raphson for Single-Parameter Models** For models with a single parameter  $\lambda$ , the Newton-Raphson update formula simplifies to:

$$\lambda_{\text{new}} = \lambda_{\text{old}} - \frac{l'(\lambda_{\text{old}})}{l''(\lambda_{\text{old}})}$$

Here,  $l'$  and  $l''$  denote the first and second derivatives of the log-likelihood function, respectively. The iterative process continues until the relative error  $\frac{|\lambda_{\text{new}} - \lambda_{\text{old}}|}{|\lambda_{\text{new}}|}$  falls within predefined acceptable limits.

**Newton-Raphson for Multi-Parameter Models** For models with multiple parameters, the Newton-Raphson method generalizes to handle a parameter vector  $\boldsymbol{\theta} = [\theta_1, \theta_2, \dots, \theta_p]$ . The generalized iterative update formula is:

$$\boldsymbol{\theta}_{\text{new}} = \boldsymbol{\theta}_{\text{old}} - \mathbf{H}^{-1}(\boldsymbol{\theta}_{\text{old}}) \nabla \mathcal{L}(\boldsymbol{\theta}_{\text{old}})$$

Where:

- $\mathbf{H}(\boldsymbol{\theta})$  is the Hessian matrix, detailed in Appendix E.
- $\nabla \mathcal{L}(\boldsymbol{\theta})$  is the gradient vector of the log-likelihood function.

The iterative procedure for multi-parameter models is analogous to the single-parameter case but operates in a multidimensional parameter space. Convergence is assessed using the relative error metric:

$$\text{Relative Error} = \frac{\|\boldsymbol{\theta}_{\text{new}} - \boldsymbol{\theta}_{\text{old}}\|}{\|\boldsymbol{\theta}_{\text{new}}\|}$$

Iteration continues until the relative error falls within predefined acceptable limits for all parameters.

#### 4.2.5 Assessing Models

This section covers the proposed approach to assessing the models using AIC, Goodness-of-Fit testing and visualisation.

**Akaike Information Criterion** The Akaike Information Criterion (AIC) can be used to determine which model is more likely given the lifetime data. AIC is chosen for its simplicity and in providing an initial comparison between different models. The formula for AIC is:

$$\text{AIC} = -2 \ln(\text{Likelihood}) + 2k \quad (37)$$

In the AIC formula,  $\ln(\text{Likelihood})$  denotes the natural logarithm of the model's likelihood given the data, while  $k$  signifies the number of model parameters. Lower AIC values suggest a model is more probable given the observed data. As a penalty

against overfitting, models with more parameters are subject to a higher AIC. Taking the Weibull and Exponential distributions as an example: if both yield the same likelihood for a dataset, the Exponential, having only one parameter compared to the Weibull's two, will possess a lower AIC. This is because the AIC inherently favors simplicity, penalizing the added complexity of the Weibull's extra parameter. By balancing goodness of fit with model complexity, AIC provides a streamlined method for initial model comparison.

**AIC Rule of Thumb** The general rule of thumb for comparing AIC scores posits that a difference of less than two points implies the models are essentially indistinguishable in performance. A difference of exactly two points provides moderate evidence favoring one model over the other, while a difference exceeding four points constitutes strong evidence for a substantial difference between the models [11]. In a specific case where a Weibull model has an AIC of 200 and an Exponential model has an AIC of 202, the two-point difference suggests moderate evidence in favor of the Weibull model.

**Goodness-of-Fit Testing** To further evaluate the performance of the statistical models, the study employs Goodness-Of-Fit (GOF) tests. Unlike the AIC, which focuses on balancing model fit and complexity for the purpose of model selection [11], GOF tests provide a direct measure of how closely a model's predictions align with the observed data. This makes GOF tests a critical tool for assessing the empirical validity of a model. By using both AIC and GOF tests, the study aims to achieve a comprehensive evaluation, facilitating a more robust comparison between the Exponential and Weibull models.

To see if the model fits the data, the first step is to set up two opposing statements: the null hypothesis  $H_0$  and the alternative hypothesis  $H_1$ .

$$H_0 : F = F_0 \quad \text{vs} \quad H_1 : F \neq F_0 \quad (38)$$

In this study,  $F$  denotes the empirical cumulative hazard function, estimated using Nelson-Aalen, while  $F_0$  denotes a theoretical distribution, such as the Exponential or Weibull models. To evaluate these hypotheses, a statistical metric known as the p-value is employed. This metric quantifies the likelihood of observing data at least as extreme as the sample data, under the assumption that the null hypothesis is true.

First, a test statistic  $D_n$  is computed based on the original dataset. Subsequently, bootstrapping methods are employed to create multiple simulated datasets from the observed data. For each simulated dataset, an individual test statistic is calculated, resulting in a distribution of test statistics. The p-value is then derived by assessing the proportion of these test statistics that meet or exceed the value of the original  $D_n$ . The p-value effectively gauges the probability that the observed test statistic could arise by random chance, under the assumption that the null hypothesis is true.

**Censored Data** Dealing with censored data introduces complexity in statistical analysis. Specifically, censored data complicates the calculation of the test statistic, the application of bootstrapping methods, and the determination of the empirical distribution. The key challenge arises because the exact lifetime values ( $t_i$ ) are unknown, which hinders the precise estimation of empirical distributions and test statistics. To handle the data censoring, this study employs a modification of the Leveraged Bootstrap Method [24]. The original method uses an empirical distribution function, while this study uses interval midpoints to replace interval-censored lifetimes. Validation is provided by a statistical test in Appendix F, and the p-values obtained confirm the approach's validity within the scope of this thesis.

**Kolmogorov-Smirnov Test** In terms of deriving the test statistic, the study utilizes the Kolmogorov-Smirnov (KS) test. The selection of the KS test is motivated by its ease of application and its well-documented use in reliability analysis [16]. The KS test aims to identify the largest difference between the empirical cumulative distribution  $F_n$  and the theoretical cumulative distribution  $F_0$ , which serves to assess the fit of the model to the data. The KS test formula is given by:

$$D_n = \sup_{t_i} |F_n(t_i) - F_0(t_i)| \quad (39)$$

**Visual Assessment of Statistical Models** This study incorporates both numerical and visual assessment techniques to ensure a robust evaluation of the statistical models. Visual assessment serves several critical roles:

- **Model-Data Alignment:** The initial set of plots compares the Exponential and Weibull models to the empirical data points. These plots serve as a qualitative check for model fit. The rationale is that numerical metrics alone may not capture subtle deviations or patterns in the data. A visual inspection thus provides an additional layer of validation.
- **Test Statistic Distribution:** The second tool involves density plots that represent the distribution of test statistics, generated from bootstrapped datasets for each model. These plots can identify whether the model is consistently fitting the data well across multiple samples. Such a distributional view can signal potential issues like overfitting or underfitting, which may not be immediately apparent from single-value metrics.
- **Cumulative Hazard Function Assessment:** The final tool consists of plots that juxtapose the empirical cumulative hazard function with the fitted models. These plots not only gauge the model's fidelity to real-world data but also reveal nuances in the rate of failure over time. This is crucial for understanding the reliability and limitations of the model in practical applications.

By employing these visual tools in conjunction with numerical assessments, the study aims for a methodologically sound, multi-faceted evaluation. This dual approach en-

ables a more nuanced understanding of the model fits, ultimately leading to more reliable conclusions.

### 4.3 User Interface and Database

The software architecture is designed with modularity and scalability in mind, suitable for both current utilization and future expansions. The code repository for this project has been comprehensively documented and can be accessed for further details [10].

**Technological Components** The technological components are carefully selected based on their performance, flexibility, and compatibility:

- **Database Management with SQLAlchemy (2.0.10):** Employed for its robust object-relational mapping capabilities.
- **User Interaction through FastAPI (0.95.1):** Implemented for its RESTful capabilities and compatibility with Uvicorn.
- **User Interface via Swagger UI:** Chosen for its user-friendly design.
- **Data Processing and Calculations with Pandas and NumPy:** Integrated for efficient data manipulation and numerical computation.

**Performance and Efficiency** Parallel computing techniques are utilized to enhance computational efficiency, particularly when managing large datasets or complex calculations.

**Structure and Design** The architecture comprises three layers:

1. *Database Layer:* Manages data storage and retrieval.
2. *Middleware Layer:* Handles user requests, serving as an interface between the database and the user.
3. *User Interface Layer:* Facilitates user interaction via a graphical interface.

Three figures are included to provide a visual overview: Figure 11 illustrates the user interface, while Figures 12 and 13 represent the input schema and plot output, respectively.

default	
GET	/distribution-model/fit/parameters/exponential/ Get Fitted Exponential Distribution
GET	/calculate-lifetimes/count/ Calculate Lifetimes Count
GET	/calculate-lifetimes/ Calculate Lifetimes
GET	/distribution-model/exponential/plot/ Get Exponential Model Cdf Plot
GET	/distribution-model/fit/parameters/ Get Fitted Distributions
POST	/distribution-model/fit/parameters/weibull/initial-guess Get Fitted Weibull Distributions Using Initial Guess
POST	/distribution-model/goodness-of-fit/test Get Fit Statistics
POST	/distribution-model/fit/parameters/test Get Fit Parameters
POST	/distribution-model/weibull/plot/ Get Weibull Model Cdf Plot
POST	/distribution-model/plot/hazard-function/ Get Hazard Function Plot
POST	/object/upsert/ Upsert Objects
POST	/failure-type-code/upsert/ Upsert Failure Type Codes
POST	/maintenance-group/upsert/ Upsert Maintenance Groups
POST	/malfunction/upsert/ Upsert Malfunctions

Figure 11: Overview of User Interface

Figure 12: Input Interface

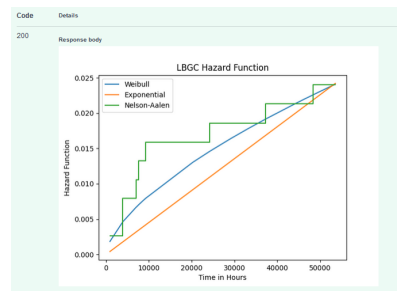


Figure 13: Plot Output Interface

For further elaboration on the technological choices, specifically the rationale behind the selection of Python packages, refer to Appendix G

#### 4.4 Summary

This chapter addresses the key research question: How can statistical methods be used to challenge the constant failure rates assumption in storm surge barriers? The chapter outlines a framework that incorporates Type-codes as failure scenarios. These

Type-codes specify failure modes, relate to recorded malfunctions, and correspond to various system components. To examine the assumption of constant failure rates, the chapter details a structured methodology that employs the Nelson-Aalen estimator and two statistical models: the Exponential and Weibull distributions.

The Nelson-Aalen estimator serves to estimate the cumulative hazard function. A linear increasing cumulative hazard function is indicative of constant failure rates, while a non-linear shape suggests variable failure rates.

The analysis suggested in the framework begins by contrasting two models: the Exponential, which assumes a constant failure rate, and the Weibull, which allows for variation in failure rates. To assess the relative performance of these models, AIC is employed. The AIC provides a measure of model quality that penalizes unnecessary complexity to prevent overfitting. Additionally, hypothesis testing offers further validation. Specifically, the Kolmogorov-Smirnov test, along with bootstrapping methods for p-value calculation, enables a direct comparison of the models to the actual lifetime data of SVKO components. Should the data lead to the rejection of the Exponential model, whilst accepting the Weibull model, it could imply that failure rates vary over time. This chapter introduces a critical evaluation of the models, preparing the way for more detailed empirical investigation in subsequent sections.

However, applying the proposed methods can be difficult due to data censoring. Fitting models often requires numerical methods, which can be complex and time-consuming. The Exponential model offers a simpler approach for complete and right-censored data. Nevertheless, most scenarios involve complicated equations that are hard to solve. Although this can be overcome using numerical methods like the Newton-Raphson algorithm, these can be problematic. They may not find the best solution, but settle for a local maximum, and the initial guess can significantly affect the results. Future research should aim to apply more reliable methods for fitting the distribution models to censored data.

## 5 Assessment of Component Failure Rates via Statistical Framework

This chapter will attempt to answer a question that remains unexplored in prior research on storm surge barriers: does a time-variable failure rate model provide a statistically better fit to the existing data than a constant rate model? Prior studies tend not to focus on validating the underlying model of the data, instead focusing on updating failure rates [4, 8].

To answer the research sub-question, the chapter uses component lifetime data of the SVKO, discussed in section 3.2. This data is assessed through a statistical framework described in section 4. Under the current approach to storm surge barrier reliability failure rates are assumed to be constant in time [2,19,31]. A constant failure rate can be represented by the exponential distribution [16], real-world conditions suggest a more intricate landscape, which is discussed in Chapter 2. Factors like the repair of hydraulic cylinders can lead to non- “as-new” conditions, potentially altering the established constant failure rate,  $\lambda$  [18]. Given the potential complexities in real-world conditions, this chapter will evaluate whether an Exponential or a Weibull model fits better to the data. The Weibull model, with its shape parameter  $\beta$ , is designed to accommodate time-variable failure rates. A superior fit from the Weibull model, especially if its  $\beta$  parameter differs from one, is evidence for failure rates being variable [16,18].

The chapter begins with background on prior work that evaluates component lifetimes, followed by the method to apply the statistical framework, the results and a discussion to answer the sub research question.

### 5.1 Background

Statistical models are crucial for assessing the reliability of storm surge barriers by determining component failure rates. In relation to the SVKO, a previous study used an assumed statistical model to describe the component lifetimes with the primary aim of updating these failure rates [8]. This model, however, was not validated using the observed data.

The lack of validation in the previous work is noteworthy. Additionally, the prior study simplified the analysis by omitting important data characteristics like censoring, which might influence the reliability estimate, and choice of methods used.

This study distinguishes itself by being the first to use the available maintenance system data from the SVKO for validating lifetime models. It is also unique in its consideration of data censoring. Practical implications of knowing the model are additional insight into whether the failure rates are constant or vary over time, which is valuable information for resource allocation and effective maintenance, as discussed in Chapter 2.

The aim of this chapter is to validate the underlying statistical models for the life-

times of SVKO components. The SVKO component data described in Chapter 3 will be analysed using the statistical framework discussed in Chapter 4. The primary goal is to determine which model offers the best fit for describing the lifetimes of these components.

## 5.2 Method

The research subquestion addressed is: "Does a time-variant failure rate model provide a superior fit to the data compared to a constant rate model?" To answer this question, models are fitted to lifetime data. The dataset under consideration, obtained from the

SVKO, is outlined in Chapter 3.2. A statistical framework, detailed in Chapter 4, is utilized. This framework has two main components: 1) a non-parametric estimation of the hazard function to provide an empirical representation of failure rates over time, and 2) parametric model fitting, specifically employing the Exponential and Weibull models.

Two models are evaluated: the Exponential and the Weibull models. The Exponential model assumes a constant failure rate, while the Weibull model allows for a time-variant failure rate. These models are assessed using the Akaike Information Criterion (AIC) for model selection and the Kolmogorov-Smirnov (KS) tests for Goodness-of-Fit. The KS tests in tandem with bootstrapping are used to calculate the p-value to quantify the adequacy of the model fit to the observed data.

If the Weibull model is a better fit and its shape parameter is not equal to 1, it indicates that failure rates vary over time. A non-linear pattern in the cumulative hazard function would substantiate this conclusion.

The methodology consists of the following steps:

1. **Data Preparation** Raw data are processed for statistical analysis. Datasets with lifetimes in hours are generated for each failure scenario.
2. **Model Fitting:** Both Exponential and Weibull models are fitted to the unmodified lifetime data for each failure scenario using Maximum Likelihood Estimation (MLE).
3. **Model Assessment:** AIC values are computed for preliminary model selection. Bootstrapping generates new lifetime datasets, which are fitted to Exponential and Weibull models. The KS test then quantitatively evaluates the fit, producing a p-value for each model.
4. **Visualization:** Visualizations such as plots and graphs are generated to provide a qualitative assessment of the models, complementing the numerical criteria.

### 5.2.1 Data Preparation

The data used in this study originates from the BMS+ system and focuses on the failure rates within the SVKO. The dataset spans from May 20, 2010, to June 30, 2016. For further details on the raw data, refer to Section 3.2. This dataset allows for the analysis of 17 unique failure scenarios, which are summarized in Table 6.

For each failure scenario, a dataset is constructed that captures the lifetimes of the components in hours. These lifetimes are then categorized into one of three types: complete, right-censored, or interval-censored, as illustrated in Figure 14. The red dashed line for right censoring indicates that the failure occurs sometimes in the future, and is not yet observed. The categorization of lifetime data is crucial as it imposes specific requirements on the statistical models used for the analysis. The mathematical treatment of these different types of lifetime data is elaborated in Chapter 4.

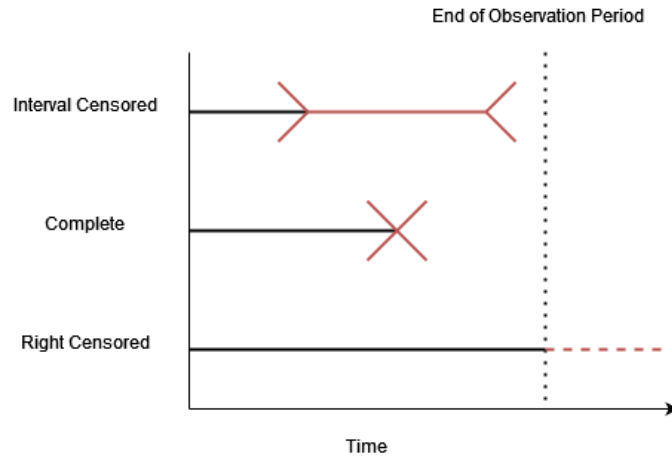


**Figure 14:** Illustration of component lifetime types: complete, interval-censored, and right-censored data.

### 5.2.2 Model Fitting

To evaluate which of the two models, Exponential or Weibull, best fits the component lifetime data, a statistical framework is adopted. This framework is described in Chapter 4, which aims to identify the model that best represents the observed failure rates in the data.

In reliability engineering, the term "failure rate" is often synonymous with the "hazard function" [16]. The Exponential and Weibull models are chosen for their differing underlying hazard functions. Specifically, the Exponential model assumes a constant hazard function, given by Equation 40. On the other hand, the Weibull model allows for a time-varying hazard function, as described by Equation 41.

$$h(t) = \lambda \tag{40}$$

$$h(t) = \frac{\kappa}{\lambda} \left( \frac{t}{\lambda} \right)^{\kappa-1} \tag{41}$$

Models are initially fitted to lifetime data using MLE, adapted to account for censored data, as elaborated in Chapter 4. Given the constraints introduced by data censoring, numerical solvers such as the Newton-Raphson method are employed in the MLE process. For ensuring global convergence, initial parameter values are initially optimized using the AIC iteratively. For instance, an initial fit is conducted using rudimentary parameter estimates, which are then iteratively refined using the AIC to guide the Newton-Raphson method toward global convergence.

### 5.2.3 Model Assessment

The AIC quantitatively assesses model fit, penalizing excessive complexity to deter overfitting. It inherently addresses censored data by utilizing the likelihood function, which is adapted for such datasets. A lower AIC value for the Weibull model implies that its additional parameters, particularly the shape parameter, provide a meaningful improvement in describing the data over the Exponential model, affirming its statistical significance.

Censored data presents unique challenges for goodness-of-fit testing. To overcome this, a bootstrap approach, based on leveraging data midpoint imputation, is employed to approximate the incomplete data. This preparation allows for the application of the KS test, where the empirical distribution is compared against the hypothesized model to ascertain the congruity between observed data and model predictions.

The KS tests are used in the calculation of a p-value, reflecting the probability that the observed data could plausibly be generated by the specified model. For instance, suppose a p-value of 0.03 for the Exponential model and 0.07 for the Weibull model are obtained. The p-value for the Exponential model being below 0.05 suggests that the data does not fit well with a constant failure rate assumption, and thus, this model is rejected. On the contrary, the Weibull model with a p-value above 0.05 is not rejected, which implies that incorporating the shape parameter provides a significantly better fit. This indicates that the failure rates are not constant and vary over time. Conversely, if both models yield p-values above 0.05, for example 0.08 for the Exponential and 0.10 for the Weibull, it indicates that both models are statistically plausible and the data does not provide a strong reason to prefer one over the other based on the KS test alone. However, if the Weibull model has a lower AIC than the Exponential, it would suggest that despite both models fitting within the acceptable range, the Weibull model, with its varying failure rate assumption, provides a more nuanced understanding of the data.

The structured process for model evaluation and selection consists of the following steps:

1. **Initial Model Fitting and AIC Calculation:** Fit the models to the raw data and compute AIC values.
2. **Data Preparation:** Simplify censored data using the aforementioned method to enable robust GoF testing.
3. **KS Test on Simplified Data:** Conduct the KS test using the simplified data.
4. **Bootstrapped Model Fitting:** Generate bootstrapped data sets based on the simplified data.
5. **Test Statistic and P-Value Calculation:** Apply the KS test to the bootstrapped data sets to compute test statistics. Which are used to determine the p-values.
6. **Final Model Evaluation:** Assess the suitability of the model based on the p-values.

Supplementary to these quantitative analyses, the following visual methods are also used:

- **Graphical Comparisons:** Direct graphical comparisons between the fitted models and empirical data.
- **Density Plots:** Study density plots based on test statistics from the bootstrapped data sets to understand model adequacy in more detail.
- **Empirical Cumulative Hazard Function:** Observe how the hazard function evolves over time to assist in model selection.
- **Empirical Survival Function:** Facilitates direct comparison between the fitted and observed hazard functions.

#### 5.2.4 Assumptions and Limitations

This study relies on several assumptions to enable the analysis of component reliability. Both the assumptions and the inherent limitations of the dataset could influence the findings and should be considered when interpreting the results.

The dataset is limited in its scope in time, covering only six years of operation while the SVKO has been in service for 37 years. This limitation could affect the reliability estimations related to component lifetimes and failure rates. The dataset of this study also omits certain failure scenarios, including only those scenarios for which malfunctions have actually been recorded. If a failure scenario has not occurred, all lifetime data for that scenario is set equal to the length of the observation period. This is problematic because a dataset with zero variance cannot inform parameter estimations. In

addition, the dataset lacks key information like test times for components and does not establish a link between component replacements and recorded malfunctions.

1. **Analysis Timeframe:** The dataset spans from May 20, 2010, to June 30, 2016. Failures occurring outside this period are not accounted for, even though the SVKO continues to operate.
2. **Test Times:** To mitigate the limitation of incomplete data, an additional dataset containing SVKO test dates is used to infer component test times. This data are the test closures, it is assumed that these lead to the hidden malfunctions being discovered.
3. **Failure Event Characteristics:** Each failure event is characterized by a unique combination of component type and failure type. Components are assumed to be as good as new post-maintenance, indicating that their pre- and post-failure conditions are independent.
4. **Immediate Replacement:** The study assumes immediate replacement of failed components, ensuring a constant number of units at risk throughout the observation period. This assumption facilitates a streamlined analysis, although it may not accurately represent real-world situations where delays in replacement are typical. Such delays could lead to overestimated component lifetimes, as the time taken for replacement is not accounted for. Regarding the variation of the failure rate over time, the immediate replacement assumption could potentially flatten the observed trend. This would make the failure rate appear more constant over time than it actually is, as immediate replacement would artificially reduce the perceived rate of failure, particularly for components with shorter lifetimes.

## 5.3 Results

This section details the results obtained by applying the framework constructed in 4 to the data detailed in 3.2.

### 5.3.1 Failure Scenarios and Object Lifetimes

Building upon the 17 unique failure scenarios identified in the dataset, the lifetime of each component is analysed. In Table 6, 9 of these failure scenarios were found to be interval-censored, and 8 were right-censored.

Each component in the dataset was further classified based on the nature of its failure. If a component is operational at the end of the observation period, it is considered right-censored. Components that failed during this period and were observable are categorized as complete, whereas those that are unobservable are classified as interval-censored. This classification is also highlighted in Table 6. Figures 15 and 16 represent

the component lifetimes of failure scenarios 5-LBPRC and 6-LBQENM. The figures use various symbols to indicate the nature of the failure, a  $\bullet$  represent an observable failure, a  $\triangleright$  and  $\triangleleft$  represent the start and end of an interval in which an unobservable failure occurred. The blue lines represent lifetimes that have not ended at the end of the observation period.

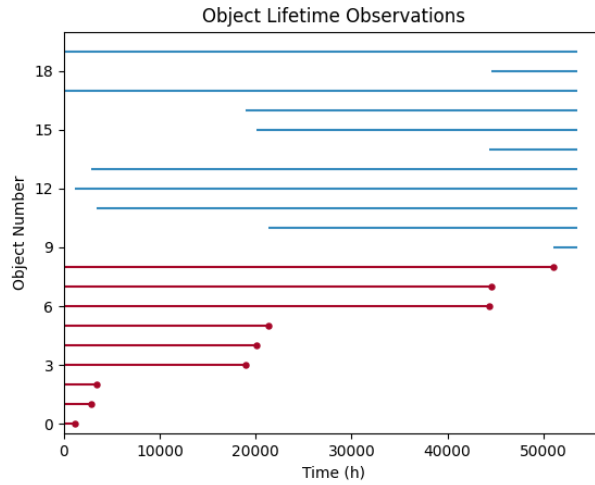


**Figure 15:** Lifetimes of objects experiencing the observable LBPRC failure scenario. Red lines concluding with a  $\bullet$  symbolize observed failure scenarios. Blue lines depict objects subject to right censoring.

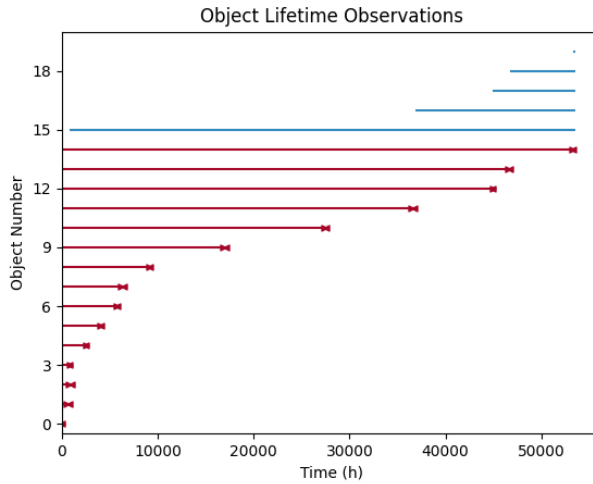


**Figure 16:** Lifetimes of objects subject to the unobservable LBQENM failure scenario. Red lines indicate objects with interval censoring, with the ▷ and ◁ symbols specifying the start and end of the interval. Blue lines illustrate objects subject to right censoring.

### 5.3.2 Model Fits

The Exponential and Weibull models have been fitted to the lifetime datasets for 17 failure scenarios, for which malfunctions relevant to the closure reliability are observed. The model parameters estimated using MLE are provided in Table 7. In case of the exponential model, the failure rate  $\lambda$  is estimated, whereas both the shape  $\kappa$  and scale  $\lambda$  parameters are derived in for Weibull model.

In Table 7 specific cases such as the 1-LBDIM scenario with  $\kappa = 1.3$  indicate an increasing failure rate, while the 5-LBPRC scenario with  $\kappa = 0.7$  reveals a decreasing failure rate. Table 8 lists the AIC values, p-values, and a single KS test statistic obtained from applying the Exponential and Weibull models to various failure scenarios.

Based on AIC values, 12 out of the total failure scenarios show a preference for the Exponential model, while the Weibull model performs better for 4 scenarios (7-LBQENM, 9-LBSWAM, 13-LERA38, and 16-LHGR). For 5-LBPRC, the AIC values are identical. Importantly, the difference in AIC values between the two models is smaller than two for most scenarios, suggesting both models are equally well suited to describe the data [11]. The difference in the AIC values for the models is likely due to the penalty for model complexity [11]. Figure 17 depicts the difference in AIC values between the models, and shows that scenario 7-LBQENM stands out for its large difference, over 13, and preference for Weibull.

In evaluating the fit of both Exponential and Weibull models to the data, the p-values

from hypothesis testing for all failure scenarios exceed 0.05. This means that there is insufficient statistical evidence to reject the null hypothesis, which in this context is that the observed data can be modeled adequately by either an Exponential or a Weibull distribution.

Based on the statistical indicators in Table 8 the Weibull model has a lower absolute distance to the empirical distribution for the original lifetime data for 7 failure scenarios 3-LBGC, 4-LBKLO, 5-LBPRC, 6-LBPRNI, 7-LBQENM, 15-LESS, 16-LHGR, there are 2 ties, 11-LEDGSN, 17-LHSV, and the remaining 8, 1-LBDIM, 2-LBDINM, 8-LBREL, 9-LBSWAM, 10-LBSWB, 11-LEDSSN, 13-LERA38, 14-LEVSSN, the remainder Exponential results in a lower test statistic value. Note that this is just one test statistic calculate for each failure scenario, hence it cannot be readily used to determine if one or the other model is better, and serves more a quantitative indicator for how well the models fit to the data for this moment in time.

**Table 7:** Comparison of Exponential and Weibull model parameters for each component.

F. Scenario	Exponential	Weibull	
	Rate ( $\lambda$ )	Scale ( $\lambda$ )	Shape ( $\kappa$ )
1-LBDIM	2.1e-08	1.1e07	1.3
2-LBDINM	4.2e-08	2.2e07	1.0
3-LBGC	4.5e-07	2.0e07	0.6
4-LBKLO	6.2e-06	1.7e05	0.9
5-LBPRC	6.5e-07	6.3e06	0.7
6-LBPRNI	7.2e-08	4.0e06	1.2
7-LBQENM	2.8e-07	7.7e8	0.4
8-LBREL	1.5e-08	9.0e7	1.0
9-LBSWAM	1.5e-07	7.5e05	1.8
10-LBSWB	7.3e-08	6.6e5	1.1
11-LEDGSN	5.2e-05	4.9e4	0.9
12-LEDSSN	3.7e-06	4.0e05	0.9
13-LERA38	2.4e-07	8.5e04	9.5
14-LEVSSN	2.7e-06	3.5e05	1.0
15-LESS	1.1e-06	6.4e06	0.6
16-LHGR	2.7e-06	1.9e06	0.6
17-LHSV	4.9e-08	1.2e7	1.1

**Table 8:** Comparison of Exponential and Weibull model AIC values, KS test statistics, and p-values for each component.

Failure Scenario	Exponential			Weibull		
	AIC	p-value	KS	AIC	p-value	KS
1-LBDIM	77	0.76	3.24e-4	78	0.69	3.77e-4
2-LBDINM	100	0.88	4.08e-4	102	0.86	4.18e-4
3-LBGC	187	0.53	9.40e-3	188	0.58	5.76e-3
4-LBKLO	18	0.83	1.48e-1	19	0.83	1.27e-1
5-LBPRC	277	0.70	8.96e-3	277	0.79	6.27e-3
6-LBPRNI	37	0.85	3.69e-3	40	0.85	3.67e-3
7-LBQENM	338	0.53	6.34e-3	324	0.85	2.00e-3
8-LBREL	29	0.79	1.98e-5	31	0.79	1.22e-4
9-LBSWAM	70	0.84	9.50e-4	69	0.75	2.56e-3
10-LBSWB	37	0.85	3.78e-3	40	0.81	5.32e-3
11-LEDGSN	259	0.28	2.22e-1	260	0.27	2.22e-1
12-LEDSSN	35	0.56	8.22e-2	37	0.55	8.97e-2
13-LERA38	35	0.58	8.22e-2	34	0.46	6.54e-2
14-LEVSSN	100	0.64	3.24e-2	101	0.68	3.31e-2
15-LESS	21	0.87	4.08e-2	23	0.87	3.18e-2
16-LHGR	251	0.53	4.37e-2	249	0.71	2.95e-2
17-LHSV	26	0.40	2.25e-3	28	0.85	2.25e-3

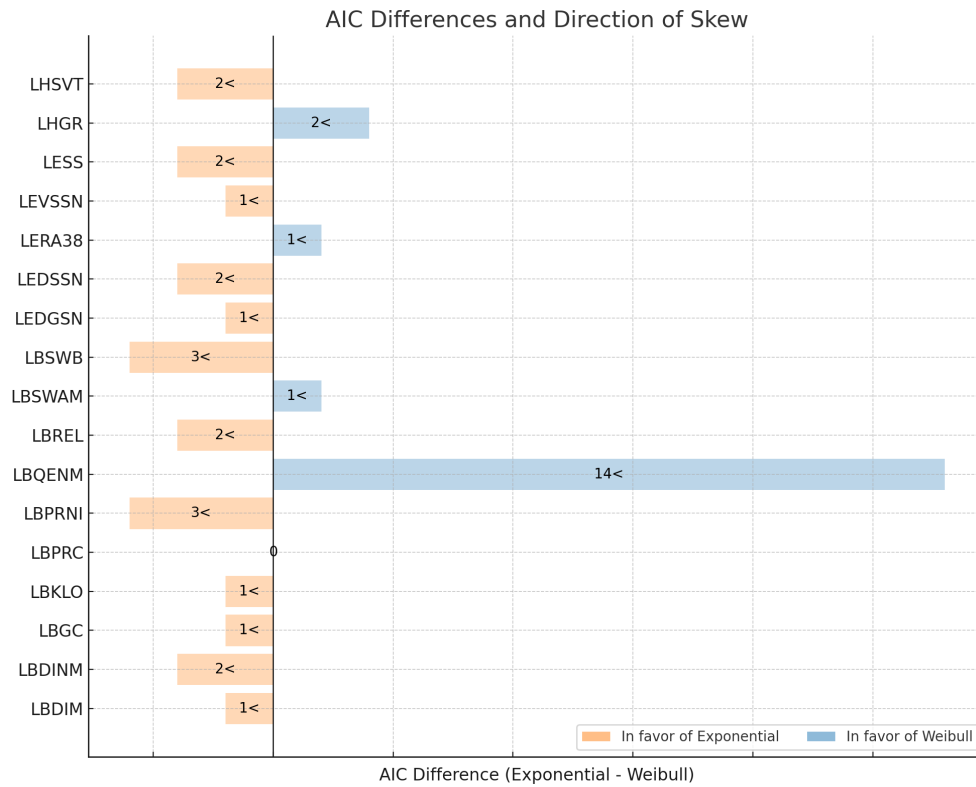


**Figure 17:** Diverging bar chart comparing the AIC values of the Exponential and Weibull models across different failure scenarios. Bars extending to the left and colored in orange indicate a lower AIC value for the Exponential model, making it more favorable. Bars extending to the right and colored in blue indicate a lower AIC value for the Weibull model. The symbol <math>j</math> indicates that the actual difference is lower than, e.g.

### 5.3.3 Graphical Assessment of Model Fits

Graphical evaluations for both Exponential and Weibull models are documented in Appendix H. Two key findings are presented:

- For datasets with low variability and fewer average failures, both models generally exhibit poor fit. These datasets do not appear to be suitable for rigorous model assessment using the framework based on the visualisation.
- For datasets with higher variability and a greater number of failures, the Weibull model typically performs as well as or better than the Exponential model.

Since a Weibull model with a shape parameter of 1 functions similarly to an Exponential model, it is expected that datasets showing a constant failure rate are well-captured by both models. For datasets indicating a varying hazard rate—a feature not accommodated by the Exponential model—the Weibull model is expected to perform better.

This behavior is supported by the visualisation presented in Appendix H. For a more comprehensive understanding, Appendix I categorizes these failure scenarios based on how well each model fits the empirical data. Key metrics from this analysis are consolidated in Table 9. Notably, the table highlights that the average number of failures in well-fitting scenarios is 10.29, significantly higher than in poorly-fitting scenarios, which average 1.30 failures. Additionally, the minimum number of failures in well-fitting scenarios (4) is double the maximum number of failures in poorly-fitting scenarios (2).

**Table 9:** Key Findings: Summary Statistics of Good Fits vs Poor Fits. For detailed information, see Appendix I.

Metric	Good Fit Scenarios	Poor Fit Scenarios
Mean Number of Failures	10.29	1.30
Maximum Number of Failures	20	2
Minimum Number of Failures	4	1
Mean Number of Components	504.71	429.90
Mean Lifetime-to-Component Ratio	1.21	1.05

**Case-by-Case Graphical Assessment** A detailed analysis is provided for specific scenarios, comparing the graphical assessments with previous quantitative analyses. Five distinct cases are examined: one where both models are similarly not very effective, two where both models seem to offer a comparable fit, and two where the Weibull model is seen to be preferable. These assessments corroborate the quantitative analyses, offering nuanced insights into the suitability of each model for different failure scenarios.

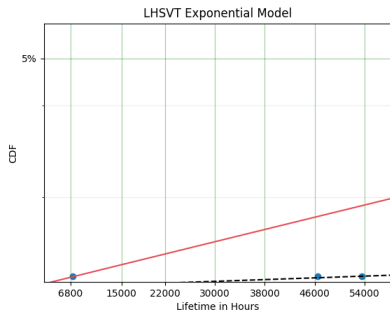
**17-LHSV T Analysis** Table 8 reveals that the Exponential and Weibull models have similar AIC scores in the 17-LHSV T scenario, implying that their fit to the data is comparably adequate. Despite this, their p-values are high enough to prevent statistical rejection. However, a closer look through visual analysis points to a poor fit for early failure times. The single component failure out of 384 suggests that the data lacks sufficient variability to differentiate between the models' performance, resulting in a potential overestimation of their fit.

Figure 20 displays the bootstrapped test statistics for the dataset (detailed in Table 6) as clustering at distinct values, with no intermediate data points. This phenomenon arises because the dataset predominantly consists of a single failure time

(e.g., 1000 hours) with only one or two component lifetimes deviating from this central tendency (e.g., at 1100 and 1200 hours). The absence of gradation between the clusters signifies that the bootstrap method, given the original dataset's limited variability, does not yield a continuous range of outcomes necessary for a nuanced model fit assessment. Consequently, caution must be exercised when interpreting these results, as the test statistics derived may not accurately reflect the models' goodness-of-fit.

The empirical cumulative hazard function, depicted as a near-horizontal line in Figure 21, signals an absence of failure events, leading to a potentially misleading zero-failure-rate inference. This suggests that the dataset is not sufficiently informative to assess the failure rate accurately or to compare model efficacy. The lack of failures to analyze means that reliability assessments are based on a dataset that may not reflect the true failure behavior.

In light of these findings, interpreting other failure scenarios with a similar pattern should be approached with skepticism. Specifically, it is advisable to question the informativeness of the dataset and consider seeking additional data. When encountering a near-horizontal empirical cumulative hazard function, it may suggest an insufficient number of events to validate a model's assumptions or to capture the potential complexity of the failure process, necessitating a cautious approach to model selection and validation.



**Figure 18:** Exponential model fit for the failure scenario LHSV T.

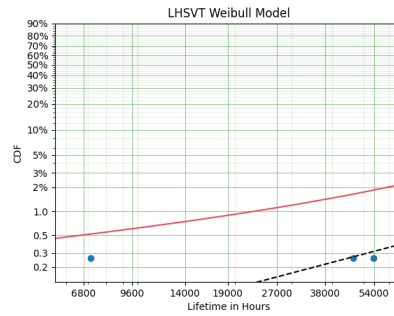


**Figure 19:** Weibull model fit for the failure scenario LHSV T.

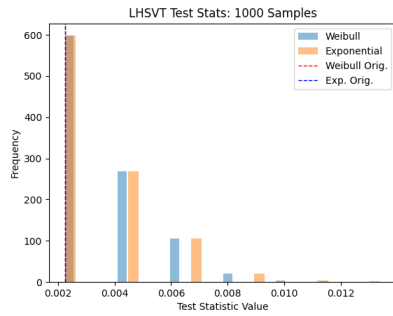


**Figure 20:** Histogram of TS values for failure scenario LHSV T.

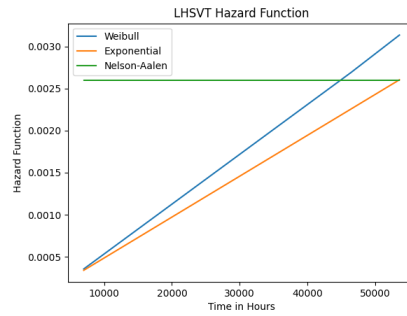


**Figure 21:** Hazard function for failure scenario LHSV T.

**11-LEDGSN Analysis** For the 11-LEDGSN scenario, the Weibull model fit for the data is clearly depicted in the Cumulative Distribution Function (CDF) plot, which shows lifetimes of 11-LEDGSN on the x-axis. The plotted data points follow the Weibull model curve fairly closely, especially for lifetimes ranging approximately between 8700 and 43000 hours, as indicated in Figure 22. Outside this range, the data points tend to diverge from both the Exponential and Weibull model curves.

The density plot in Figure 24 showcases overlapping Test Statistic (TS) distributions for both the Exponential and Weibull models derived from 1000 samples. The overlapped distributions of both models suggest their comparable fit to the 11-LEDGSN data. Notably, the two vertical lines representing the original test statistics from the Weibull and Exponential models are quite close, reaffirming the observation of similar performance by both models.

Figure 25 compares the hazard functions of the Exponential and Weibull models against the empirical Nelson-Aalen estimator. The Weibull and Exponential models seem to provide a good fit to the data, with both aligning closely with the Nelson-Aalen estimator, particularly for lifetimes up to about 40000 hours. Beyond this point, there is a noticeable divergence. This divergence suggests that the underlying risk factors or processes governing the hazard rate might change after 40000 hours. Moreover, it emphasizes the importance of considering time-varying effects or more flexible models when assessing long-term reliability or risk.

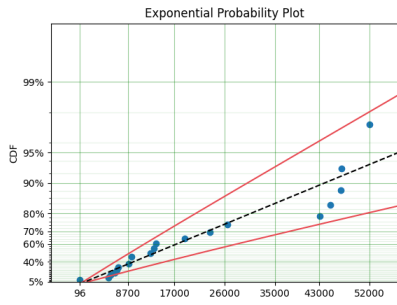


**Figure 22:** Exponential model fit for the failure scenario LEDGSN.

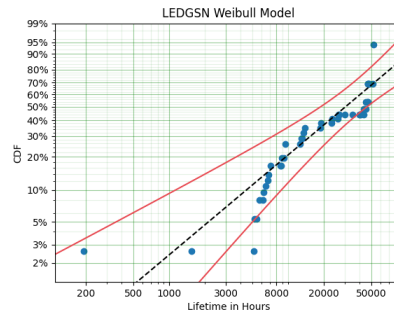


**Figure 23:** Weibull model fit for the failure scenario LEDGSN.

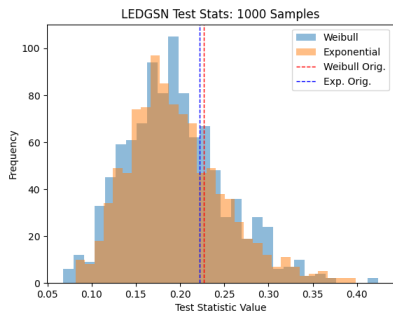


**Figure 24:** Histogram of TS values for failure scenario LEDGSN.

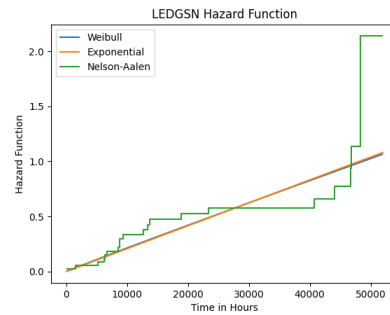


**Figure 25:** Hazard function for failure scenario LEDGSN.

**14-LEVSSN Analysis** Table 8 summarizes the results derived from the LEVSSN dataset. Both the Exponential and Weibull models yield comparable performances, as indicated by their similar AIC values. Furthermore, neither model is rejected based on their respective p-values.

The fit of these models to the dataset can also be visually assessed. Figures 26 and 26 demonstrate that both the Exponential and Weibull models closely align with the data points, reinforcing the statistical tests' findings.

Further evidence for the suitability of both models comes from the distribution of the test statistics values. As seen in Figure 28, the TS distributions for the Exponential and Weibull models overlap, suggesting an equivalent fit to the data.

The cumulative hazard function also provides insights into the models' characteristics. For the Nelson-Aalen, Exponential, and Weibull models, a linearly increasing hazard function is observed. This is indicative of a constant failure rate over time.

Notably, the Weibull model fitted to the failure data also has a shape parameter of 1, further supporting the notion of a constant failure rate.

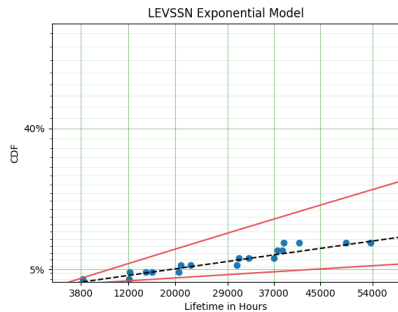


**Figure 26:** Exponential model fit for the failure scenario LEVSSN.

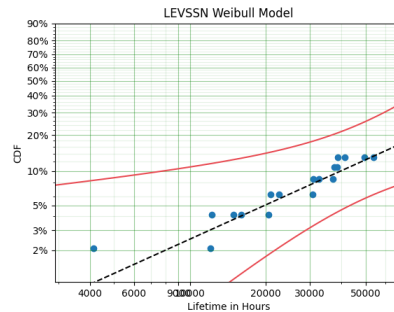


**Figure 27:** Weibull model fit for the failure scenario LEVSSN.

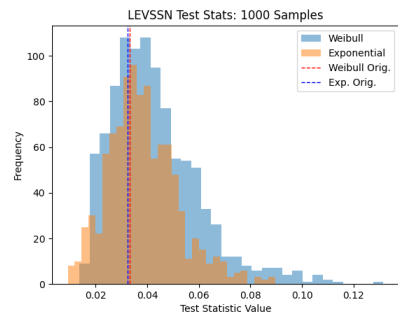


**Figure 28:** Histogram of TS values for failure scenario LEVSSN.

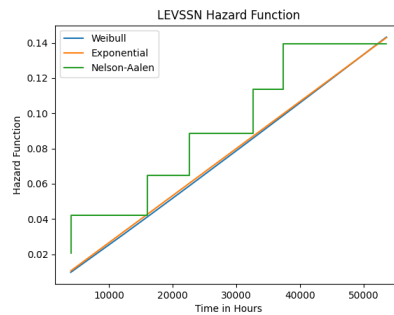


**Figure 29:** Hazard function for failure scenario LEVSSN.

**3-LBGC Analysis** For the 3-LBGC scenario, the statistical indicators in Table 8, such as the AIC, do not show a clear preference for one model over the other, graphical evidence provides additional insights.

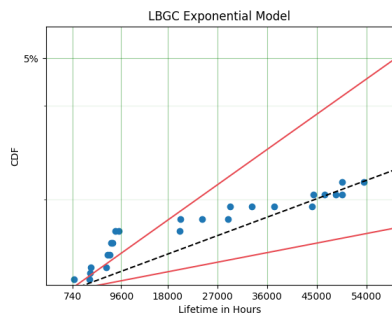
Figures 30 and 31 display the fit of the Exponential and Weibull models, respectively, to the observed data in the 3-LBGC scenario. The Exponential model appears to have limitations in accurately representing lifetimes below 8700 hours, with some estimates lying outside the 95% confidence interval. The Weibull model, in contrast, displays a tighter fit, encapsulating all lifetimes within the 95% confidence bounds. However, caution should be exercised in overinterpreting the superiority of the Weibull model based solely on this visualization.

Figure 32, a density plot derived from bootstrap samples, highlights the distributions

of the test statistic values for both models. While the Weibull model often registers lower TS values, indicating a closer alignment with the bootstrapped data, it's essential to note the overlap in the TS distributions of the two models. This overlap suggests that, based on the test statistic alone, neither model is definitively superior.

The survival rate comparison in Figure 33 further emphasizes the nuanced differences between the two models. The Weibull model appears to align more closely with the empirical hazard function, derived using the Nelson-Aalen estimator, particularly at specific intervals.

Additionally, the shape parameter of 0.58 of the Weibull model, as presented in 8 indicates that the failure rate is decreasing over time [16]. The hazard function itself appears to show a decreasing steepness in time, a decrease of cumulative hazard function steepness indicates a decreasing failure rate over time [16]. inligh with the shape parameter of the fitted model.



**Figure 30:** Exponential model fit for the failure scenario LBGC.

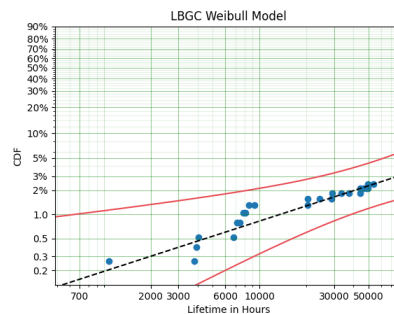


**Figure 31:** Weibull model fit for the failure scenario LBGC.

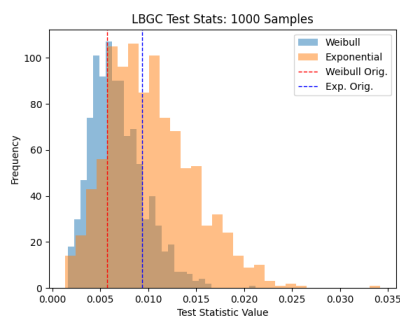


**Figure 32:** Histogram of TS values for failure scenario LBGC.

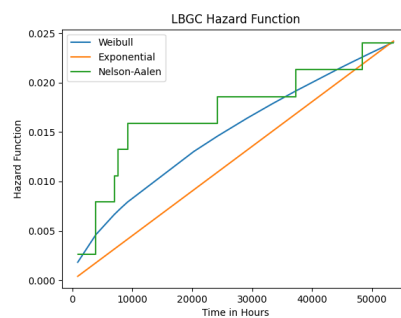


**Figure 33:** Hazard function for failure scenario LBGC.

**7-LBQENM Analysis** For the 7-LBQENM scenario, the Weibull model exhibits a different trend compared to the Exponential model, a fact supported by the AIC value in Table 8. The discrepancy between the two models is further evidenced in the Cumulative Distribution Function (CDF) plot, displayed in Figure 35.

The density plot presented in Figure 36 shows less overlap between the test statistic distributions for the Exponential and Weibull models, unlike the 11-LEDGSN scenario. This divergence implies that the models offer different fits to the 7-LBQENM data.

As depicted in Figure 37, a stark contrast is evident between the cumulative hazard functions of the Exponential and Weibull models. The Exponential model's cumulative hazard function shows a consistent linear increase over time, aligning with its presupposition of constant failure rates. In contrast, the Weibull model's cumulative hazard function displays a variable rate of increase. Notably, the function's slope lessens over time, which resonates with a shape parameter of 0.4, as documented in Table 7. This non-linear behavior of the Weibull cumulative hazard function indicates variable failure rates, corroborated by the empirical cumulative hazard data. These observations suggest a dynamic failure rate pattern over time, which is more comprehensively captured by the Weibull model due to its ability to account for changing failure rates—an aspect that the Exponential model, with its assumption of constancy, fails to encapsulate.

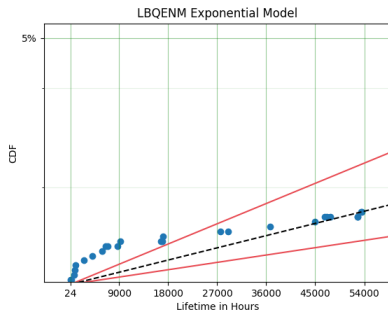


**Figure 34:** Exponential model fit for the failure scenario LBQENM.

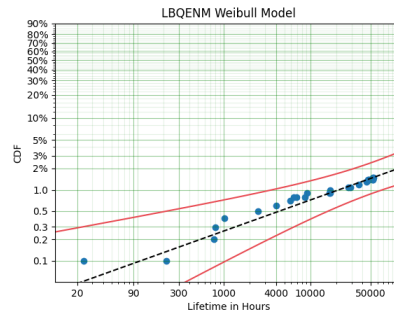


**Figure 35:** Weibull model fit for the failure scenario LBQENM.

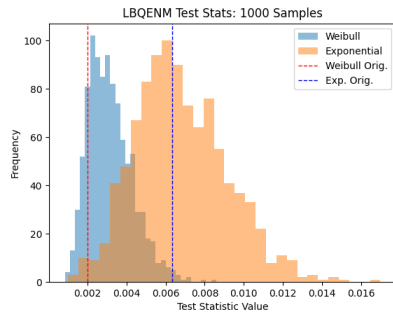


**Figure 36:** Histogram of TS values for failure scenario LBQENM.

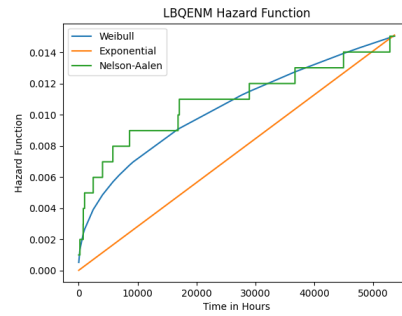


**Figure 37:** Hazard function for failure scenario LBQENM.

## 5.4 Summary

The research sub-question “Does a time-variable failure rate model provide a statistically better fit to the existing data than a constant rate model?” is addressed by comparing the Weibull and Exponential models across various failure scenarios using the framework suggested in Chapter 4. The analysis reveals that the Weibull model does not consistently offer a superior fit compared to the Exponential model based on the existing data.

A key determinant in model selection is the AIC, which suggests near equivalence in model performance with no clear preference for most failure scenarios, as the difference in AIC values is within 2 points. Notable exceptions where AIC indicates a preference are scenarios 6-LBPRNI and 10-LBSWB favoring the Exponential model, and 7-LBQENM showing a preference for the Weibull model.

Statistical hypothesis testing fails to decisively reject either model across the scenarios, implying that within a 95% confidence level, both models are statistically viable for describing the failure data. This outcome is supported by p-values that do not fall below the significance threshold of 0.05.

Graphical evaluation of the models’ fit to the data provides additional insights. For seven out of the seventeen failure scenarios reviewed, namely 2-LBDINM, 3-LBGC, 5-LBPRC, 7-LBQENM, 11-LEDGSN, 14-LEVSSN, and 16-LHGR, the model appear visually to fit adequately. Particularly for scenarios 3-LBGC, 5-LBPRC, 7-LBQENM, and 16-LHGR, the Weibull model, with its time-varying failure rate feature, provides a more accurate description of failure behavior. Especially, Weibull more closely follows the empirical cumulative hazard function. In contrast, scenario 11-LEDGSN exhibits a pattern of increasing failures towards the end of the observation period that neither model captures effectively, suggesting an anomaly or a wear-out effect. The remaining scenarios demonstrate that both the Weibull and Exponential models are comparably effective, both seeming to approximate the empirical cumulative hazard function,

which appears to be linearly increasing. In these cases, the Weibull model approaches the characteristics of the Exponential model as its shape parameter nears 1.

Correlating the scenarios that exhibit appropriate model fits visually, as identified in Appendix H, with the principal characteristics of their lifetime datasets presented in Table 9, it becomes evident that datasets with a higher average number of failures typically correspond to a more satisfactory fit from the models compared to those characterized by a lesser frequency of failure instances.

The implications of these results are multifaceted. The Weibull model's comparable or superior performance in some scenarios underscores its potential in depicting complex failure dynamics. Its added flexibility with an additional parameter makes it a robust option for reliability modeling, particularly beneficial for strategies requiring adaptive maintenance and enhanced predictive risk assessments. Nevertheless, the Exponential model's simplicity and convenience remain valuable, especially when data is limited. In scenarios where both models perform similarly, it could reflect either insufficient data differentiation or inherently constant failure rates. Therefore, the choice between models may depend on the specific scenario, with the Weibull model offering greater flexibility and the Exponential model providing a simpler alternative.

#### 5.4.1 Implications

The analysis conducted does not uniformly support the superiority of the Weibull model over the Exponential model for all failure scenarios. This uncertainty in model efficacy indicates that the appropriateness of a time-variable failure rate model like Weibull versus a constant rate model like Exponential may depend on the nuances of the specific data set. The findings imply that when failure rates are not evidently variable, the additional complexity of the Weibull model may not yield significant benefits over the simpler Exponential model. Conversely, when there is an indication of non-constant failure rates, the Weibull model's extra parameter, which allows for the adjustment of the failure rate over time, could potentially offer a more nuanced understanding of the system's reliability.

#### 5.4.2 Recommendations for Future Research

Future research should consider the following strategies to enhance the robustness of reliability model comparisons:

- **Data Expansion:** More comprehensive datasets with an increased number of failure events could provide a stronger statistical basis for model evaluation and could lead to more conclusive evidence regarding the appropriateness of different models.
- **Model Exploration:** Given the limitations of the Weibull and Exponential models in certain scenarios, such as 11-LEDGSN, investigation into alternative

models that capture wear-out effects or non-standard failure patterns is recommended. These models should be able to account for complexities not addressed by the models fitted in this thesis.

- **Methodological Advancements:** For datasets characterized by low variance, the development of specialized methodologies is advisable. Extreme value analysis, or similar statistical methods, may offer more suitable insights for datasets that include infrequent or outlier failure events.

Enhanced datasets and refined analytical methods could improve the accuracy of statistical comparisons, providing clearer evidence for or against the superiority of time-variable failure rate models over constant rate models, directly addressing the research sub-question.

## 6 Discussion and Conclusion

### 6.1 Discussion

The study centered around the research question: “Is the assumption of constant failure rates over time for storm surge barriers valid?” The analysis presents a nuanced picture: some data supports the assumption, while other data contradicts it, indicating variable failure rates. The evaluation of Weibull and Exponential models, in the context of storm surge barrier failure rates, indicates that no single model adequately captures the nuances across all observed failure instances. Therefore, it is not feasible to categorically affirm the constancy of failure rates for these structures.

Literature supports the presence of variable failure rates in safety-critical systems, a finding which resonates with the observations from the current analysis that shows a Weibull model more aptly describing certain failure scenarios. In the majority of the failure scenarios analyzed, the Weibull and Exponential models performed comparably, as reflected by their AIC scores with minimal differences. This similarity in performance does not substantiate a clear preference for either model in those scenarios. However, one scenario notably diverged, with the Weibull model’s AIC score significantly lower, suggesting a better fit and pointing to the possibility of variable failure rates in that instance.

The analysis, informed by p-values from hypothesis testing, does not provide clear evidence to reject the Exponential model or the Weibull model conclusively across the studied scenarios. In an ideal analysis, if the Exponential model is unsuitable, it would be rejected, leaving the Weibull model as the more appropriate choice if it is not rejected, and vice versa. This kind of outcome would offer clear evidence as to which model better characterizes the data for a specific scenario. However, the study does not demonstrate such a definitive outcome. Therefore, it is not possible to firmly support the hypothesis of constant failure rates, nor to unambiguously affirm that failure rates are variable for storm surge barriers. The ambiguous p-values suggest that neither the dataset at hand nor the statistical methods applied are sufficient to arrive at a conclusive judgment, allowing for the possibility that both constant and variable failure rates could be present.

Visual inspection of the SVKO component data provides additional insight into failure rate trends. Out of seventeen scenarios, seven demonstrate a good visual fit with the proposed models. Scenarios 2-LBDINM and 14-LEVSSN, in particular, show linear trends, suggesting the potential for constant failure rates, as both the Exponential and Weibull models indicate.

Conversely, scenarios such as 3-LBGC, 5-LBPRC, 7-LBQENM, and 16-LHGR, exhibit non-linear trends, implying variability in failure rates. The stark outlier is scenario 1-LEDGSN, where the observed increase in failure rate is not captured by either model, challenging their predictive accuracy.

In summary, the examination of storm surge barrier failure rates through this re-

search reveals that the assumption of constant failure rates may not hold universally across different scenarios. The inconclusive evidence from statistical tests, the comparative analysis of the Weibull and Exponential models, and the visual assessment of failure data collectively suggest that both constant and variable failure rates may exist in different components.

## 6.2 Conclusion

The research into the consistency of failure rates over time for storm surge barriers presents a nuanced view of predictive modeling in this area. The analysis comparing Weibull and Exponential models does not conclusively favor one over the other. This suggests that flexibility in model selection based on specific circumstances could be more appropriate than a uniform approach.

The study hints at the possibility that a generic approach to failure rate prediction might not capture the full complexity of the issue. The observed low variability when applying a single model across the board indicates that a strategy tailored to the individual characteristics of each component may offer advantages. Such a strategy would involve selecting the most fitting model that accounts for the unique failure patterns over time, potentially leading to improved maintenance planning and reliability of barriers. This nuanced modeling could accommodate variations in failure rates, enhancing the accuracy of predictions, which is essential for effective flood risk management.

In conclusion, the research contributes preliminary insights into the failure patterns of storm surge barriers and points towards the need for further investigation into more refined and potentially adaptive modeling techniques. This direction may be important for advancing our understanding of flood defense reliability.

## 6.3 Contributions

The presented research advances the understanding of storm surge barrier reliability by examining the behavior of failure rates over time, rather than assuming their constancy. It merges theoretical analysis with practical application, resulting in several key contributions:

- **Statistical Framework:** A framework is introduced for the comparative analysis of constant and variable failure rates using Exponential and Weibull distributions. The framework utilizes standard statistical tests, including the Kolmogorov-Smirnov test, and incorporates a version of bootstrapping designed to manage censored data within the lifespan of storm surge barrier components.
- **Code Repository Release:** To support the research community, a code repository has been made publicly available. This repository aids in the creation of databases and interfaces for statistical analysis of component data, facilitating standardization and collaboration within the field of reliability engineering.

- **Methodology for Closure Data Analysis:** An approach to analyzing closure data is detailed in an appendix, which could be instrumental for evaluating the reliability of storm surge barriers. The corresponding code repository provides standardized procedures for data handling and analysis, contributing to methodological consistency in this research area.

## 6.4 Recommendations

To further the applicability of theoretical models to real-world scenarios, the study proposes the following recommendations:

- **Sustained and Comprehensive Data Collection:** It is suggested that data collection should be both extensive and ongoing, with an emphasis on enhancing the detail and accuracy of data for improved reliability assessments. Strategies may include developing databases that capture detailed malfunction records for storm surge barrier components. The current system employed by the SVKO is a strong model that could be further augmented by including the time to replacement data for each malfunction record, which would enrich the information regarding component lifetimes.
- **Further Evaluation of Failure Rates:** In light of observed variations in failure rates within limited datasets, it is recommended to employ the available data to assess failure rate dynamics. This could involve empirical analysis of cumulative hazard functions or the application of models, such as the Weibull distribution, to gain insights into failure patterns over time. Furthermore, enhancing the recording of individual components and their lifetimes would contribute to a deeper understanding of failure rates and maintenance needs.
- **Adoption of Malfunction Recording Systems:** Other storm surge barriers are encouraged to adopt malfunction recording systems akin to that used by the SVKO, BMS+. Such systems are invaluable, not only for the data they provide, also for the potential improvements they can prompt in maintenance practices. A comprehensive database that includes timing and details of replacements would offer significant benefits for predictive maintenance and reliability forecasting.

### 6.4.1 Future Research Strategies

The study indicates several avenues for future research:

- **Data Expansion:** Broadening the data collection to encompass more complete operational data can enhance the potential insights. Such data should be available for the SVKO, assuming that BMS+ maintenance management software is still in active use.
- **Model Exploration:** The exploration of statistical models that can accommodate complex and non-standard failure behaviors, such as those due to wear-out

effects, is recommended to supplement Exponential and Weibull models in the analysis of component lifetimes.

- **Methodological Advancements:** Advancing methodologies capable of analyzing data with infrequent failures or high variability is encouraged, potentially involving the application of extreme value analysis or other sophisticated statistical techniques that cater to the prediction of rare, significant failure events.

## References

- [1] Nederlandse waterwet, 2017. Accessed on 2023-03-16.
- [2] BAKKER, A., MOOYAART, L., HAMERSLAG, E. J., AND VAN GIJZEN, L. Towards probabilistic asset management of storm surge barriers under rapidly changing circumstances. Tech. rep., EasyChair, 2022.
- [3] BOU-HAMAD, I., LAROCQUE, D., AND BEN-AMEUR, H. A review of survival trees. *Statistics Surveys* 5 (2011), 44–71.
- [4] CASTELEIJN, A., BREE, B. v., DELHEZ, R., BAKKER, A., PLICHT, N. v. d., AND OVERMAN, J. Standaard faalkansen voor frequent sluitende keermiddelen, 2019.
- [5] CASTELEIJN, A., AND VAN BREE, B. Werkwijze bepalen kans op niet sluiten per sluitvraag met scoretabellen, 2017.
- [6] CROW, L. H. Reliability analysis for complex repairable systems. Tech. Rep. 6, 1974.
- [7] CROW, L. H. Confidence intervals on the reliability of repairable systems. In *Annual Reliability and Maintainability Symposium 1993 Proceedings* (1993), IEEE, pp. 126–134.
- [8] DE GROOT, P. Data-update 2016: Faalkansanalyse stormvloedkering oosterschelde. Technical Report 23755/16.140356, Nuclear Research & consultancy Group VOF (NRG), mar 2017.
- [9] EPEMA, J. H. Closure Reliability Database API Software, Sept. 2023.
- [10] EPEMA, J. H. Component Lifetime Database API Software, Sept. 2023.
- [11] GREENWOOD, M. C. *Intermediate Statistics with R*. Montana State University Open Education Resource LibreTexts Project, Culbertson Hall, 100, Bozeman, MT 59717, USA, 2014. Accessed on 2023-10-23.
- [12] KHAROUBI, Y., VAN DEN BOOMEN, M., HERTOOGH, M., AND VAN DEN BOGAARD, J. Foundation for risk-based asset management for storm surge barriers. In *Life-Cycle of Structures and Infrastructure Systems*, 1st ed. CRC Press, 6000 Broken Sound Parkway, NW, (Suite 300), 2023, pp. 3214–3221.
- [13] KUIJKEN, W. Deltaprogramma 2015, 9 2015. Accessed on 2023-06-04.
- [14] LAMBERT, P. C., ROYSTON, P., ET AL. Flexible parametric alternatives to the cox model. *UK Stata User Group 2009* (2009).
- [15] LANTRONIX. Component lifespan considerations for industrial iot oems, 2023. Accessed on 2023-10-12.

- [16] LAWLESS, J. F. *Statistical Models and Methods for Lifetime Data*, 2nd ed., vol. 362. John Wiley & Sons, 2011.
- [17] LEMOINE, N. P. Moving beyond noninformative priors: why and how to choose weakly informative priors in bayesian analyses. *Oikos* 128, 7 (2019), 912–928.
- [18] LITTLEWOOD, B., ASCHER, H., AND FEINGOLD, H. Repairable systems reliability: Modelling, inference, misconceptions and their causes. *Journal of the Royal Statistical Society. Series A (General)* 148, 2 (1985), 165.
- [19] MAARTEN, A. v. Guidelines on performance-based risk analyses (pra) – enabling asset management based on system performance. Technical Report 5333, ProBo Support Desk, Rijkswaterstaat, March 2018. Accessed on 2023-10-12.
- [20] MINISTERIE VAN INFRASTRUCTUUR EN WATERSTAAT, R. R. Bescherming tegen het water, 2022. Accessed on 2023-06-08.
- [21] MINISTERIE VAN INFRASTRUCTUUR EN WATERSTAAT, R. R. De deltawerken, 2022. Accessed on 2023-08-15.
- [22] MOUBRAY, J. *Reliability-centered Maintenance*, 2nd ed. Industrial Press Inc., 2001.
- [23] POPOVA, E., YU, W., KEE, E., SUN, A., RICHARDS, D., AND GRANTOM, R. Basic factors to forecast maintenance cost and failure processes for nuclear power plants. *Nuclear Engineering and Design* 236, 14-16 (2006), 1641–1647.
- [24] REN, J.-J. Goodness of fit tests with interval censored data. *Scandinavian Journal of Statistics* 30, 1 (2003), 211–226.
- [25] RIJKSWATERSTAAT. Alarmoproepen osk, 2023. Accessed on 2023-07-05.
- [26] RONGEN, G., AND MAASKANT, B. Systeemanalyse hollandsche ijssel: Uitwerking conform boi uitgangspunten. Tech. Rep. PR3925.10, HKV LIJN IN WATER, 4 2019. Accessed on 2023-01-19.
- [27] STRACHAN, R. W., AND DIJK, H. K. v. Bayesian model selection with an uninformative prior\*. *Oxford Bulletin of Economics and Statistics* (Dec 2003).
- [28] TOBIAS, P., AND TRINDADE, D. *Applied Reliability*, 3rd ed. Taylor & Francis, 2011.
- [29] TSANG, A. H. Condition-based maintenance: tools and decision making. *Journal of quality in maintenance engineering* 1, 3 (1995), 3–17.
- [30] TUYL, F., GERLACH, R., AND MENGERSEN, K. The rule of three, its variants and extensions. *International statistical review* 77, 2 (2009), 266–275.
- [31] VAN DEN BOGAARD, J., AND VAN AKKEREN, K. *Guidelines for Risk-based Operations and Maintenance*, 1st ed. Drukkerij Rekafa bv, 2012. Copyright: RWS/Steunpunt ProBO.

- [32] VEENDORP, M., AND NIEMIJER, J. Leidraad kunstwerken. Tech. Rep. L15 DWW2003-059, May 2003. © 2003 Rijkswaterstaat.
- [33] WECKMAN, G. R., SHELL, R., AND MARVEL, J. Modeling the reliability of repairable systems in the aviation industry. *Computers & Industrial Engineering* 40, 1-2 (2001), 51–63.

## A Maintenance Groups SVKO

This appendix provides an overview of the maintenance groups associated with the Storm Surge Barrier Control System (SVKO). The groups included in the table are specifically relevant to the reliability of the storm surge barrier's closure mechanism. Each entry contains details about the total number of failures, the number of failures that are relevant to the closure reliability, and the total components within each maintenance group. For a comprehensive understanding, see the original report [8].

**Table 10:** Records of Maintenance Groups [8]

Maintenance Group	Description	Failures (No.)	Relevant Failures (No.)	Components (No.)
B-DI	Digital input module	7	6	1786
B-DO	Digital output module	0	0	704
B-DS	S16 Switch (Safety Operation)	0	0	3
B-GC	Graycode sensor	12	9	372
B-GC-C	Graycode sensor CCF 1v3 North or South	1	1	124
B-GV	Stabilized power supply VSL	0	0	6
B-GV-T	General stabilized power supply VSL	0	0	1
B-KL	'Safe closing line' cable	1	1	6
B-KL-T	General 'Safe closing line' cable	0	0	1
B-PM	I-O bus/network communication controller/module	16	6	260
B-PM-T	General I-O bus/network communication controller/module	6	4	248
B-QE	QE Module (AND gates)	10	10	992
B-QE-T	QE-22 (2 out of 3 selection)	6	5	62
B-QS	QESI Module	0	0	124

Continued on next page

**Table 10 Continued**

Maintenance Group	Description	Failures (No.)	Relevant Failures (No.)	Components (No.)
B-QS-T	Optocouplers for safe closing line	0	0	62
B-SF	LCC Software	2	0	62
B-SS	Safety operation key switch	0	0	1
B-SW	Switch	3	3	256
E-ATD	ATD (=A02+00*CB2:23-U130)	0	0	1
E-BC	Control signal from LC4 to 10kV Transformer field	2	1	17
E-BT	Battery (Transformer field)	6	0	63
E-DG	Diesel generator	8	3	10
E-DG:AKD	Diesel generator control cabinets	14	7	30
E-DG:ALG	General diesel generator	6	3	40
E-DG:BAT	Diesel generator battery	0	0	10
E-DG:DB	Diesel generator day tank + fuel pump	4	0	10
E-DG:GEN	Diesel generator generator	2	2	10
E-DG:MCP	Diesel generator engine control panel	1	1	10
E-DG:MOT	Diesel generator engine	13	5	10
E-DG:VJ	Diesel generator fan + radiator	1	0	20
E-GRS	Charging rectifier (24 V)	20	9	63
E-KLL	Low voltage cables (400V)	0	0	13
E-KLM	Medium voltage cable (10 kV)	0	0	10
E-MCK	Switch (400V) Barrier	1	0	26

Continued on next page

**Table 10 Continued**

Maintenance Group	Description	Failures (No.)	Relevant Failures (No.)	Components (No.)
E-MCTEB	Switches (400V) Topshuis Own Business	0	0	4
E-MCTFF	Switches (400V) Topshuis Flip-Flop	0	0	2
E-RD	Diesel switching re- lay (NSTA box)	0	0	1
E-RHK	Relay	1	1	1240
E-RHK-T	General relay	0	0	62
E-RL1	Low voltage rail (400V) CB1:21 and CB1:27	0	0	2
E-RLE	Low voltage rail (400V) Topshuis Own Business	0	0	2
E-RLK	Low voltage rail (400V) Barrier	2	1	79
E-RLS	Control voltage rail (24V)	0	0	62
E-RLT	Low voltage rail (400V) Topshuis CBB 23	0	0	1
E-RMT	Medium voltage rail (10kV Top- shuis)	0	0	5
E-RN	Down relay	0	0	1
E-RS	Medium voltage re- lease relay	0	0	6
E-SR	Load switch Q020	0	0	17
E-SVH	24V fuse auxiliary voltage	0	0	17
E-TFD	Diesel transformer	1	0	10
E-TFK	Barrier transformer	3	0	17
E-TFT	Topshuis trans- former	1	0	4
E-VM1	Motor-operated switch TRRR (10 kV Barrier)	1	0	8
E-VM2	Motor-operated switch TRRb (10 kV Barrier)	4	2	42

Continued on next page

**Table 10 Continued**

Maintenance Group	Description	Failures (No.)	Relevant Failures (No.)	Components (No.)
E-VM3	Motor-operated switch TRRo (10kV Roompot-sluis)	1	0	3
E-VMD	Motor-operated switch (10 kV Diesels)	34	2	10
E-VMT	Motor-operated switch (10 kV Topshuis)	23	4	20
E-VSL	Delta Nuts Switch	2	1	1
H-BG	Hydraulic tank compensator (POS50)	0	0	65
H-DV	Pressure control valve (POS16)	0	0	130
H-FL	Filter (POS05/13)	18	0	260
H-GK	Controlled check valve Cylinder (POS35)	2	0	124
H-KC	Ball valve Cylinder (POS21/22)	5	0	260
H-MP	Pump (POS02)	13	0	130
H-MPB	Motor control cabinet (MBS)	1	0	130
H-NK	Emergency choice switch	4	0	130
H-NK-T	Emergency hydraulic choice	1	0	62
H-SL3	Hose 30-33 (POS75)	0	0	124
H-SL6	Hose 61	0	0	130
H-SM	Flow control valve (POS34)	1	0	124
H-SV5	Solenoid valve POS15	9	0	130
H-SV7	Solenoid valve POS17	8	1	130
H-SV8	Solenoid valve POS38	15	0	124

Continued on next page

**Table 10 Continued**

Maintenance Group	Description	Failures (No.)	Relevant Failures (No.)	Components (No.)
H-TKT	Check valve (POS04/43/47)	3	0	390
H-VT	Tank (POS60)	3	0	65
H-VV2	Safety valve POS12	0	0	130
H-VV9	Safety valve POS19	1	0	130
H-ZC	Cylinder	7	0	124
L-LCC	Lightning strike LCC	0	0	62
L-VSL	Lightning strike VSL	0	0	1
N-BP	Backplane	0	0	5
N-CP	CPU	0	0	5
N-DI	Digital input module	0	0	4
N-DO	Digital output module	0	0	4
N-GV	24V D.C. NSTA	1	0	2
N-NS	Level measurement	0	0	6
N-PL	Valves / pipe pile inlets	0	0	2
N-PM	Power module	0	0	5
N-RI	RS232 module	0	0	6
N-RLS	NSTA 24 volt distribution	0	0	2
N-SF	Software Inwin units	0	0	1
N-US	UPS NSTA	1	0	2

## B Type-codes SVKO

This appendix provides an overview of the Type Codes associated with the Storm Surge Barrier Oosterschelde. The Type codes included in the table are specifically relevant to the reliability of the storm surge barrier's closure mechanism. Each entry holds the Code and the description [8].

**Table 11:** Type Codes and their English Descriptions

Type Code	Description (Translated to English)
LBBL	Failure Frequency Buslock LCC (LC-1,2,3)
LBBO	Failure Frequency Bus Interruption LCC (LC-1,2,3)
LBDI <sub>m</sub>	Failure Frequency Digital Input Module (noticeable)
LBDI <sub>nm</sub>	Failure Frequency Digital Input Module (not noticeable)
LBDO <sub>m</sub>	Failure Frequency Digital Output Module (noticeable)
LBDO <sub>nm</sub>	Failure Frequency Digital Output Module (not noticeable)
LBDS	Failure Frequency Push-button Switch
LBGC	Failure Frequency Graycode Sensor 1 North Not Functioning
LBGV	Failure Frequency Stabilized Supply VSL (-35V/+35V)
LBKLA	Failure Frequency Earth Short Circuit Safe Close Line
LBKLO	Failure Frequency Interruption Safe Close Line
LBPRC	Failure Frequency Processor Module
LBPRNI	Failure Frequency Processor Module Network Interface
LBQEn <sub>m</sub>	Failure Frequency QE22 Module Fails Not Noticeably
LJQEn <sub>m</sub>	Failure Frequency QE22 Module Fails Not Noticeably, Tested Annually
LBQSn <sub>m</sub>	Failure Frequency QESI Module/Channel Not Noticeable
LBREL	Failure Frequency Relay Does Not Switch
LBSS	Failure Frequency Key Switch
LBSWAm	Failure Frequency Switch Type A in LCC in the Middle of a Section
LBSWB	Failure Frequency Switch Type B in LCC
LEBT	Failure Frequency 24V Batteries in Electrocontainer
LEDGSN	Failure Frequency Diesel Generator Does Not Start
LEDGSV	Failure Frequency Diesel Generator Stops Prematurely
LEDSSN	Failure Frequency Switch of Diesel Generator Does Not Close
LEEBOM	Failure Frequency Switching to Own Operation Fails
LEKLL	Failure Frequency Low Voltage Coupling Cable
LEKLRG	Failure Frequency 10kV Cables Roompot White or Black, Ground Segment
LEKLRK	Failure Frequency 10kV Cables Roompot White or Black, Conduit Segment
LEKLSG	Failure Frequency 10kV Cables Hammen/Schaar White or Black, Ground Segment

Continued on next page

**Table 11 Continued**

<b>Type Code</b>	<b>Description (Translated to English)</b>
LEKLSK	Failure Frequency 10kV Cables Hammen/Schaar White or Black, Conduit Segment
LEMCSN	Failure Frequency Low Voltage Switch Does Not Close
LEMCSO	Failure Frequency Low Voltage Switch Opens Spontaneously
LERA	Failure Frequency Rail Earth/Fault
LERA24	Failure Frequency 24V Rail (Room A2) in Electrocontainer to Earth
LERA38	Failure Frequency 380V Rail Transformer Container to Earth
LERARW	Failure Frequency 10kV Rails Roompot White to Earth
LERARZ	Failure Frequency 10kV Rails Roompot Black to Earth
LERASW	Failure Frequency 10kV Rails Hammen/Schaar White to Earth
LERASZ	Failure Frequency 10kV Rails Hammen/Schaar Black to Earth
LESD	Failure Frequency Fuse (open)
LESRL	Failure Frequency Disconnect Switch Q020 Transformer Container Does Not Open
LESRSO	Failure Frequency Disconnect Switch Q020 Transformer Container Opens Spontaneously
LESS	Failure Frequency No Control Signal from LC4 to 10kV A01 Transformer Field
LETR	Failure Frequency Transformer Barrier (in operation)
LETRDG	Failure Frequency Transformer Diesel/Switching Station Defective
LEVSON	Failure Frequency Delta Switch Does Not Open
LEVSSN	Failure Frequency Power Switch Does Not Close
LEVSSO	Failure Frequency Power Switch Opens Spontaneously
LHBG	Failure Frequency Ball Valve Leakage
LHDV	Failure Frequency Pressure Control Valve Does Not Regulate
LHFL	Failure Frequency Filter Blocked
LHGKON	Failure Frequency Controlled Check Valve Does Not Open
LHGKSN	Failure Frequency Controlled Check Valve Does Not Close
LHGR	Failure Frequency Charging Rectifier Not Functioning
LHHKOM	Failure Frequency Hand Valve Not Switchable
LHMPSN	Failure Frequency Pump Does Not Start
LHMPSV	Failure Frequency Pump Stops Prematurely
LHOV	Failure Frequency Hydraulically Controlled Valve Does Not Open
LHRA24	Failure Frequency Earth Short Circuit 24V DC Distribution
LHRA38	Failure Frequency Earth Short Circuit 380V AC Distribution
LHSL	Failure Frequency Hose Leak/Break
LHSM	Failure Frequency Flow Control Valve Blocked
LHSTK	Failure Frequency Check Valve Does Not Open
LHSVS	Failure Frequency Solenoid Control Valve Switches Spontaneously
LHSVT	Failure Frequency Solenoid Control Valve Does Not Switch

Continued on next page

**Table 11 Continued**

<b>Type Code</b>	<b>Description (Translated to English)</b>
LHVT	Failure Frequency Tank Leakage
LHVVOS	Failure Frequency Pressure Protection Opens Spontaneously
LHZCLK	Failure Frequency Cylinder Not Functioning (Leakage)
LHZCMS	Failure Frequency Cylinder Not Functioning (Blocking)
LNBP	Failure Frequency Backplane
LNCA	Failure Frequency Carrier
LNCPI	Failure Frequency CPU Fails
LNCPPM	Failure Frequency CPU Fails Noticeably
LNCPPN	Failure Frequency CPU Fails Not Noticeably
LNDIMI	Failure Frequency DI Module, Total, Inwin
LNDIR	Failure Frequency DI Module, Process, Test Relay
LNDIV	Failure Frequency DI Module, Process, Full Test
LNDOR	Failure Frequency DO Module, Test Relay
LNDOV	Failure Frequency DO Module, Full Test
LNMM	Failure Frequency Memory
LNPM	Failure Frequency Power Module
LNRA24	Failure Frequency NSTA 24 Volt Distribution
LNRI	Failure Frequency RS232 Module
LNRS	Failure Frequency Relay Does Not Close
LNRSMS	Failure Frequency Medium Voltage Relay Does Not Close
LNUSM	Failure Frequency UPS Fails Noticeably
LNUSN	Failure Frequency UPS Fails Not Noticeably

## C Unified Modeling Language

Unified Modeling Language (UML) for classes is used to model the data. In UML applied to data modelling a class is an object with a name and attributes. The class name is based on the data type. The class attributes are the characteristics of the data type. Every table in the database is essentially a class. Its attributes are the table columns. The class objects are the table records.

There exist multiple data relations. The two relevant types are aggregations and compositions. An example is presented in figure 38. The first is an aggregation. Where one object owns the other but both can exist without the other. The second is a composition. In this case, an object is part of another and cannot exist without the parent.

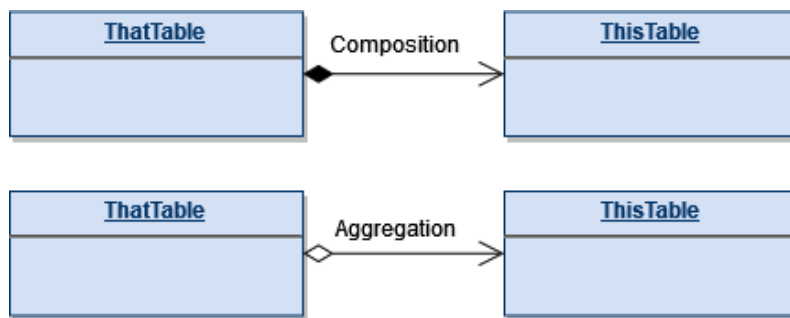


**Figure 38:** Data relations

The multiplicity of tables details the records of a table that take part in a relationship between tables.

**Table 12:** Multiplicity table

Symbol	Meaning
1	Exactly 1
0..1	0 or 1
1..*	1 or more
0..*	0 or more

## D Type-codes: Detailed Breakdown

In Table 6, several abbreviations are used to describe different failure scenarios and components. Below, we detail each abbreviation and provide a brief description of the respective scenarios and components.

**Table 13:** Detailed Descriptions of Type Codes

Type Code	Detailed Description
LBDIM	Failure digital input module (Observable): Refers to observable failures occurring in the digital input module, which is a part of the control system where digital signals are inputted.
LBDINM	Failure digital input module (Unobservable): Pertains to unobservable failures in the digital input module, indicating scenarios where the failure is not immediately noticeable or detectable.
LBGC	Bug gray code module (Unobservable): Indicates unobservable issues within the gray code module, a unit responsible for handling gray code, a binary numeral system.
LBKLO	Interruption safely closure cable (Unobservable): Involves unobservable interruptions in the safety closure cable, potentially affecting the secure closure of systems or components.
LBPRC	Failure I-O digital module (Observable): Refers to observable failures in the Input-Output (I-O) digital module, affecting the proper functioning of digital signal processing.
LBPRNI	Failure network interface I-O module (Observable): Indicates observable failures occurring in the network interface of the I-O module, which could affect network communications.
LBQENM	Failure QE module (Unobservable): Pertains to unobservable failures in the QE module, where QE refers to a specific type of module in the system (the exact function should be detailed according to the system specifics).
LBREL	Failure relay (Unobservable): Involves unobservable failures in relay components, which are electrically operated switches.
LBSWAM	Computer bug switch type A in mid section (Observable): Refers to observable computer bugs affecting type A switches in the mid section of the system, potentially affecting the switching operations.
LBSWB	Computer bug switch type B (Observable): Indicates observable computer bugs affecting type B switches, which can have implications on the performance of the switch.
LEDGSN	Failure start diesel generator (Unobservable): Pertains to unobservable failures occurring during the start-up of diesel generators.
LEDSSN	Failure motor controlled switch (Unobservable): Indicates unobservable failures in motor-controlled switches, affecting the operation of motors in the system.

Continued on next page

**Table 13 Continued**

<b>Type Code</b>	<b>Detailed Description</b>
LERA38	Failure 380V transformer container earth leakage (Observable): Refers to observable failures due to earth leakage in 380V transformer containers, a serious issue that can affect the safety and functionality of the electrical system.
LEVSSN	Failure motor controlled switch of 10kV transformer (Unobservable): Pertains to unobservable failures in the motor-controlled switches of 10kV transformers, which can affect the proper functioning of the transformers.
LESS	Signal failure local computer to 10kV transformer field (Unobservable): Indicates unobservable signal failures between the local computer and the 10kV transformer field, which can affect the monitoring and control of the transformer field.
LHGR	Function failure charging rectifier (Observable): Refers to observable functional failures in the charging rectifier, a device that converts AC voltage to DC voltage.
LHSV T	Switching failure solenoid (Observable): Indicates observable switching failures in solenoids, which are a type of electromagnet where the wound wire is in tight coils, creating a magnetic field when electricity is passed through it.

## E Hessian Matrix

The Hessian matrix  $\mathbf{H}$  is a square matrix comprising the second-order partial derivatives of a function, usually denoted as  $\mathcal{L}(\boldsymbol{\theta})$  in the context of MLE. For a function with  $p$  parameters, the Hessian is a  $p \times p$  matrix defined as:

$$\mathbf{H}(\boldsymbol{\theta}) = \begin{pmatrix} \frac{\partial^2 \mathcal{L}}{\partial \theta_1^2} & \frac{\partial^2 \mathcal{L}}{\partial \theta_1 \partial \theta_2} & \cdots & \frac{\partial^2 \mathcal{L}}{\partial \theta_1 \partial \theta_p} \\ \frac{\partial^2 \mathcal{L}}{\partial \theta_2 \partial \theta_1} & \frac{\partial^2 \mathcal{L}}{\partial \theta_2^2} & \cdots & \frac{\partial^2 \mathcal{L}}{\partial \theta_2 \partial \theta_p} \\ \vdots & \vdots & \ddots & \vdots \\ \frac{\partial^2 \mathcal{L}}{\partial \theta_p \partial \theta_1} & \frac{\partial^2 \mathcal{L}}{\partial \theta_p \partial \theta_2} & \cdots & \frac{\partial^2 \mathcal{L}}{\partial \theta_p^2} \end{pmatrix}$$

## F Validation Simplified Bootstrap Method

The purpose of this appendix is to validate the efficacy of a simplified bootstrap method for estimating the parameters of a statistical model, within the constraints and context of this study. The validation is carried out by using a Z-test to compare the original parameters of the model to those obtained via bootstrapping.

The Z-test is applied to two parameters,  $k$  and  $\lambda$ , which are estimated both through the original method and the simplified bootstrap method. The following steps outline the process:

1. **Calculate Descriptive Statistics:** For each parameter  $k$  and  $\lambda$ , the mean  $\mu$  and standard deviation  $\sigma$  are calculated from the bootstrapped samples.

$$\mu_k = \frac{1}{n} \sum_{i=1}^n k_i$$
$$\sigma_k = \sqrt{\frac{1}{n} \sum_{i=1}^n (k_i - \mu_k)^2}$$

Similarly for  $\lambda$ .

2. **Compute Z-scores:** The Z-scores for the original parameters  $k_{\text{original}}$  and  $\lambda_{\text{original}}$  are calculated using the formula:

$$Z_k = \frac{k_{\text{original}} - \mu_k}{\sigma_k}$$
$$Z_\lambda = \frac{\lambda_{\text{original}} - \mu_\lambda}{\sigma_\lambda}$$

3. **Calculate P-values:** Using the calculated Z-scores, p-values are obtained assuming a standard normal distribution.

$$p_k = 2 \times (1 - \Phi(|Z_k|))$$
$$p_\lambda = 2 \times (1 - \Phi(|Z_\lambda|))$$

where  $\Phi$  is the cumulative distribution function of the standard normal distribution.

4. **Significance Test:** The p-values are compared to a pre-defined significance level  $\alpha = 0.05$ .

If the p-values obtained are above  $\alpha$ , the null hypothesis that the parameters estimated by the original and simplified methods are statistically equivalent cannot be rejected. In other words, it confirms that the simplified bootstrap method produces

estimates that are statistically indistinguishable from those obtained through the original method.

**Note:** The conclusions drawn here are not to be considered definitive proof of the efficacy of the simplified bootstrap method. They are shown to be effective only within the context and limitations of this thesis.

The data used for this Z-test is derived from taking the midpoints of interval-censored lifetimes.

**Table 14:** Z-test Results for Different Datasets

Dataset	$p_{\text{Exponential (Lambda)}}$	$p_{\text{Weibull (Kappa)}}$
LBDINM	0.93	0.87
LBGC	0.98	0.88
LBPRC	0.98	0.86
LBQENM	0.98	0.91
LEDGSN	0.95	0.75
LEVSSN	0.97	0.97
LHGR	0.99	0.81

**Nelson-Aalen Estimator in Constant Risk Settings:** The Nelson-Aalen estimator is often used for estimating the cumulative hazard function  $H(t)$  in survival analysis. In settings where the number of components under risk remains constant, the estimator becomes simplified.

**Hazard Rate:** The hazard rate  $h(t_i)$  at each distinct time  $t_i$  is calculated using the constant number of components at risk  $n$  and the number of events (failures)  $d_i$  at that time:

$$h(t_i) = \frac{d_i}{n} \quad (42)$$

**Cumulative Hazard Function:** In the case of a constant number of components under risk, the cumulative hazard function  $H(t)$  can be calculated by summing the hazard rates at each event time  $t_i$  less than or equal to  $t$ :

$$H(t) = \sum_{i:t_i \leq t} h(t_i) \quad (43)$$

**Advantages and Applications:** The advantage of having a constant number of components under risk is that it simplifies the calculations and the interpretation of the cumulative hazard function. It is applicable in contexts where the risk population is fixed, such as specific engineering settings where the number of components does not change over time.

**Summary:** In situations where the number of components at risk remains constant, the Nelson-Aalen estimator provides a straightforward method for calculating the cumulative hazard function. Its simplicity makes it an effective tool for reliability analysis in such specialized settings.

## G Detailed Description of Python Packages

This appendix aims to elucidate the rationale behind the selection of specific Python packages in the project. A comprehensive understanding of each package's functional role aids in both present comprehension and potential future modifications or scaling.

### G.1 Pandas

Pandas is employed for its robust data manipulation capabilities, specifically data cleaning, transformation, and analysis. Its DataFrame structure offers a flexible and efficient way to handle large sets of structured data.

### G.2 FastAPI

FastAPI is utilized for developing the RESTful API layer. It is chosen for its speed, validation capabilities, and compatibility with Swagger UI and Uvicorn, which serve as the web server gateway interface.

### G.3 SQLAlchemy

SQLAlchemy is implemented for database management. Its object-relational mapping features allow seamless interaction between Python objects and the database, offering a versatile yet strong layer for data storage and retrieval.

### G.4 Python-DotEnv

The Python-DotEnv package is used to read key-value pairs from a .env file and add them to the environment variable, providing a secure way to configure application settings.

### G.5 Uvicorn

Uvicorn serves as the ASGI server, providing a production-ready platform to host the FastAPI application. It is known for its speed and robustness.

### G.6 NumPy

NumPy is employed for its efficient handling of numerical operations, array manipulations, and statistical functions. Its performance is critical in tasks involving complex calculations.

### G.7 Psycopg2

This package acts as a PostgreSQL database adapter for Python. It offers functionalities to connect to PostgreSQL databases, enabling direct manipulation and transactional control.

## **G.8 Reliability**

The Reliability library is used for statistical analysis pertinent to reliability engineering. Its specialized functions are vital for performing survival analysis and generating reliability models.

## **G.9 Alembic**

Alembic is a database migration tool for SQLAlchemy. It is implemented to manage changes to the database schema, ensuring a consistent and version-controlled database structure.

## **G.10 Surpyval**

Surpyval is specifically integrated for survival analysis, offering a plethora of parametric models, non-parametric estimators and statistical tests to aid in reliability engineering.

## H Plots of Failure Scenarios

For each failure scenario, four main visual analyses are provided:

1. Fit of the Exponential model.
2. Fit of the Weibull model.
3. Histogram of test statistic (TS) values.
4. Hazard function comparison.

### H.1 Failure Scenario - LBDIM

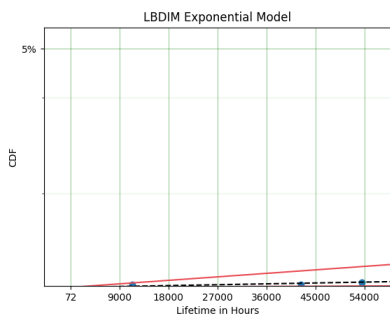


**Figure 39:** Exponential model fit for the failure scenario LBDIM.

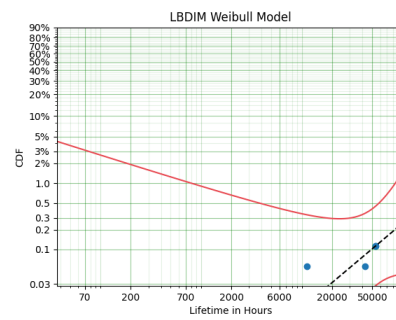


**Figure 40:** Weibull model fit for the failure scenario LBDIM.

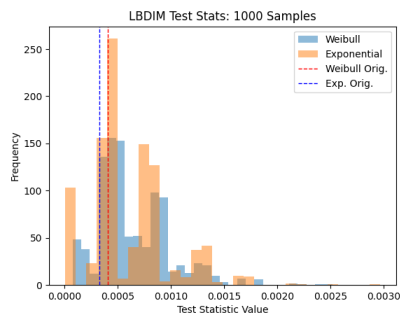


**Figure 41:** Histogram of TS values for failure scenario LBDIM.

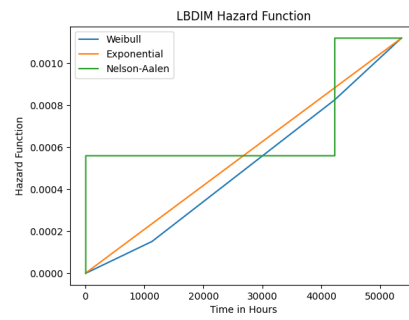


**Figure 42:** Hazard function for failure scenario LBDIM.

## H.2 Failure Scenario - LBDINM

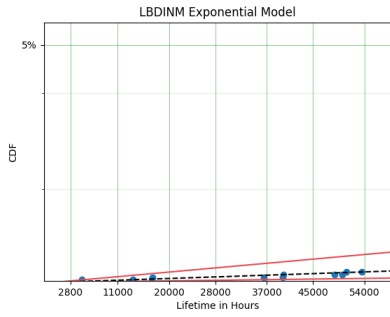


**Figure 43:** Exponential model fit for the failure scenario LBDINM.

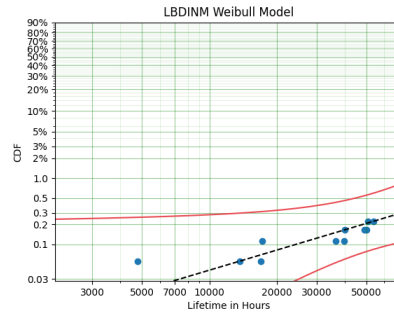


**Figure 44:** Weibull model fit for the failure scenario LBDINM.

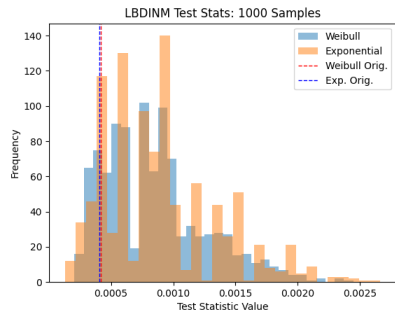


**Figure 45:** Histogram of TS values for failure scenario LBDINM.

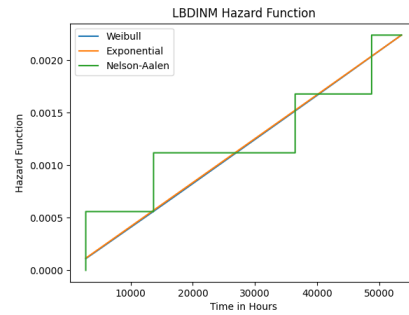


**Figure 46:** Hazard function for failure scenario LBDINM.

### H.3 Failure Scenario - LBGC

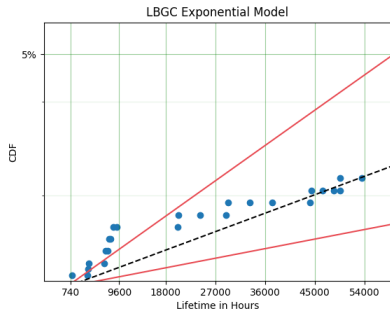


**Figure 47:** Exponential model fit for the failure scenario LBGC.

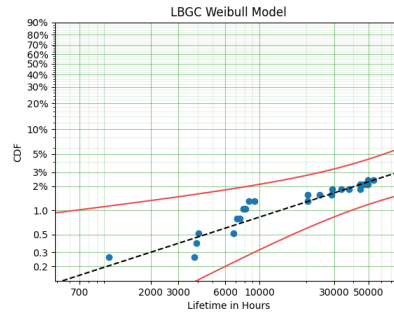


**Figure 48:** Weibull model fit for the failure scenario LBGC.

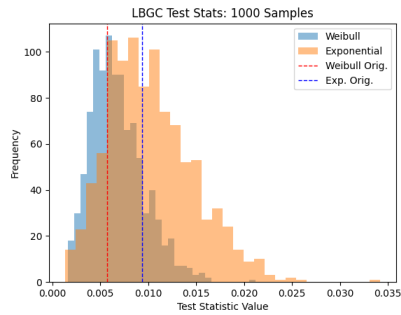


**Figure 49:** Histogram of TS values for failure scenario LBGC.

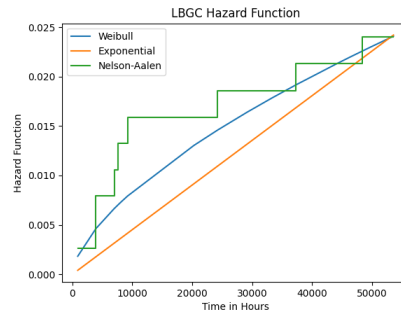


**Figure 50:** Hazard function for failure scenario LBGC.

## H.4 Failure Scenario - LBKLO

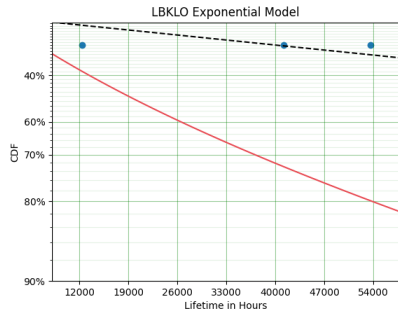


**Figure 51:** Exponential model fit for the failure scenario LBKLO.

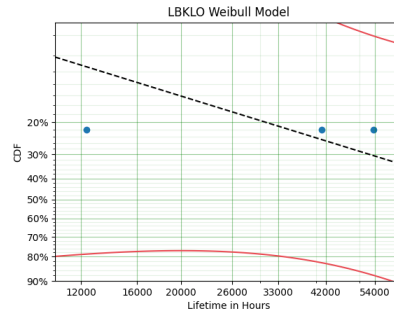


**Figure 52:** Weibull model fit for the failure scenario LBKLO.

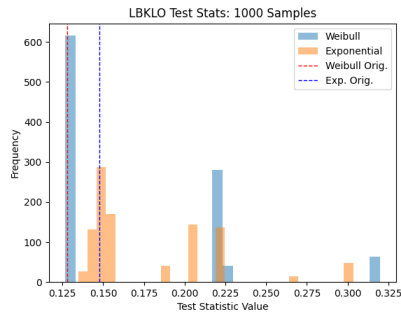


**Figure 53:** Histogram of TS values for failure scenario LBKLO.

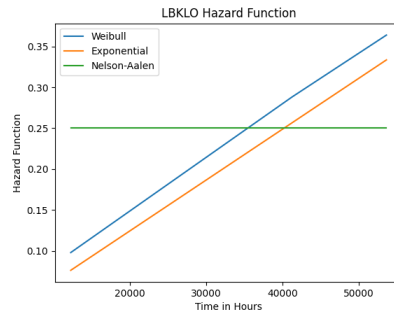


**Figure 54:** Hazard function for failure scenario LBKLO.

## H.5 Failure Scenario - LBPRC

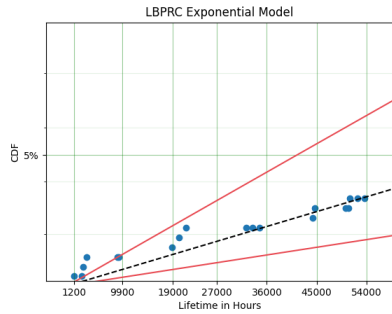


**Figure 55:** Exponential model fit for the failure scenario LBPRC.

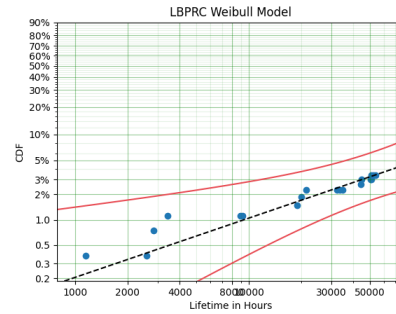


**Figure 56:** Weibull model fit for the failure scenario LBPRC.

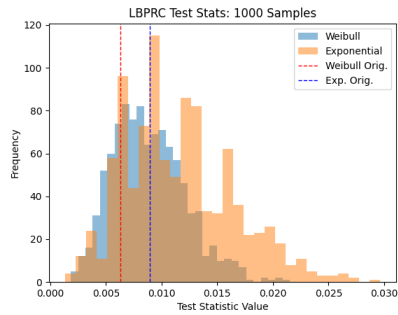


**Figure 57:** Histogram of TS values for failure scenario LBPRC.

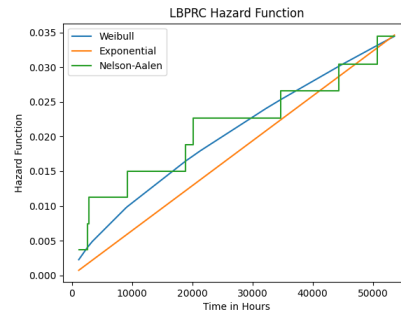


**Figure 58:** Hazard function for failure scenario LBPRC.

## H.6 Failure Scenario - LBPRNI

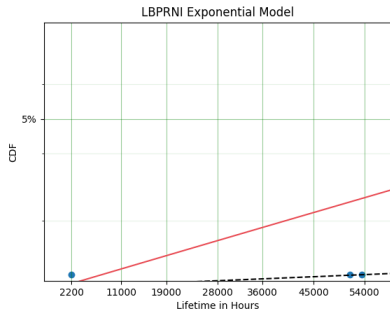


**Figure 59:** Exponential model fit for the failure scenario LBPRNI.

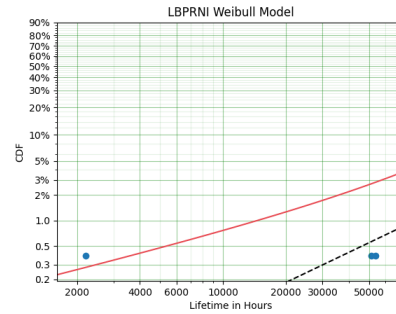


**Figure 60:** Weibull model fit for the failure scenario LBPRNI.

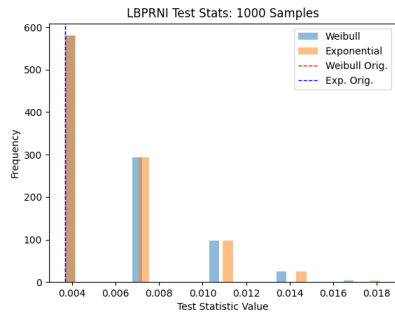


**Figure 61:** Histogram of TS values for failure scenario LBPRNI.

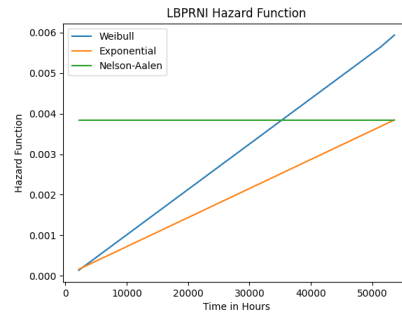


**Figure 62:** Hazard function for failure scenario LBPRNI.

## H.7 Failure Scenario - LBQENM

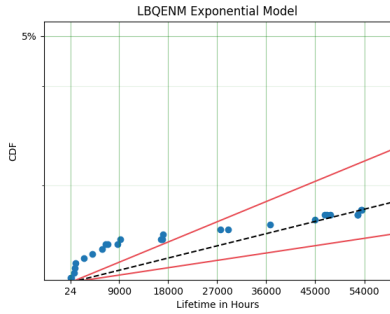


**Figure 63:** Exponential model fit for the failure scenario LBQENM.

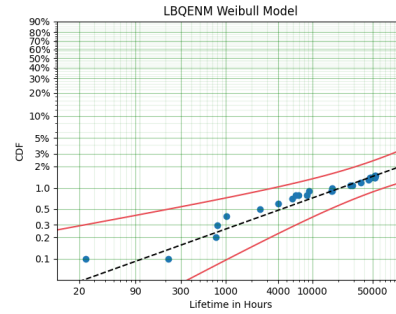


**Figure 64:** Weibull model fit for the failure scenario LBQENM.

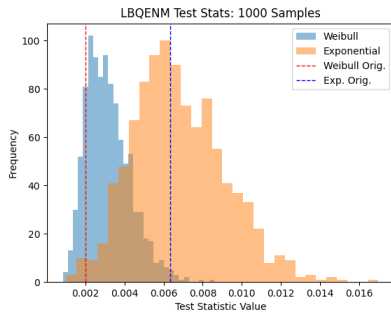


**Figure 65:** Histogram of TS values for failure scenario LBQENM.

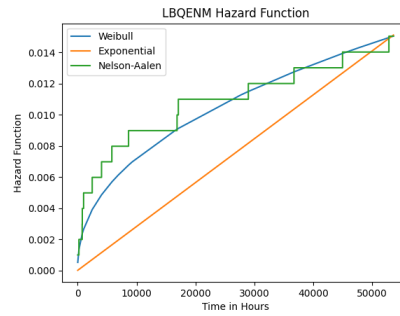


**Figure 66:** Hazard function for failure scenario LBQENM.

## H.8 Failure Scenario - LBREL

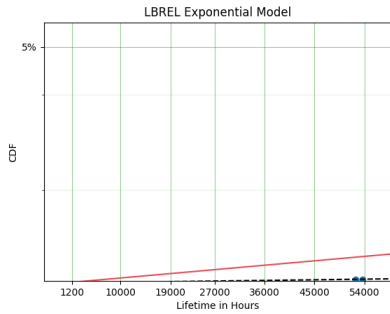


**Figure 67:** Exponential model fit for the failure scenario LBREL.

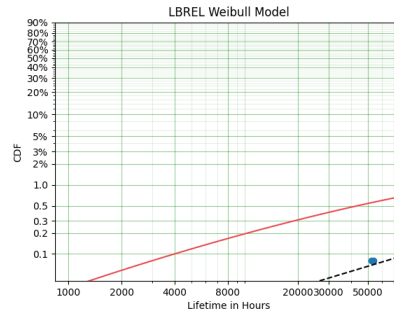


**Figure 68:** Weibull model fit for the failure scenario LBREL.

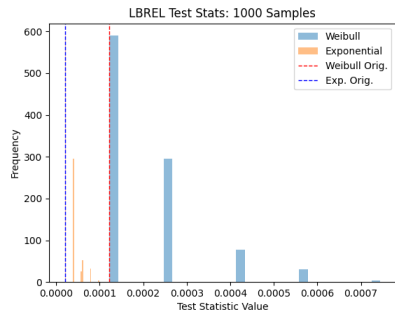


**Figure 69:** Histogram of TS values for failure scenario LBREL.

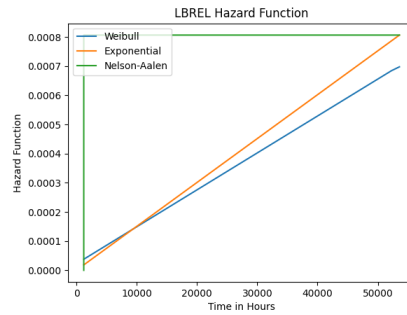


**Figure 70:** Hazard function for failure scenario LBREL.

## H.9 Failure Scenario - LBSWAM

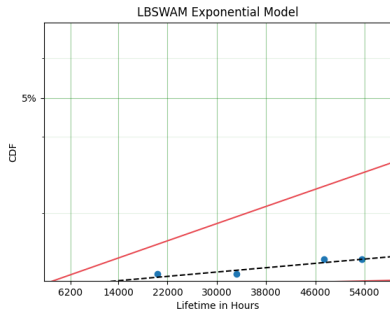


**Figure 71:** Exponential model fit for the failure scenario LBSWAM.

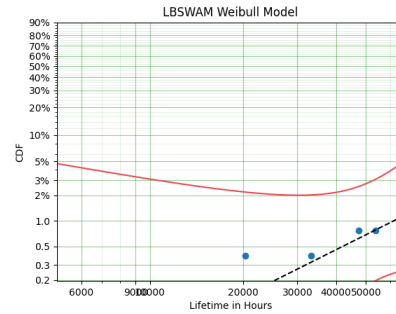


**Figure 72:** Weibull model fit for the failure scenario LBSWAM.

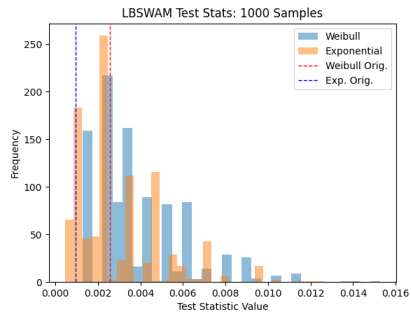


**Figure 73:** Histogram of TS values for failure scenario LBSWAM.

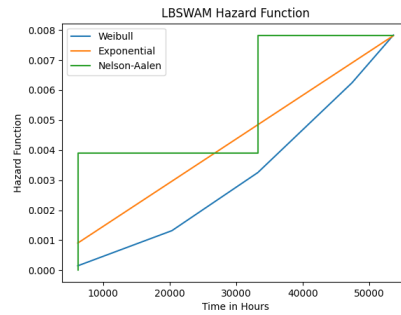


**Figure 74:** Hazard function for failure scenario LBSWAM.

## H.10 Failure Scenario - LBSWB

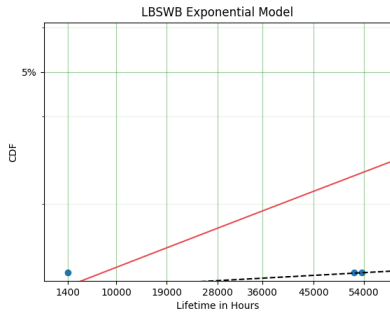


**Figure 75:** Exponential model fit for the failure scenario LBSWB.

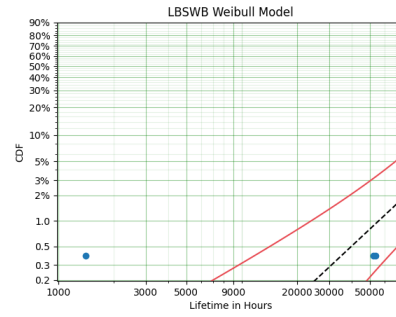


**Figure 76:** Weibull model fit for the failure scenario LBSWB.

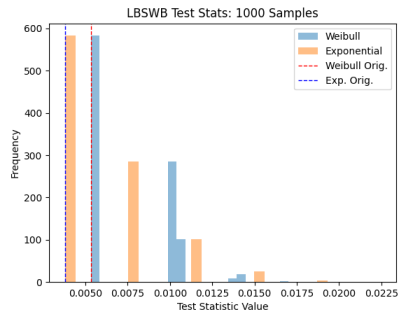


**Figure 77:** Histogram of TS values for failure scenario LBSWB.

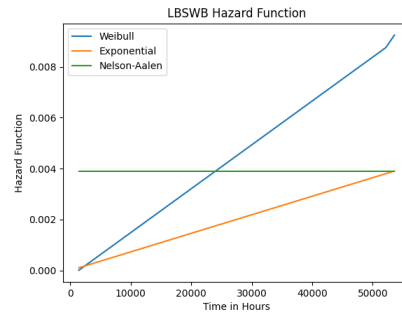


**Figure 78:** Hazard function for failure scenario LBSWB.

## H.11 Failure Scenario - LEDGSN

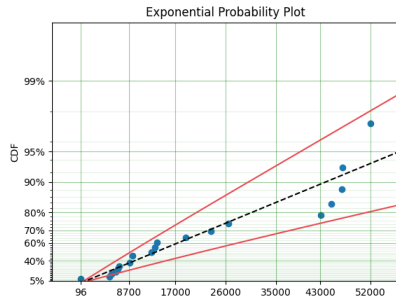


**Figure 79:** Exponential model fit for the failure scenario LEDGSN.

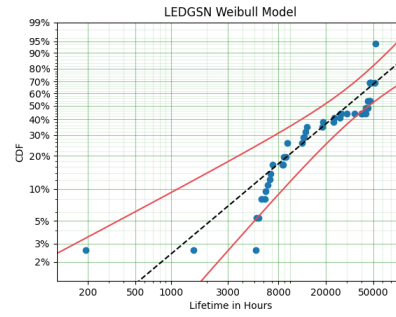


**Figure 80:** Weibull model fit for the failure scenario LEDGSN.

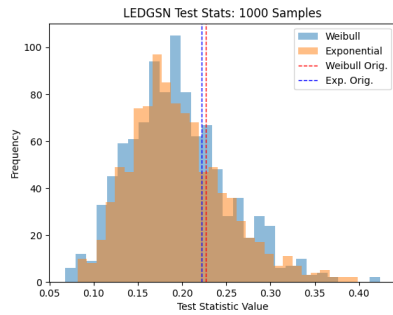


**Figure 81:** Histogram of TS values for failure scenario LEDGSN.

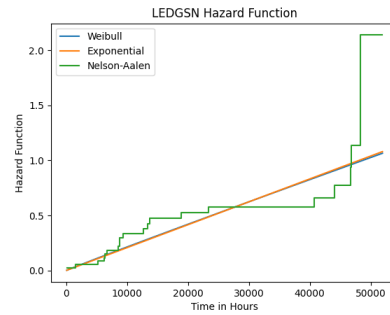


**Figure 82:** Hazard function for failure scenario LEDGSN.

## H.12 Failure Scenario - LEDSSN

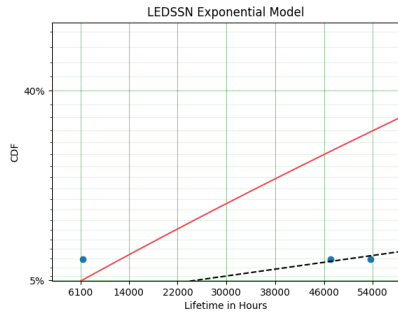


**Figure 83:** Exponential model fit for the failure scenario LEDSSN.

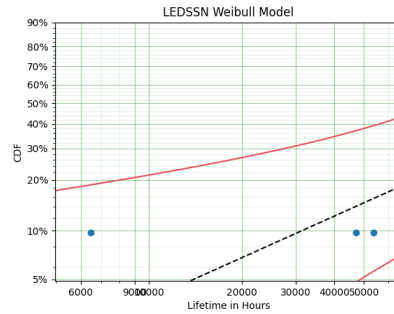


**Figure 84:** Weibull model fit for the failure scenario LEDSSN.

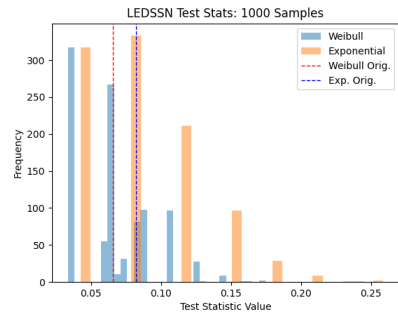


**Figure 85:** Histogram of TS values for failure scenario LEDSSN.

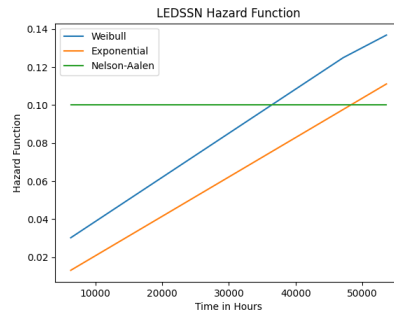


**Figure 86:** Hazard function for failure scenario LEDSSN.

### H.13 Failure Scenario - LERA38

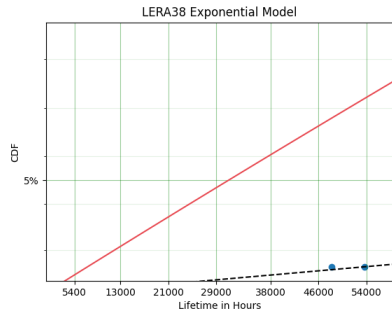


**Figure 87:** Exponential model fit for the failure scenario LERA38.

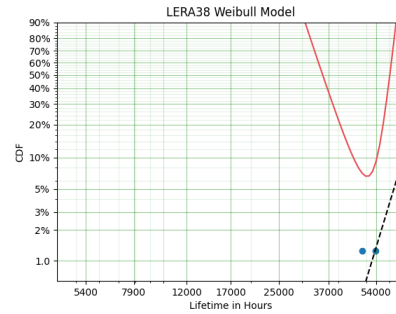


**Figure 88:** Weibull model fit for the failure scenario LERA38.

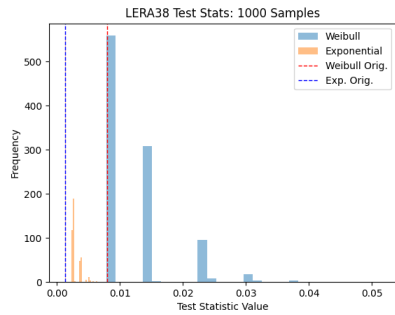


**Figure 89:** Histogram of TS values for failure scenario LERA38.

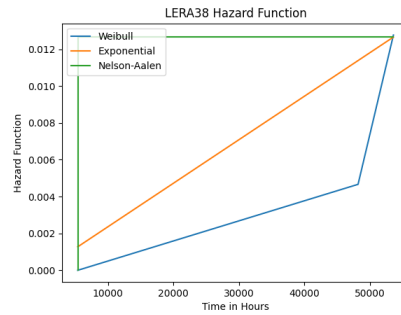


**Figure 90:** Hazard function for failure scenario LERA38.

## H.14 Failure Scenario - LEVSSN

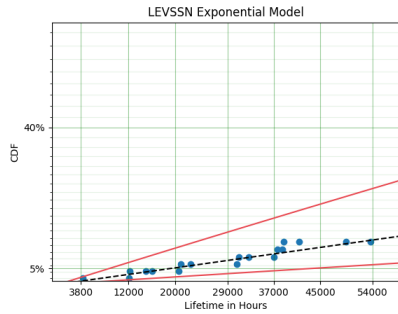


**Figure 91:** Exponential model fit for the failure scenario LEVSSN.

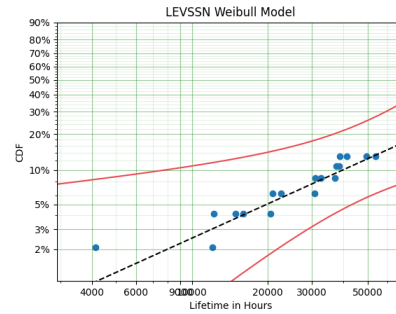


**Figure 92:** Weibull model fit for the failure scenario LEVSSN.

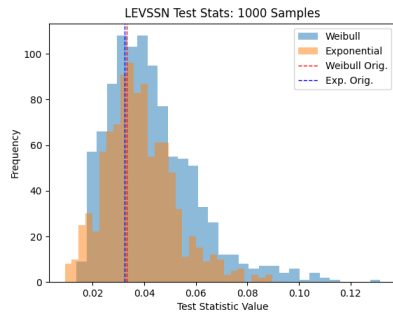


**Figure 93:** Histogram of TS values for failure scenario LEVSSN.

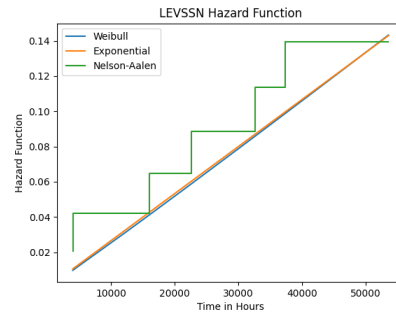


**Figure 94:** Hazard function for failure scenario LEVSSN.

## H.15 Failure Scenario - LESS

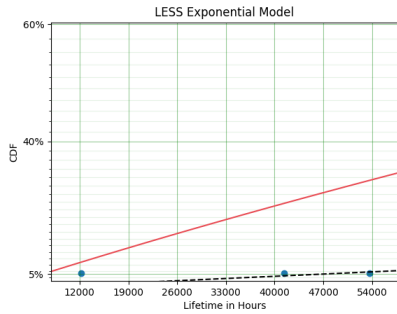


**Figure 95:** Exponential model fit for the failure scenario LESS.

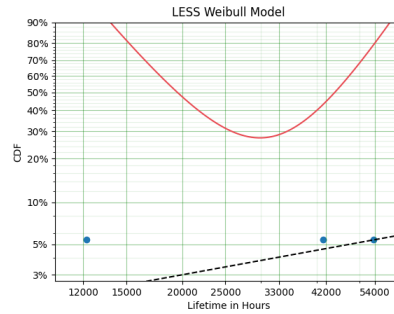


**Figure 96:** Weibull model fit for the failure scenario LESS.

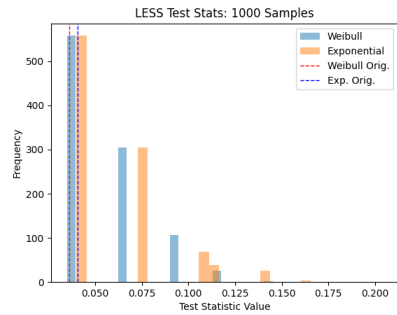


**Figure 97:** Histogram of TS values for failure scenario LESS.

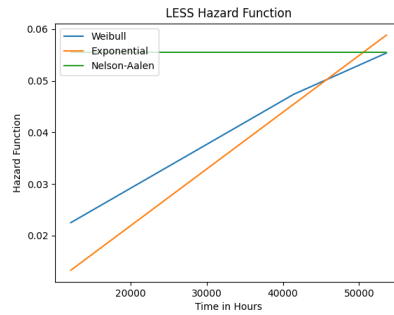


**Figure 98:** Hazard function for failure scenario LESS.

## H.16 Failure Scenario - LHGR

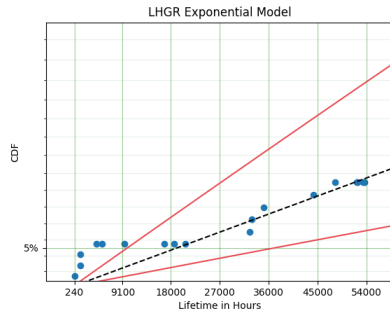


**Figure 99:** Exponential model fit for the failure scenario LHGR.

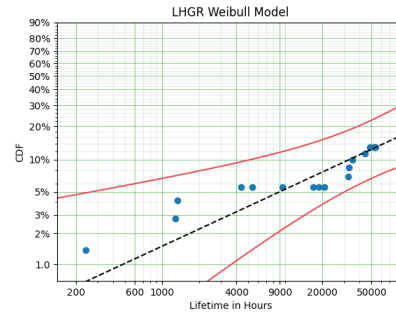


**Figure 100:** Weibull model fit for the failure scenario LHGR.

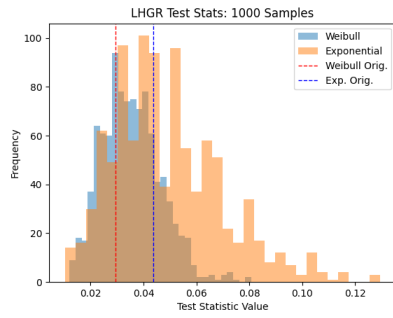


**Figure 101:** Histogram of TS values for failure scenario LHGR.

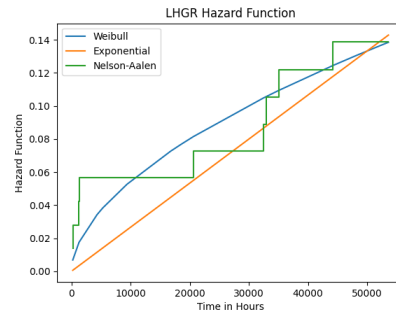


**Figure 102:** Hazard function for failure scenario LHGR.

## H.17 Failure Scenario - LHSVT

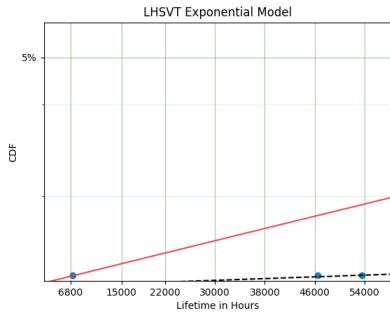


**Figure 103:** Exponential model fit for the failure scenario LHSVT.

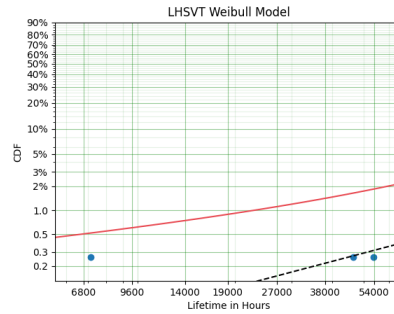


**Figure 104:** Weibull model fit for the failure scenario LHSVT.

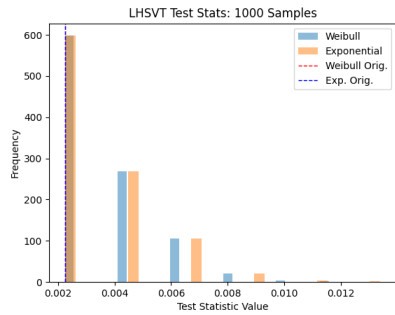


**Figure 105:** Histogram of TS values for failure scenario LHSVT.

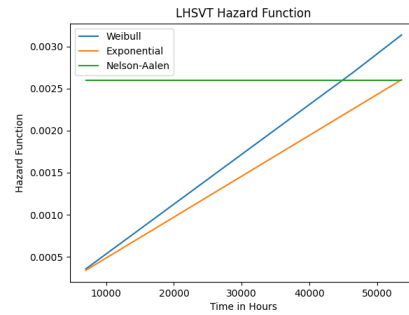


**Figure 106:** Hazard function for failure scenario LHSVT.

# I Comparative Analysis of Failure Scenarios Based on Model Fits

This appendix provides a detailed analysis comparing failure scenarios that yielded good model fits with those that yielded poor fits. Table 15 summarizes the metrics for both categories, including the Lifetime to Component Ratio and Number of Failures. Table 16 enumerates the Lifetime to Component Ratios for each failure scenario. Lastly, key observations and implications stated.

The key observations are:

- **Lifetime to Component Ratio:** Scenarios with good fits demonstrate a higher mean Lifetime to Component Ratio of 1.21, compared to 1.05 in scenarios with poor fits. This suggests that scenarios with a higher ratio may be more suitable for detailed modeling.
- **Number of Failures:** Scenarios with good fits have a significantly higher mean number of failures (10.29) as opposed to those with poor fits (1.30). The higher variability in scenarios with good fits indicates that they capture a broader range of conditions.
- **Minimum and Maximum Failures:** The minimum number of failures in scenarios with good fits is 4, which is twice as high as the maximum number of failures in scenarios with poor fits (2). This implies that scenarios in the poor fit group may require additional data or alternative methodologies for effective reliability modeling.

**Table 15:** Summary Statistics for Good and Poor Fits

Metric	Good Fit Scenarios	Poor Fit Scenarios
Mean Number of Failures	10.29	1.30
Max Number of Failures	20	2
Min Number of Failures	4	1
Mean Number of Components	504.71	429.90
Mean Lifetime to Component Ratio	1.21	1.05

**Table 16:** Lifetime to Component Ratio for Each Failure Scenario

<b>Scenario Code</b>	<b>Good Fits</b>	<b>Poor Fits</b>
LBDINM	1.002	–
LBGC	1.024	–
LBPRC	1.035	–
LBQENM	1.015	–
LEDGSN	2.111	–
LEVSSN	1.143	–
LHGR	1.143	–
LBDIM	–	1.001
LBKLO	–	1.333
LBPRNI	–	1.004
LBREL	–	1.001
LBSWAM	–	1.008
LBSWB	–	1.004
LEDSSN	–	1.111
LER38	–	1.013
LESS	–	1.059
LHSV7	–	1.003

## J Data Types

In computer science and information technology, a byte is a basic unit of data storage. It represents a group of eight binary digits (bits) and can store a single character, such as a letter or number. The term "byte" is used to specify the amount of storage capacity of storage mediums and the memory size.

In database management, various data types are used to define the type of data that can be stored in a particular column of a table. Below are explanations for some of the data types used in the SVKO component database:

**varchar(36):** A variable-length character string data type. It allows for storing strings with a maximum length of 36 characters. The 'varchar' type is efficient for storing strings as it only uses storage equivalent to the length of the string entered, plus an additional 2 bytes for overhead. If a string with a length of 5 characters is stored in a 'varchar(36)' column, it will only use 7 bytes of storage.

**int4:** Represents a four-byte (or 32-bit) integer data type. It can store whole numbers in the range of -2,147,483,648 to 2,147,483,647.

**float8:** An eight-byte (or 64-bit) floating-point number data type. It is used to store numbers that require decimal precision. The 'float8' type can store numbers with up to 15 decimal digits of precision.

**date:** Represents a date value. It is used to store date values without time. The typical format for a date is 'YYYY-MM-DD'. It does not store time information.

**time:** A data type used for storing time values without the date. The typical format for time is 'HH:MM:SS'.

**bool:** Represents a Boolean data type. It can store only two possible values: 'true' or 'false'. It's often used for fields that have a binary nature, such as "Is Active?" or "Is Deleted?".

Choosing the correct data type for each field in a database is crucial. It ensures that the data stored is accurate and valid, optimizes storage space, and can improve the speed and efficiency of database operations.

## K Closure Data Analysis

### K.1 Literature Review

This literature review aims to investigate data-driven techniques for evaluating the reliability of storm surge barrier closures. Emphasis is laid on methods that are apt for analysing closures with constant failure rates and scarce failure data.

#### K.1.1 Challenges in Failure Data Analysis

The primary obstacle in the analysis of storm surge barrier closures is the limited availability of failure data. The paucity of such data arises from the high success rate of barrier closures and the overall limited number of existing storm surge barriers. Traditional statistical methods, like maximum likelihood estimation, tend to underestimate the failure rate due to this data scarcity [16].

#### K.1.2 Review of Data-Driven Methods

**Rule of Three** The Rule of Three (R3) serves as a specialized technique for estimating the upper confidence limit of failure rates, especially when no failures are observed. It is particularly applicable for rare event scenarios and relies on the binomial distribution [30].

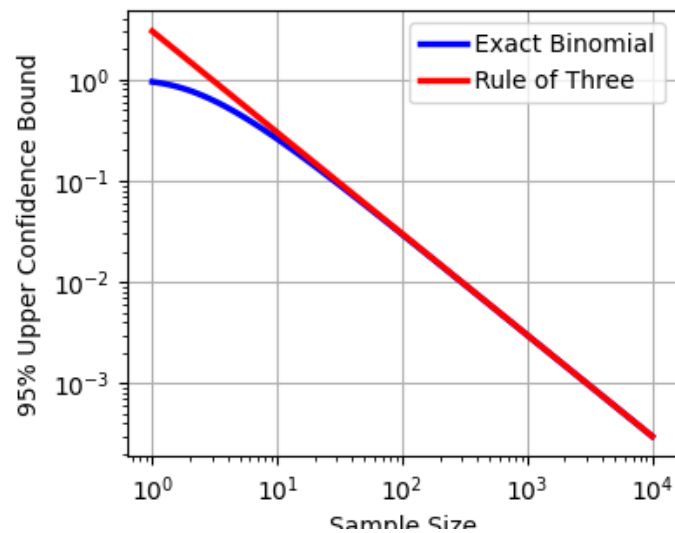


**Figure 107:** Graphical representation of the convergence of the Rule of Three with a binomial distribution. Convergence start at approximately 100 occurrences

The study Bakker et al. (2019) utilises Bayesian analysis to account for the failure probability in storm surge barrier closures. They calculate this by considering the ratio of failure events to total events. This yields an accurate estimate, whilst also accommodating statistical uncertainties associated with random failure events by modeling the probability distribution around the failure rate [4].

### K.1.3 Methodological Implications for This Thesis

The integration of the Rule of Three and Bayesian analysis suggests a balanced methodology for this thesis. The Rule of Three focuses on empirically observed data, whereas Bayesian analysis adds layers of complexity by considering prior knowledge and uncertainties. This dual approach could potentially compensate for the limitations posed by scarce data in storm surge barrier analysis. Specifically, the Rule of Three could be applied to observed patterns, while Bayesian methods could be used to update the prior estimates using observations.

## K.2 Methodology

### K.2.1 Methodology Framework

In light of the literature review, which underscores the potential of data-driven methods like the Rule of Three (R3) and Bayesian analysis, this section delineates the methodological approach adopted for assessing storm surge barrier closure reliability. The assessment of storm surge barrier closure reliability necessitates a methodology that is both robust and attuned to the intricacies of the data. While traditional methods have their merits, they often prioritize historical data and engineering judgments. To provide a more comprehensive approach, the Rule of Three (R3) is considered for its data-centric perspective.

The methodology introduced evolves around the hypothesis that using data can potentially result in a more realistic storm surge barrier closure reliability, it takes the following steps to achieve this:

1. **Application of Rule of Three (R3):** As a starting point, the Rule of Three, tailored for binomially distributed data sets without observed failures, is applied. This provides an initial estimate of the upper confidence bounds based on the observed data, laying the groundwork for a deeper reliability assessment.
2. **Bayesian Analysis with a Uniform Prior:** Subsequently, Bayesian statistics is employed with an initial uniform prior. This approach yields a posterior distribution derived from observed data, without being influenced by strong prior assumptions.
3. **Refinement with a Weakly Informed Prior:** To enhance the analysis, domain-specific insights and historical data are incorporated to establish a weakly informed prior. This step refines the posterior distribution, potentially leading to a more realistic estimate of the failure rate.

The synergy between R3's empirical foundation and the comprehensive nature of Bayesian statistics forms the essence of this framework. While R3 offers preliminary estimates, Bayesian statistics further refines these by integrating prior knowledge, such as expert insights and historical data. By juxtaposing this combined approach with traditional methodologies, the potential advantages of a data-driven methodology in storm surge barrier closure reliability assessments are potentially highlighted.

### K.2.2 Rule of Three and Closure Reliability

The Rule of Three (R3) serves as a statistical methodology tailored for binomial distributions with infrequent events. It asserts that if no failures are detected over  $n$  trials, the upper boundary for the 95% confidence interval of the failure probability is approximately  $\frac{3}{n}$  [30]. This method is instrumental in estimating the maximum likelihood of failure, especially when no failures are evident. For instance, in the context of 100 trials with zero failures, the 95% confidence boundary for a failure is  $\frac{3}{100} = 0.03$  or 3%. A detailed proof of this principle can be found in appendix M.

Delving into the implications of the R3 for storm surge barrier closures:

1. **Empirical Basis:** The R3, anchored in observed data, provides an empirical alternative to models that might predominantly rely on historical data or engineering-based assumptions.
2. **Flexibility:** The foundational principle of R3 is adaptable. It can be modified to address more complex scenarios or to integrate additional data, highlighting its versatility in reliability assessments.

The integration of the Rule of Three (R3) into the reliability assessment framework for storm surge barrier closures aims to balance traditional methods with data-driven insights. This approach seeks to anchor the assessment in empirical data, potentially capturing a more nuanced understanding of closure reliability.

### K.2.3 Bayesian Analysis in the Context of Storm Surge Barrier Closures

Bayesian analysis provides a methodological framework that integrates prior knowledge with new data, facilitating a deeper understanding of complex scenarios. This approach proves particularly relevant when examining storm surge barrier closures, a domain often constrained by limited data and the rarity of failures. [8]

Central to Bayesian inference is the principle of refining beliefs about a model parameter  $\theta$  based on new data  $D_n = \{x_1, x_2, \dots, x_n\}$ . This principle is encapsulated by Bayes' theorem:

$$p(\theta|D_n) \propto p(D_n|\theta) \times p(\theta) \tag{44}$$

Breaking down the components:

- $p(\theta|D_n)$ : The updated belief after incorporating the data.
- $p(D_n|\theta)$ : The likelihood of observing the data under the assumption of  $\theta$ .
- $p(\theta)$ : The initial stance or belief about  $\theta$  prior to data observation.

For a deeper exploration, readers are directed to Appendix L.

The Bayesian procedure for storm surge barrier closures will follow these methodical steps:

1. **Selection of a Prior:** Determine an initial belief before incorporating data.
2. **Computation of the Posterior:** Integrate the initial belief with the observed data to derive an updated belief.
3. **Estimation of Failure Rates:** Utilize the updated belief to make predictions about potential failures.

**Selection of a Prior:** In the context of storm surge barrier closures, individual closures can result in two outcomes: failure or success. Thus, when considering multiple closures, their outcomes can be described by a binomial distribution. Given this scenario, the Beta distribution is often employed to represent beliefs about these outcomes. The formulas for these distributions are:

$$p(D_n|\theta) = \binom{n}{k} \theta^k (1 - \theta)^{n-k} \quad (45)$$

$$p(\theta|\alpha, \beta) = \frac{1}{B(\alpha, \beta)} \theta^{\alpha-1} (1 - \theta)^{\beta-1} \quad (46)$$

When beliefs are updated using the Beta distribution in conjunction with new data, the updated beliefs continue to follow a Beta distribution:

$$p(\theta|D_n) \propto p(D_n|\theta) \times p(\theta|\alpha, \beta) \quad (47)$$

$$= \theta^{k+\alpha-1} (1 - \theta)^{n-k+\beta-1} \quad (48)$$

A more detailed proof can be found in Appendix N.

When determining the prior, several considerations come into play:

- **Uninformative Prior:** Adopted when there is minimal prior knowledge and a neutral starting point is desired [27].
- **Weakly Informative Prior:** Employed when there exists a modicum of prior information [17].

In this thesis both a uniformed and informed prior are used. First, an *Uninformative Prior* will be utilized for storm surge barrier closures, reflecting the desire to commence with a neutral perspective. Once data is assimilated, the posterior distribution will be computed, providing an updated belief about the failure rates. Subsequently, an *Informed Prior* will be introduced, drawing upon any available data or domain-specific insights. Again, the posterior distribution will be derived, this time reflecting the combined influence of the informed prior and the observed data.

By comparing the results derived from both priors and their respective posteriors, the influence of starting beliefs on the conclusions can be assessed. Furthermore, the posterior distributions will be analyzed to estimate failure rates, determine confidence intervals, and make predictions about future barrier closures.

This dual approach not only aids in understanding the significance of initial beliefs but also demonstrates the utility of the posterior in making informed decisions and predictions.

#### K.2.4 Combining Different Closure Types for Enhanced Data Analysis

The quest for a robust analysis often requires maximizing the available data. While storm closures are the primary focus, their sporadic occurrence might not provide ample data for a comprehensive analysis. An option to augment this data scarcity is to amalgamate storm closures with operational and test closures, thereby enriching the dataset. However, there are three main challenges:

1. **Diverse Operating Conditions:** Storm closures typically occur under distinct conditions compared to operational or test closures. The urgency and potential threat during a storm closure are considerably elevated.
2. **Flexibility of Test Closures:** Test closures possess the distinct advantage of being abortable if conditions are deemed suboptimal. This preemptive measure ensures that potential failures, which might have manifested under continued suboptimal conditions, are averted. Such a safety net is absent during storm closures, where the stakes are high and the margin for error is minimal.
3. **Potential for Data Bias:** Merging data from varied conditions might introduce biases. The reliability metrics from test or operational closures might not be directly translatable to storm closures due to the differing stakes and conditions.

To navigate these challenges, the following two strategies will be employed:

1. Clearly demarcate and label data from different closure types.
2. Conduct individual analyses for each closure type before amalgamation, to discern individual reliability metrics.

By adopting this meticulous approach, the study aims to harness the benefits of a combined dataset while being acutely aware of its inherent challenges. The objective is to strike a balance between data richness and analytical precision.

### K.2.5 Comparative Analysis and Evaluation of Conservatism

This research investigates whether data-driven methods for storm surge barrier closure reliability yield less conservative estimates than traditional models rooted in historical data and engineering insights. The evaluation is based on the following criteria:

- **Comparison Against  $P_{\text{historic}}$ :** The conservatism in traditional methods can be assessed by comparing  $P_{\text{historic}}$  with estimates from  $P_{\text{R3}}$  and  $P_{\text{Bayesian}}$ . A significant difference in values suggests potential overestimation by the conventional approach.
- **Correlation between R3 and Bayesian Estimates:** A high correlation between  $P_{\text{R3}}$  and  $P_{\text{Bayesian}}$  would validate the reliability of data-driven methods. Consistent results from both methods indicate their robustness.

In essence, this analysis aims to highlight any conservatism in current methodologies. If data-driven methods consistently deviate from traditional models, it signals a need for re-evaluation. The ultimate goal is to base storm surge barrier assessments on up-to-date and accurate data, ensuring a realistic evaluation of barrier closure reliability.

### K.2.6 Assumptions, Limitations, and Evaluation of Methods

The methodology employed in this study is underpinned by two foundational assumptions:

- Each closure event is independent of others.
- The failure rate of closures remains consistent over time.
- Each closure only has one of two outcomes, either success or failure.

These assumptions find their basis in consultations with barrier operators and are in line with the guidelines presented in "Leidraad Kunstwerken" [32]. Any significant deviation from these assumptions could impact the study's validity.

The specific failure rates for the closures of the HIJK, MLK, and HK are derived from the Dutch Waterwet § 2. Normen waterkering Artikel 2.2 [1]. For the HIJK this is 1 in 200, whilst both the MLK and HK have a failure rate of 1 in 100. Additionally, the unique multi-gate structure of the SVKO is considered. According to the operator's criteria, an SVKO failure is defined as a scenario where 90% (or 56) or fewer of its gates successfully close. The implications of 6 gates failing to close are elaborated upon in the NRG Report 2017, with the failure rate being approximately 1 in 1700 [8].

### Evaluation of Methods:

- **Rule of Three (R3):** The R3 offers a direct approach to determine an upper confidence bound from observed data. Its constraints encompass:
  - A presumption of binomial distribution, which may not align with all real-world data and only comes into effect at a set number of observations. For R3 this is around 100.
  - A focus solely on the upper bound, potentially neglecting other aspects of reliability.
  - Optimal utility in the absence of observed failures, which restricts its applicability across diverse datasets.
- **Bayesian Analysis:** The Bayesian methodology excels in melding prior knowledge with current observations, showcasing its adaptability and depth. Yet, it is not without its challenges:
  - The selection of the prior can substantially sway the outcomes. Misguided priors can yield skewed posterior distributions.
  - The computational demands can escalate, especially when dealing with non-conjugate priors or extensive datasets.
  - The efficacy of the method hinges on the accuracy and timeliness of the prior information. Outdated or unreliable priors can distort the results.

To encapsulate, both the R3 and Bayesian methodologies provide insightful perspectives on storm surge barrier closure reliability. However, their inherent limitations necessitate a cautious interpretation of the results, ensuring that conclusions are drawn with an understanding of these constraints.

## K.3 Results

This section delves into the reliability of storm surge barriers by analyzing observed closure data. The HIJK barrier is particularly noteworthy due to its elevated count of storm-induced closures. Through the Rule of Three, certain barriers exhibited discrepancies between their stated failure rates and the 95% upper confidence bounds. Further examination using Bayesian analysis, incorporating both non-informative and weakly informative priors, indicated that most storm surge barriers present posterior closure failure rates that are more favorable than their stated rates, especially when considering all types of closures. This comprehensive analysis offers a clearer perspective on the closure reliability of storm surge barriers.

### K.3.1 Observed Closure Data

Table 17 enumerates the closure events associated with each storm surge barrier. Notably, the HIJK barrier recorded **240 closures** attributed to storms, contrasting sharply with the MLK and HK barriers, which reported only two such closures each.

**Table 17:** Observed storm surge barrier closures: Number of storm, non-storm and test closures for the four storm surge barriers that are analysed in the thesis.

	Storm Closures	Operational Closures	Test Closures
HIJK	239	70	71
SVKO	29	-	354
MLK	2	-	25
HK	2	-	25

### K.3.2 Rule of Three Analysis

The Rule of Three was employed to deduce the 95% upper confidence bound of the closure failure rate based on observed closures for each type. As illustrated in Table 18, the upper confidence bounds for the storm surge barriers' closure failure rates significantly exceed the stated rates. For instance, the HIJK barrier, despite having the highest number of storm-induced closures, has a **95% upper confidence bound of 1 in 80**, contrasting with its stated failure rate of 1 in 200.

**Table 18:** Observed storm surge barrier closures and corresponding upper confidence bounds (95% percentile) for failure rates calculated using the Rule of Three.

	Storm Closures		Operational Closures		Test Closures	
	Number	95% CI	Number	95% CI	Number	95% CI
HIJK	239	1:80	70	1:24	71	1:24
SVKO	29	1:10	-	-	354	1:118
MLK	2	1:0.67	-	-	25	1:9
HK	2	1:0.67	-	-	25	1:9

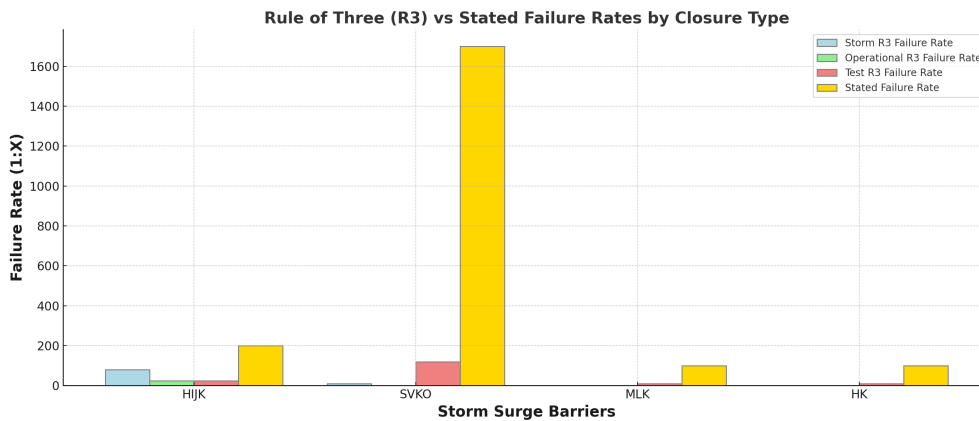


**Figure 108:** Comparison of R3 Failure Rates for Different Types of Closures (Storm, Operational, Test) with the Stated Failure Rates for Each Storm Surge Barrier.

Given the limited data on storm closures, understanding storm surge barrier closure reliability becomes potentially challenging. Table 19 offers insights into this by presenting the observed closures alongside their upper confidence bounds, derived from the Rule of Three. For the HIJK barrier with 239 closures, the 50% confidence interval suggests a closure failure rate upper bound of 1 in 344, more favorable than its stated 1 in 200. Conversely, the SVKO barrier's 50% confidence interval indicates a less favorable rate of 1 in 42, compared to its stated 1 in 1700.

**Table 19:** Observed storm surge barrier storm closures and corresponding upper confidence bounds calculated using rules derived from the Rule of Three.

Storm Surge Barrier	Storm Closures	50% CI	75% CI	90% CI
HIJK	239	1:344	1:172	1:104
SVKO	29	1:42	1:21	1:13
MLK	2	1:3	1:1.5	1:0.86
HK	2	1:3	1:1.5	1:0.86

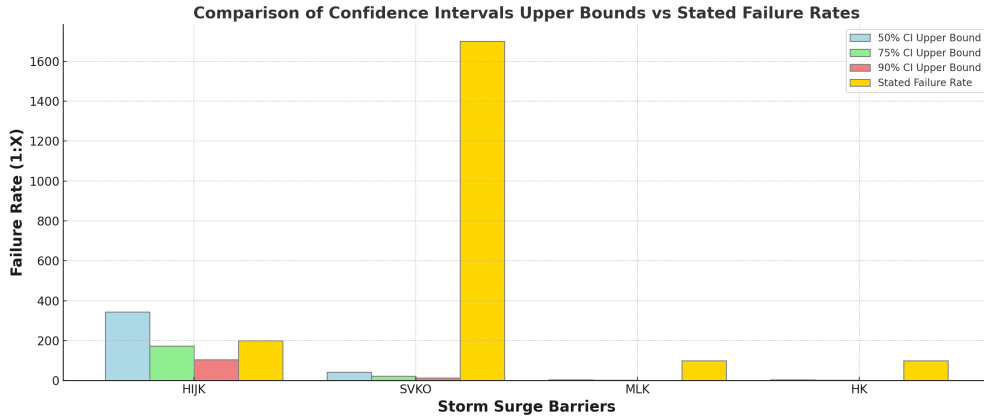


**Figure 109:** Comparison of Confidence Intervals Upper Bounds (50%, 75%, 90%) Based on Storm Closures with the Stated Failure Rates for Each Storm Surge Barrier.

To address the scarcity of individual storm closure data, an aggregation of all closure types, including operational and test closures, was considered. This consolidated approach, especially when paired with lower confidence intervals, offers a clearer perspective on upper confidence bounds, as demonstrated by the Rule of Three in Table 20. Notably, the HIJK barrier's 50% confidence interval suggests a favorable failure rate of 1 in 548, surpassing its stated rate of 1 in 200. Conversely, other barriers exhibit 50% confidence interval rates that exceed their respective stated failure rates.

**Table 20:** Observed storm surge barrier closures and corresponding upper confidence bounds for failure rates based on total number of closures.

Storm Surge Barrier	Total Closures	50% CI	75% CI	90% CI	95% CI
HIJK	380	1:548	1:274	1:165	1:127
SVKO	383	1:552	1:276	1:166	1:128
MLK	27	1:39	1:20	1:12	1:9
HK	27	1:39	1:20	1:12	1:9

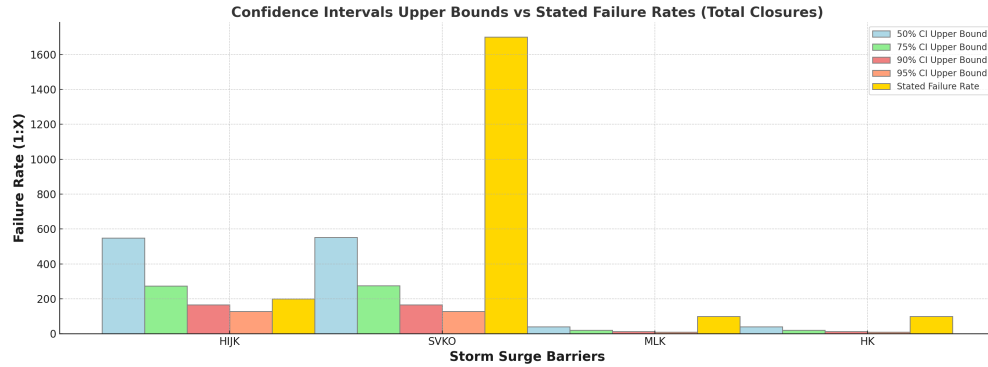


**Figure 110:** Comparison of Confidence Intervals Upper Bounds (50%, 75%, 90%, 95%) Based on the Total Number of Closures with the Stated Failure Rates for Each Storm Surge Barrier.

### K.3.3 Bayesian Analysis

The failure rates of each storm surge barrier were assessed using a Bayesian approach with the Beta distribution as the prior. The analysis began with a non-informative prior, later integrating an informed prior to account for existing knowledge on barrier performance.

Table 21 details failure rates based solely on storm closures, highlighting the barriers' robustness during specific weather events. Notably, the HIJK barrier exhibits a **posterior rate of 1 in 241**, which is more favorable than its stated rate of 1 in 200.

**Table 21:** Failure Rates Derived from Storm Closures (Uninformed Prior)

Barrier	Prior Rate	Posterior Rate	95% CI Lower	95% CI Upper
HIJK	1:2	1:241	1:9,482	1:66
SVKO	1:2	1:31	1:1,185	1:9
MLK	1:2	1:4	1:119	1:1.4
HK	1:2	1:4	1:119	1:1.4

For a comprehensive assessment of barrier reliability, all closure types—operational, test, and storm closures—were analyzed. The findings are detailed in Table 22. Notably, the HIJK barrier’s posterior failure rate is more favorable than its stated rate. In contrast, other barriers exhibit posterior rates that exceed their stated rates. However, all stated failure rates lie within the 95% confidence interval, suggesting that the observed data is consistent with the stated rates, even if the most likely rates differ.

**Table 22:** Failure Rates Derived from Total Closures (Uninformed Prior)

Barrier	Prior Rate	Bayesian Rate	95% CI Lower	95% CI Upper
HIJK	1:2	1:382	1:15,090	1:104
SVKO	1:2	1:385	1:15,312	1:105
MLK	1:2	1:29	1:1,107	1:8
HK	1:2	1:29	1:1,107	1:8

Incorporating a weakly informative prior offers a refined view of the data. As illustrated in Table 23, not only does the HIJK barrier’s posterior failure rate align favorably with its stated rate, but the SVKO, MLK, and HK barriers also exhibit posterior rates of 1 in 1728 and 1 in 102, respectively, which are more favorable than their stated rates. Crucially, all these stated rates are encompassed within the 95% confidence intervals.

**Table 23:** Failure Rates Derived from Storm Closures (Weakly Informative Prior)

Barrier	Prior Rate	Posterior Rate	95% CI Lower	95% CI Upper
HIJK	1:200	1:439	1:17,301	1:119
SVKO	1:1700	1:1728	1:68,259	1:469
MLK	1:100	1:102	1:3,990	1:28
HK	1:100	1:102	1:3,990	1:28

To achieve a potentially more thorough assessment of the closure reliability, all closure types were incorporated into the analysis. As detailed in Table 24, the posterior failure rates for all storm surge barriers are more favorable than their stated rates. While the 95% confidence intervals present even more favorable lower and upper bounds, it is noteworthy that the stated failure rates consistently lie within these intervals for all barriers.

**Table 24:** Failure Rates Derived from Total Closures (Weakly Informative Prior)

Barrier	Prior Rate	Posterior Rate	95% CI Lower	95% CI Upper
HIJK	1:200	1:580	1:23,023	1:157
SVKO	1:1700	1:2082	1:82,239	1:564
MLK	1:100	1:126	1:4,940	1:34
HK	1:100	1:126	1:4,940	1:34

## **K.4 Discussion**

This section outlines the methodology utilized in determining the failure rates of storm surge barrier closures, underpinned by observational data and analytical strategies including the Rule of Three (R3) and Bayesian analyses. Subsequent paragraphs delve into the data employed, scrutinize the limitations of the existing strategies, and present the findings.

### **K.4.1 Reflecting on Data**

The dataset, formulated from publicly available reports and operator inputs, could potentially be incomplete. Despite adherence to the Dutch Water Law [1] by operators, there may be instances of human error in record-keeping or difficulties in data access, thereby impacting the comprehensiveness of the dataset. Therefore, an acknowledgment of the potential for missing data is crucial, and it is recommended that future studies extend and refine the data collection to enhance the reliability assessment of storm surge closures.

The current dataset classification divides closures into "successful" or "failed," missing out on the significant intermediary group of "aborted closures." Such closures, prominently featured in the SVKO dataset, are initiated but halted due to considerable technical complications, thus not clearly fitting into the success or failure categories. Ignoring this category could potentially lead to an overoptimistic view of the reliability assessment, neglecting the early signs of trouble that led to the abortion of the procedure. Recognizing and studying "aborted closures" is crucial as it paints a more comprehensive picture of the system performance, encompassing insights into emerging technical issues. Therefore, including "aborted closures" in the classification could refine the reliability assessment of storm surge barrier closures.

The existing dataset has a notable limitation – the lack of detailed information on the performance of individual gates during barrier closures, as seen in the HIJK dataset where it remains unclear whether the first, second, or both gates were functional during the closures. This omission restricts a detailed reliability analysis of the storm surge barriers as the overall reliability is tied to the performance of each individual gate. Consequently, incorporating data on individual gate performances could help in understanding their reliability. Therefore, including these data points could enhance the reliability assessments of storm surge barriers, allowing for a more detailed analysis that incorporates performance of individual gates.

### **K.4.2 Reflecting on the Limitations**

The present methodology assumes a constant failure rate over time, disregarding potential variations arising from maintenance adjustments, aging, or upgrades. As delineated in section 2.3, the long-term reliability of a system is influenced by maintenance

and repair strategies, necessitating a more dynamic approach to failure rate assessment that considers these variables.

#### **K.4.3 Reflecting on the Results**

The examination of closure data employed R3 and Bayesian analysis techniques. While R3 offers a preliminary failure rate estimate based solely on closure observations, the Bayesian approach refines this estimate by incorporating additional reliability information. For a detailed explanation of these methods, refer to sections 2.1 and 2.3. The application of these techniques aims to obtain more realistic failure rate predictions, provided sufficient data is available.

The HK and MLK barriers lack closure observations, making the application of R3 not possible, and the results from Bayesian analysis uncertain and potentially uninformative. Therefore, caution must be exercised when interpreting results derived from storm surge barriers with insufficient closure data.

In contrast, the SVKO, with a substantial number of test closures, allows for a more confident application of R3 and Bayesian analyses. However, the limited storm closure data pose a constraint in applying R3 rigorously. The analyses reveal that the actual failure rate is likely less conservative than the stated rate, suggesting the necessity for revised reliability estimations.

For the HIJK barrier, the considerable amount of data enables a reliable application of both R3 and Bayesian analyses, leading to less conservative failure rate estimates. This illustrates the potential of these methods in deducing realistic closure reliability metrics when backed by substantial data, as detailed in section K.3.

## L Bayesian Inference for Parameter Estimation

Bayesian inference offers a systematic framework for refining the beliefs about a model parameter  $\theta$  based on new data, denoted by  $D_n = \{x_1, x_2, \dots, x_n\}$ . This belief refinement is captured by Bayes' theorem, which mathematically combines the prior knowledge and observed data to yield a posterior belief about  $\theta$ :

$$p(\theta|D_n) \propto p(D_n|\theta) \times p(\theta) \tag{49}$$

Where:

- $p(\theta|D_n)$  represents the **posterior** distribution of  $\theta$  after considering data  $D_n$ .
- $p(D_n|\theta)$  is the **likelihood**, indicating the probability of the observed data under a specific value of  $\theta$ .
- $p(\theta)$  constitutes the **prior** distribution, which encapsulates our preliminary beliefs about  $\theta$  before data observation.

## M Rule of three

The rule of three provides the 95% confidence bound for independent events with probability  $p$ , on the basis that the event has not occurred in  $n$  Bernoulli trials. The formula of the cumulative binomial function for zero successful events in a population of size  $n$ ,  $(1 - p)^n$ , can be used to derive the rule of three. The upper limit of the confidence interval is  $P(x = 0) = 0.05$ . This is used to deduce the rule of three:

$$\begin{aligned} (1 - p)^n &\leq 0.05 \\ \Leftrightarrow n \ln(1 - p) &\leq \ln(0.05) \simeq -2.996 \end{aligned} \quad (50)$$

A Taylor series expansion around  $x = 0$  is used to estimate  $\ln 1 - p$ .

$$f(x) = f(0) + \frac{f'(0)}{1!}(x) + \frac{f''(0)}{2!}(x)^2 + \frac{f'''(0)}{3!}(x)^3 + \dots \quad (51)$$

By inserting  $\ln 1 - p$  it is found that:

$$\begin{aligned} f(x) &= 0 + \frac{\frac{d}{dp}(\ln(1 - p)(0))}{1!} + \frac{\frac{d^2}{dp^2}(\ln(1 - p)(0))}{2!} + \frac{\frac{d^3}{dp^3}(\ln(1 - p)(0))}{3!} + \dots \\ &= -p - \frac{1}{2}p^2 - \frac{1}{3}p^3 - \dots \\ &\approx -p \text{ (for } p \text{ close to } 0) \end{aligned} \quad (52)$$

Hence, it is shown that  $-np \leq -2.996$  or more formally:

$$p \leq \frac{3}{n} \quad (53)$$

Modifications of the rule of three exist. For example, the rule of four. Which can be used to provide the upper limit of the 99% confidence interval. Naturally, the formulas for other confidence bounds can also be deduced.

## N Proof of Beta-Binomial Conjugacy

The binomial distribution models the count of successes in  $n$  independent Bernoulli trials. Its likelihood is described by:

$$p(D_n|\theta) = \binom{n}{k} \theta^k (1-\theta)^{n-k} \quad (54)$$

Given that  $\theta$  is a probability and varies between 0 and 1, the Beta distribution serves as an apt choice for the prior. This distribution is characterized by:

$$p(\theta|\alpha, \beta) = \frac{1}{B(\alpha, \beta)} \theta^{\alpha-1} (1-\theta)^{\beta-1} \quad (55)$$

Where  $B$  stands for the Beta function.

As the Beta distribution is the *conjugate prior* for the binomial distribution, it ensures that when commencing with a Beta-distributed prior and then observe binomial data, the resultant posterior is also Beta-distributed.

Combining these, the posterior distribution for  $\theta$  after observing the data becomes:

$$p(\theta|D_n) \propto p(D_n|\theta) \times p(\theta|\alpha, \beta) \quad (56)$$

$$\propto \theta^k (1-\theta)^{n-k} \times \theta^{\alpha-1} (1-\theta)^{\beta-1} \quad (57)$$

$$= \theta^{k+\alpha-1} (1-\theta)^{n-k+\beta-1} \quad (58)$$

Thus, the revised parameters for the Beta distribution are:

$$\theta|D_n \sim \text{Beta}(k + \alpha, n - k + \beta)$$

The conjugacy between the Beta and binomial distributions streamlines the Bayesian updating process, making it both intuitive and analytically manageable.

## O Storm Surge Barrier Closure Database

The Storm Surge Barrier Closure Database centralizes record-keeping for storm surge barrier closures. This adaptable tool is designed to aid agencies and researchers in efficiently monitoring and analyzing closure events.

Integrated with the FastAPI framework, the system allows users to perform CRUD operations with ease. They can access barrier details, register new barriers, and view specific closure instances. Additionally, endpoints for the rule-of-three and beta distribution calculations are available for in-depth analysis.

Relying on the PostgreSQL database, the system offers both reliability and scalability in data storage. In regions where storm surge barriers play a vital role in flood prevention, this database becomes instrumental in offering insights into operational statuses and reasons for closures.

The clean and structured codebase is designed for adaptability, allowing users to tailor it to specific requirements. The entire codebase can be accessed in the repository for modifications or further applications.

For a detailed overview, please refer to the repository maintained by Jelle Epema [9].

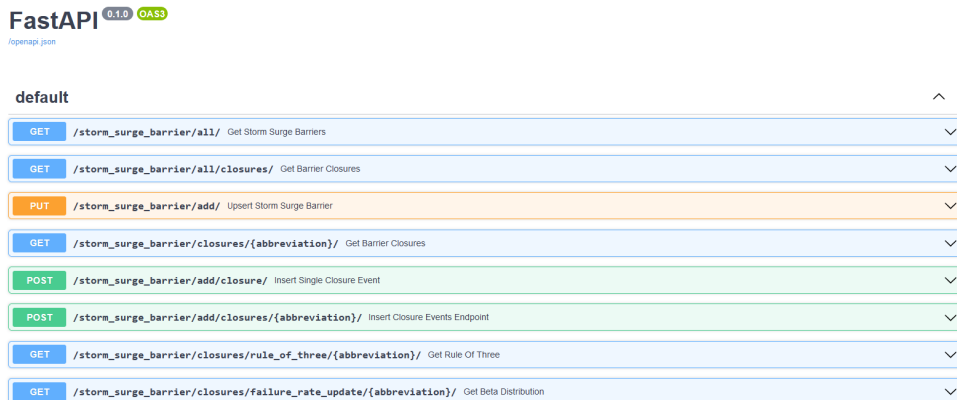


**Figure 111:** Methods available in the FastAPI interface for database interactions: PUT for updating, POST for adding, and GET for fetching data.

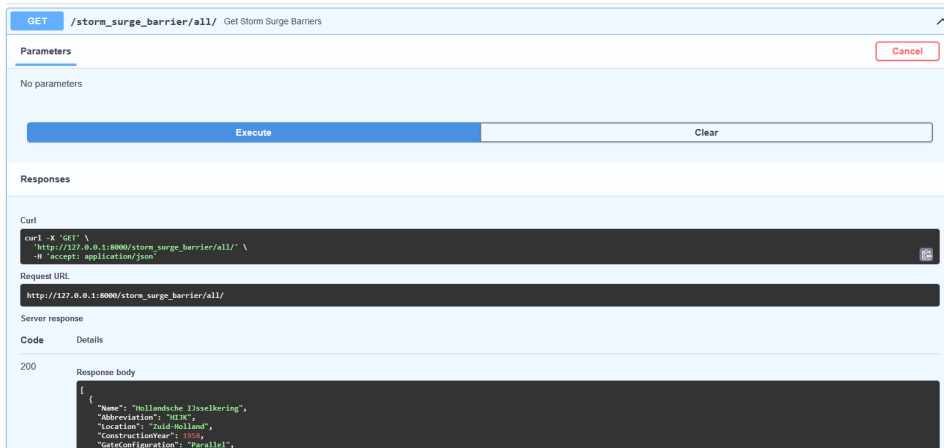


Figure 112: Interface for retrieving a comprehensive list of storm surge barriers.

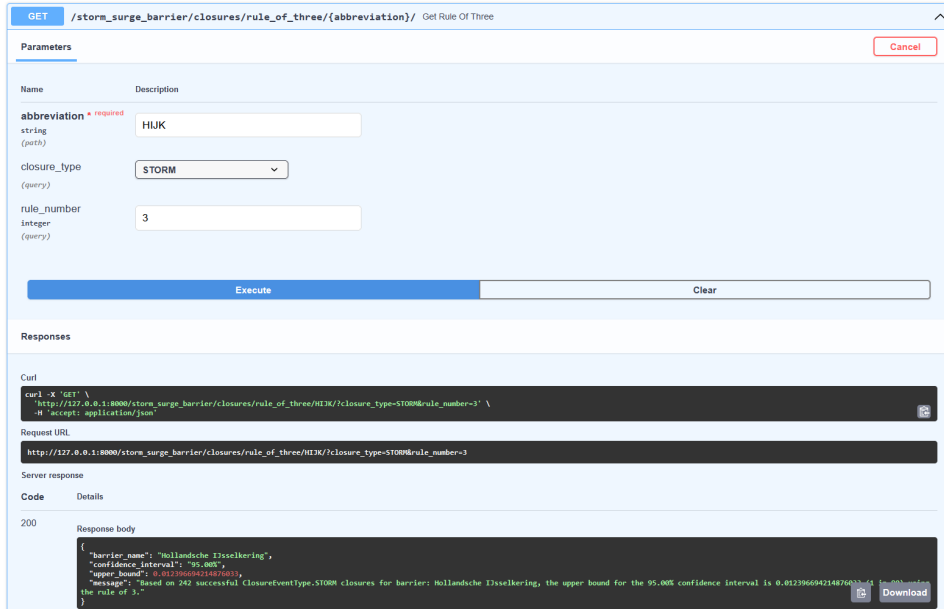


Figure 113: Procedure for analyzing closure data using the R3 method.

## P Overview of the Oosterscheldekering

Situated in Zeeland, the Oosterscheldekering, or Eastern Scheldt Storm Surge Barrier, is a significant flood defense completed in 1986. Designed to withstand extreme storms with a 1-in-40,000-year recurrence interval, it incorporates 62 vertical lift gates operated by 124 cylinder [8].

Figures 114 and 115 provide a snapshot of specific SVKO closures. For a comprehensive list, consulting original references is recommended.

		ROOMPOT BUITEN					STAVENISSE			Opmerkingen	
		Voor- alarm	Alarm	Sluiten	Sluit- peil	Verwacht hoogwater bij belasting sluiting	Astro hoog- water	Opgetr. hoog- water	Streef- peil		Opgetr. waterst.
1	20-10-1986	JA	JA	JA	+275	+261	+175	+294	---	---	Langd. gesl. tbv C-werk
2	02-11-1986	JA	---	---	+275	+250	+191	+258	---	---	---
3	16-12-1986	---	JA	---	+275	+240	+149	+236	---	---	85% open tbv C-werk
4	19-12-1986	---	JA	JA	+275	+290	+141	+273	+100	+103	---
5	19-12-1986	---	JA	JA	+275	+279	+155	+271	+100	+97	---
6	02-01-1987	---	JA	---	+275	+258	+196	+239	---	---	62% open tbv C-werk
7	05-01-1987	---	JA	---	+275	+264	+178	+220	---	---	---
8	21-11-1987	JA	JA	---	+300	+284	+195	+266	---	---	---
9	14-02-1989	---	JA	JA	+300	+300	+135	+317	+100	+170	Late sluiting
10	26-01-1990	---	JA	---	+300	+260	+146	+208	---	---	---
11	12-02-1990	JA	JA	---	+300	+262	+181	+250	---	---	---
12a	26-02-1990	JA	JA	---	+300	+257	+193	+280	---	---	---
12b	27-02-1990	---	---	JA	+300	+300	+180	+317	+100	+102	Doorlopend alarm
12c	27-02-1990	---	---	JA	+300	+329	+198	+369	+200	+206	Idem 2de top
12d	28-02-1990	---	---	JA	+300	+314	+187	+325	+100	+106	Idem 3de top
13	01-03-1990	JA	JA	JA	+300	+320	+169	+335	+100	+107	---
14	02-03-1990	JA	JA	---	+300	+273	+187	+286	---	---	---
15	19-09-1990	JA	JA	---	+300	+272	+187	+291	---	---	---
16	21-09-1990	---	JA	JA	+300	+305	+184	+292	+100	+102	---
17	07-10-1990	---	JA	---	+300	+280	+211	+280	---	---	---
18a	12-12-1990	---	JA	JA	+300	+305	+119	+280	+100	+93	---
18b	12-12-1990	---	---	JA	+300	+308	+136	+265	+200	+198	Doorlopend alarm
19	20-12-1991	---	JA	---	+300	+289	+172	+267	---	---	---
20	11-11-1992	---	---	JA	+300	+264	+183	+315	+100	+239	Late sluiting
21	26-11-1992	---	JA	---	+300	+280	+170	+275	---	---	---
22	10-01-1993	JA	JA	---	+300	+295	+211	+272	---	---	---
23	25-01-1993	JA	JA	JA	+300	+292	+179	+325	+100	+260	Late sluiting
24a	20-02-1993	JA	JA	---	+300	+285	+156	+277	---	---	---
24b	21-02-1993	---	---	JA	+300	+310	+171	+313	+100	+135	Doorlopend alarm
25a	14-11-1993	JA	JA	JA	+300	+307	+204	+337	+100	+100	---
25b	15-11-1993	---	---	JA	+300	+312	+198	+337	+200	+202	Doorlopend alarm
26	16-12-1993	JA	JA	---	+300	+258	+192	+255	---	---	---
27	28-01-1994	---	JA	JA	+300	+325	+199	+349	+100	+131	Hoog laagwater
28	30-01-1994	JA	JA	---	+300	+265	+209	+256	---	---	---
29	17-03-1994	---	JA	---	+300	+240	+167	+238	---	---	---
30a	01-01-1995	---	JA	---	+300	+281	+195	+293	---	---	---
30b	02-01-1995	---	---	JA	+300	+313	+184	+330	+100	+98	Doorlopend alarm
31	02-01-1995	---	---	JA	+300	+295	+203	+311	+200	+248	---
32	18-03-1995	JA	---	---	+300	+248	+209	+240	---	---	Eindvoorspelling lager
33	28-09-1995	JA	JA	---	+300	+292	+210	+274	---	---	---

Figure 114: SVKO closures, part 1 [25]

34	28-08-1996	JA	---	---	+300	+268	+179	+276	---	---	---	---
35a	29-08-1996	---	JA	---	+300	+279	+179	+276	---	---	---	Zelfde HW als vorige oproep
35b	30-08-1996	---	JA	---	+300	+286	+213	+264	---	---	---	Doorlopend alarm
36	29-10-1996	JA	JA	JA	+300	+324	+198	+313	+100	+94	---	---
37	28-02-1998	JA	JA	---	+300	+292	+214	+276	---	---	---	---
38a	15-09-1998	---	JA	JA	n.v.t.	+155	+116	+158	+100	+98	---	Wateroverlast door neerslag
38b	15-09-1998	---	JA	JA	n.v.t.	+155	+134	+159	+50	+50	---	Wateroverlast door neerslag
39	25-10-1998	JA	JA	---	+300	+276	+170	+269	---	---	---	---
40	04-11-1998	JA	---	---	+300	+277	+219	+258	---	---	---	---
41	04-02-1999	JA	---	---	+300	+279	+167	+269	---	---	---	---
42	16-02-1999	JA	---	---	+300	+284	+194	+280	---	---	---	---
43	03-12-1999	---	JA	---	+300	+277	+155	+282	---	---	---	---
44	24-12-1999	JA	---	---	+300	+279	+208	+245	---	---	---	---
45	22-01-2000	JA	JA	---	+300	+269	+204	+273	---	---	---	---
46	28-12-2001	JA	JA	---	+300	+281	+167	+281	---	---	---	---
47	27-10-2002	JA	JA	JA	+300	+299	+170	+251	+100	+131	---	---
48	04-02-2003	JA	JA	---	+300	+285	+175	+235	---	---	---	---
49	29-01-2003	JA	JA	---	---	---	---	---	---	---	---	Dreigende olievervuiling
50	02-04-2003	JA	JA	---	+300	+281	+172	+235	---	---	---	---
51	21-12-2003	JA	JA	JA	+300	+304	+169	+319	+100	+97	---	---
52	08-02-2004	JA	JA	JA	+300	+300	+184	+300	+100	+101	---	---
53	12-11-2004	JA	JA	---	+300	+292	+204	+293	---	---	---	---
54	12-02-2005	JA	JA	---	+300	+278	+190	+250	---	---	---	---
55a	13-02-2005	JA	---	---	+300	+284	+176	+278	---	---	---	---
55b	13-02-2005	JA	---	---	+300	+275	+176	+263	---	---	---	---
56	29-04-2005	---	JA	---	---	---	---	---	---	---	---	Vlakter onderdoor kering
57	16-12-2005	---	JA	---	+300	+278	+176	+280	---	---	---	---
58	17-12-2005	JA	---	---	+300	+278	+177	+266	---	---	---	---
59a	18-03-2007	JA	---	---	+300	+279	+184	+273	---	---	---	---
59b	18-03-2007	---	JA	---	+300	+282	+168	+271	---	---	---	Doorlopend alarm
60	20-03-2007	JA	---	---	+300	---	---	+246	---	---	---	---
61a	09-11-2007	JA	JA	JA	+300	+327	+173	+343	+100	+102	---	---
61b	09-11-2007	---	JA	---	+300	+288	+169	---	---	---	---	Doorlopend alarm
62	25-11-2007	JA	---	---	+300	+293	+208	+288	---	---	---	---
63	21-03-2008	JA	---	---	+300	+289	+173	+298	---	---	---	---
64	10-02-2009	JA	---	---	+300	---	+177	+266	---	---	---	---
65	09-12-2011	JA	---	---	+300	---	---	---	---	---	---	---
66a	06-12-2013	JA	JA	JA	+300	+332	+190	+363	+146	+151	---	Afw. streefpeil door sterk gewijzigde voorspelling
66b	06-12-2013	---	JA	---	+300	+292	+204	+278	---	---	---	Doorlopend alarm
69	22-10-2014	JA	JA	JA	+300	+308	+170	+319	+100	+102	---	---
70	29-11-2015	JA	---	---	+300	+282	+172	+268	---	---	---	Sterk gewijzigde waterstandsverwachting tijdens voorbereidingsfase
71	13-01-2017	JA	---	---	+300	+276	+182	+276	---	---	---	---
72	03-01-2018	JA	JA	JA	+300	+310	+208	+301	+100	+095	---	---
73	18-01-2018	---	JA	---	---	---	---	---	---	---	---	Wegafsluiting N57
74	05-11-2018	---	JA	---	---	---	---	---	---	---	---	Aanvaring ms Eemshorn tegen kering thv R24. Tevens wegafsluiting N57
75	08-01-2019	JA	---	---	+300	+283	+172	+283	---	---	---	---
76	10-03-2019	---	JA	---	---	---	---	---	---	---	---	Wegafsluiting N57
77	29-09-2019	JA	---	---	+300	+278	+215	+280	---	---	---	---
78	09-12-2019	---	---	---	---	---	---	---	---	---	---	Geen semafoonoproep uitgegaan bij waterstand +275
79	09-02-2020	---	JA	---	---	---	---	---	---	---	---	Windwaarschuwing (N57 niet afgesloten)
80	10-02-2020	JA	JA	JA	+300	+305	+199	311	+100	+096	---	---
81	11-02-2020	JA	---	---	+300	+290	+204	+276	---	---	---	---
82	25-09-2020	---	JA	---	---	---	---	---	---	---	---	Windwaarschuwing (N57 niet afgesloten)
83	21-10-2021	JA	---	---	+300	+279	+180	+277	---	---	---	---
84	07-11-2021	---	JA	---	+300	+275	+215	+290	---	---	---	---
85	05-01-2022	JA	---	---	+300	+290	+195	+285	---	---	---	---
86	31-01-2022	JA	JA	JA	+300	+310	+172	+324	+100	+096	---	---
87	18-02-2022	---	JA	---	---	---	---	---	---	---	---	Windwaarschuwing harde wind(>25m/s), weg afgesloten
88a	21-02-2022	JA	---	---	+300	+280	+171	+311	+100*	+280	---	*)Wegens "late sluiting" is streefpeil niet gehaald. Doorlopend alarm (zie 88b)
88b	21-02-2022	---	JA	---	+300	+280	+176	+269	---	---	---	---
		Voor- alarm	Alarm Sluiten	Verwach- peil	Verwach- hoogwater	Astro hoog- water	Opgetr- hoog- water	Streef- peil	Opgetr- waterst.			Opmerkingen

Figure 115: SVKO closures, part 2 [25]

Table 25: Dutch to English Translations.

Dutch	English
JA	YES
---	NO
Langd. gesl. tbv C-werk	Long closed for C-work
85% open tbv C-werk	85% open for C-work
Late sluiting	Late closing
Doorlopend alarm	Continuous alarm
Hoog laagwater	High low tide
Eindvoorspelling lager	Final forecast lower
Zelfde HW als vorige oproep	Same high water as previous call
Idem 2de top	Same 2nd peak
Idem 3de top	Same 3rd peak

## **Q Overview of the Hollandsche IJsselkering**

Finished in 1958 and located in Zuid-Holland, the Netherlands. In 1977 the second gate was finished. The gates are lowered by 4 winches. Failure probability per individual closure is 1 in 200 [13].

## R Overview of the Maeslantkering

Constructed between 1991 and 1997, the Maeslantkering is an automated storm surge barrier situated in the Nieuwe Waterweg at Hoek van Holland. The barrier boasts two gates, each 210 m wide, 22 m tall, and 15 m deep. Designed to counter flood waves reaching up to 5 m above the Normal Amsterdam Level (NAP), it has a failure probability of 1 in 100 per individual closure. An annual functional or test closure is executed, with a total of 25 test closures having taken place by the time of this documentation. Significant storm-induced closures are outlined in Table 26.

**Table 26:** Notable Closures of the Maeslantkering

Date	Level (m above NAP)	Details
10 May 1997	-	Test closure
3 October 1997	-	Test closure
18 September 2004	-	Test closure
1 October 2005	-	Test closure
7 October 2006	-	Test closure
29 September 2007	-	Test closure
8 November 2007	2.84	Storm condition closure
20 September 2008	-	Test closure
19 September 2009	-	Test closure
25 September 2010	-	Test closure
24 September 2011	-	Test closure
16 September 2012	-	Test closure
21 September 2013	-	Test closure
28 September 2014	-	Test closure
19 September 2015	-	Test closure
17 September 2016	-	Test closure
9 September 2017	-	Test closure
3 January 2018	2.60	Storm conditional closure
15 September 2018	-	Test closure
14 September 2019	-	Test closure
20 September 2020	-	Test closure
12 September 2021	-	Test closure
10 September 2022	-	Test closure

## S Overview of the Hartelkering

The Hartelkering (HK), completed in 1997 and located in Zuid-Holland, is a storm surge barrier that is part of the Europoortkering, which also includes the Maeslantkering. The HK features two vertical lift gates in series, spanning widths of 49 and 98 meters. These gates are raised and lowered by lifting cylinders. The system's failure probability per individual closure stands at 1 in 100. Over the years, the Hartelkering has undergone an annual Test closure, totaling 25 closures at the time of writing. Notable storm-induced closures are detailed in Table 27.

**Table 27:** Notable Closures of the Hartelkering

Date	Level (m above NAP)	Details
10 May 1997	-	Test closure
3 October 1997	-	Test closure
18 September 2004	-	Test closure
1 October 2005	-	Test closure
7 October 2006	-	Test closure
29 September 2007	-	Test closure
8 November 2007	2.84	Storm condition closure
20 September 2008	-	Test closure
19 September 2009	-	Test closure
25 September 2010	-	Test closure
24 September 2011	-	Test closure
16 September 2012	-	Test closure
21 September 2013	-	Test closure
28 September 2014	-	Test closure
19 September 2015	-	Test closure
17 September 2016	-	Test closure
9 September 2017	-	Test closure
3 January 2018	2.60	Storm conditional closure
15 September 2018	-	Test closure
14 September 2019	-	Test closure
20 September 2020	-	Test closure
12 September 2021	-	Test closure
10 September 2022	-	Test closure

## T Individual Double Degree Thesis Division

**Table 28:** Division of Thesis and European Credits Allocation

<b>Division</b>	<b>Section/Chapter</b>	<b>Total European Credits (EC)</b>
Civil Engineering	CH2: Current Methods CH2: Limitations Current Method CH2: Review of Prior Research Closure Data Analysis Closure Data Database Framework Closure Data Database Code Repository	14 EC
Mathematics	CH4: Statistical Framework CH4: Review of Models and Methods CH4: Simplified Bootstrap Approach CH4: User Dashboard Database Model and Statistical Fitting Codde Repository	16 EC
Common Part	CH1: Introduction CH3: Data Description CH3: Database structure CH5: Method Application Framework CH5: Application Framework Result CH6: Discussion	26 EC